Topics in Quantum Gravity and Quantum Field Theory

Praveen Dennis Xavier

University College
University of Oxford

A thesis submitted for the degree of
Doctor of Philosophy

Michaelmas 2021

Abstract

In this thesis, we analyse three different quantum systems via operator and path integral techniques: 'two-dimensional Causal-Dynamical-Triangulations (CDT) coupled to hard-dimers', 'scalar solitons' and 'Quantum Random Walks (QRW) on the Cayley tree'.

In our first project, we extend previous work on CDT coupled to hard dimers – which is a discretized model of two-dimensional quantum gravity coupled to matter – and solve this model exactly with all dimer types present subject to a single restriction. We find that, depending on the dimer fugacities, there are, in addition to the usual gravity phase of CDT, two tri-critical and two dense-dimer phases. We establish the properties of these phases, computing their cylinder and disk amplitudes, their scaling limits and their associated continuum Hamiltonians.

In our second project, we investigate scalar solitons in the framework of quantum field theory. We construct general soliton creation operators and compare these with like operators found by Mandelstam in the sine-Gordon model. We find evidence for the fact that the sine-Gordon soliton is the Thirring fermion only at coupling $\beta^2 = 4\pi$. We then go on to compute the first quantum corrections to the radius of the kink in the ϕ^4 model in two dimensions.

In our third project, we analyse QRWs on the Cayley tree via the generating function method and derive a set of polynomial equations which determine this model exactly. We establish properties of the spectrum of the time-evolution operator U and solve the 'perturbed' eigenvalue equation in U.

Topics in Quantum Gravity and Quantum Field Theory

Praveen Dennis Xavier

University College

University of Oxford

A thesis submitted for the degree of

Doctor of Philosophy

Michaelmas 2021

Statement of originality

Chapters 3, 4 and 5 (and their associated appendices) are based on papers authored by John F Wheater and me. (Chapter 3 is based on [1].) Everything else is written wholly by me.

Acknowledgements

I wish to express my gratitude to
-my supervisor *John F Wheater* for his unconditional support. It was a privilege and pleasure to be his student.
-*Subir Sarkar* and *Amanda Cooper-Sarkar* for helping to secure me the Oxford-Berman Scholarship to attend this course.
-the *Oxford-Berman Scholarship*.
-everyone from the department of physics.
-*my parents*, for everything.
-*my friends*, at Oxford and in London, and my better half *Kitt*.

Abstract

In this thesis, we analyse three different quantum systems via operator and path integral techniques: 'two-dimensional Causal-Dynamical-Triangulations (CDT) coupled to hard-dimers', 'scalar solitons' and 'Quantum Random Walks (QRW) on the Cayley tree'.

In our first project, we extend previous work on CDT coupled to hard dimers – which is a discretized model of two-dimensional quantum gravity coupled to matter – and solve this model exactly with all dimer types present subject to a single restriction. We find that, depending on the dimer fugacities, there are, in addition to the usual gravity phase of CDT, two tri-critical and two dense-dimer phases. We establish the properties of these phases, computing their cylinder and disk amplitudes, their scaling limits and their associated continuum Hamiltonians.

In our second project, we investigate scalar solitons in the framework of quantum field theory. We construct general soliton creation operators and compare these with like operators found by Mandelstam in the sine-Gordon model. We find evidence for the fact that the sine-Gordon soliton is the Thirring fermion only at coupling $\beta^2 = 4\pi$. We then go on to compute the first quantum corrections to the radius of the kink in the ϕ^4 model in two dimensions.

In our third project, we analyse QRWs on the Cayley tree via the generating function method and derive a set of polynomial equations which determine this model exactly. We establish properties of the spectrum of the time-evolution operator U and solve the 'perturbed' eigenvalue equation in U.

Contents

List of Figures

List of Abbreviations

h.o.t. . . . . . Higher order terms (usually in an expansion).

w.r.t. . . . . . With respect to.

resp. . . . . . Respectively.

s.t. . . . . . Such-that.

const. . . . . . Constant (usually referring to some numerical value).

cl. . . . . . Classical (usually used as a subscript).

d.o.f. . . . . . Degrees of freedom.

QCD . . . . . Quantum Chromo-Dynamics.

QFT . . . . . Quantum Field Theory.

ODE . . . . . Ordinary Differential Equation.

PF . . . . . Partition Function.

EOM . . . . . Equation of motion.

Conventions

Positions . . . . . In more than two dimensions, $x^\mu = (t, \boldsymbol{x})$ and, sometimes, x^μ will be written as x.
In two dimensions, we write $x^\mu = (t, x)$.

Flat metric . . . . . $\eta = (+, -, ..., -)$.

Natural units . . . . . $16\pi G = \hbar = c = 1$.

Conjugation . . . . . For a complex number z, we will write either z^* or $\bar{z}$ for the complex conjugate.

Everything not forbidden is compulsory.

— Murray Gell-Mann

1 Introduction

Contents

In the broadest of terms, this thesis contains the study of different quantum systems.

The first of the systems that we analyse in this thesis (in §2.1 and Chapter 3) is a lattice discretization of Quantum Gravity (QG) in two dimensions known as Causal Dynamical Triangulations (CDT) [2]. With standard QG, the trouble is either that the Hilbert space is incomplete and needs extra degrees of freedom (e.g. string theory), a different Hamiltonian must be found (e.g. Hořava-Lifshitz QG [3]), or that new-variables must be found (e.g. Loop QG). CDT is yet another approach to the problem of QG.

CDT is a lattice version of QG defined in any number of dimensions, usually with no matter fields. It defines QG via a lattice discretization of the path integral over metrics on a manifold of fixed topology, admitting a time foliation. Since CDT is a lattice version of QG, using simulations or analytic techniques (analytic techniques only work in two dimensions so far) one can investigate the non-perturbative aspects

of QG. It is hoped that this will in turn give evidence to the conjecture that QG in 3+1 dimensions is renormalizable in the deep ultraviolet regime.

The second of the systems that we analyse is solitons in two dimensions (in §2.2 and Chapter 4). These arise in standard quantum field theories, but one must make contact with classical aspects to best understand them, which is simplest to do from a Hilbert-space perspective. In particular, one has to make a rather intricate change of variables at the level of the Hilbert space to study solitons. This project was motivated by the "bound states conjecture" [4] which itself originated from black hole thought experiments and the Weak Gravity Conjecture.

The third of the systems that we analyse is the quantum random walk on a Cayley tree (in §2.3 and Chapter 5). In this system, a spin-one particle moves on the Cayley tree in discrete time. The dynamics is governed by a unitary operator, U, which evolves the system forward by one time step. U couples only neighbouring sites of the tree; so, when one studies matrix elements of U^t (for t an integer) via the path integral, the paths which contribute will involve the particle (also called the 'walker') hopping between neighbouring sites in discrete time. Therefore, the system is usually called a quantum-random-walk. Quantum random walks have applications in quantum search algorithms [5].

To orient the reader through this text, we state the following: §2.1, §2.2 and §2.3 are the prerequisites for Chapters 3, 4 and 5 respectively. Chapter 6 contains a detailed summary of Chapters 2–5. §A, §B and §C are the appendices to Chapters 3, 4 and 5 respectively. Chapters 3, 4 and 5 are our works on CDT, Solitons and QRWs respectively. Consult the 'conventions' and 'abbreviations' pages above for the conventions and abbreviations that we adopt.

1.1 Quantum Gravity

It is often said that there is no theory, yet, of quantum gravity. Classical gravity on the other hand, also known as general relativity (GR), is described by a metric satisfying Einstein's equations. Einstein's equations can be derived from variations of an action known as the Einstein-Hilbert (EH) action. Quantization of gravity is

then straightforward: define a path integral over metrics (modulo diffeomorphisms), weighted by the EH action. To actually calculate with this model, expand the metric around the Minkowski metric, $g = \eta + h$, and perform perturbation theory in h. What results is a set of rules for calculating Feynman diagrams. The new ingredients are: a graviton propagator and graviton interaction vertices. So what goes wrong with this model? It is actually non-renormalizable[1]. A non-renormalizable theory is one which can't make predictions[2]

The non-renormalizability of gravity is indicating that the theory is missing some ultraviolet degrees of freedom (d.o.f.). These d.o.f., when included, should restore renormalizability. In the non-renormalizable model described above, the only d.o.f. are the metric and matter fields.

GR is in fact a theory of metric and matter fields on a manifold M (by manifold we will mean smooth manifold). The modern definition of a manifold is a set (of the points in the manifold), equipped with a topology (these two together make a topological manifold) and a smooth structure. A smooth structure is an equivalence class of atlases, and an atlas is a collection of charts (i.e. coordinates) with smooth transition functions. (Let us recall that homeomorphisms are an equivalence relation between topological manifolds and that diffeomorphisms are an equivalence relation between smooth manifolds.) What kind of d.o.f. does a smooth manifold have? First, there is the choice of which underlying topological manifold, and then the choice of which smooth structure to equip the topological manifold with: in short, we have to choose the topology and the smooth structure – these are the d.o.f. associated with a smooth manifold. In regard to the question of smooth structure, in low dimensions (three and less), according to Moise's theorem, there is only

[1]However, there is the possibility that this model is non-perturbatively renormalizable. We will take up this possibility in §2.1 as the motivation for CDT after first exploring a different idea in this section.

[2]In a non-renormalizable theory, we must add a counter-term for every operator consistent with the symmetries of the theory [6] (p. 504), of which there are an infinite number. With each of these terms is associated a coupling constant; therefore there are an infinite number of coupling constants. Each of these couplings has to be measured in an experiment. The measured values can be used, then, to predict the amplitude of other scattering processes. Unless the infinite set of couplings are related by a infinite set of relations, (leaving behind a finite number of independant couplings), it is impossible to determine all couplings from a finite number of measurements, and therefore impossible to make any predictions.

one smooth structure (modulo diffeomorphism) that a given compact topological manifold can be equipped with[3]; in dimensions greater than three, there can be more than one (or even uncountably many) smooth structures that a given topological manifold can equipped with [7]. As we will discuss below, the d.o.f. associated with the smooth manifold should play a role in the quantum theory; while one is potentially familiar with topological d.o.f. playing a role in QG [8], it appears that the d.o.f. associated with the choice of smooth structure, when present, should also play a role; and whether these are present depends on the spacetime dimension under consideration, as highlighted above.

What does it mean to quantize a theory? The first step is to construct the Hilbert space $\mathcal{H}$. The Hilbert space of a quantum theory is the set of normalizable functions on configuration space $\mathcal{C}$[4]. Now, configuration space is the space of 'all possibilities'. It is in deciding 'all possibilities' that one defines the d.o.f. of the system. ($\mathcal{C}$ is basically the basis states of $\mathcal{H}$, and a function on $\mathcal{C}$ is a general state in $\mathcal{H}$ decomposed in the basis.) For example, the configuration space of quantum mechanics in $d+1$ dimensions is the space of all points in $\mathbb{R}^d$, and the Hilbert space is the set of normalizable functions on $\mathbb{R}^d$. The configuration space of quantum field theory in $\mathbb{R}^{d+1}$ is the set of field configurations on $\mathbb{R}^d$ (an entire field configuration is one point in $\mathcal{C}$).

Given the Hilbert space, one defines a Hamiltonian H, governing dynamics, as some diffusion operator on $\mathcal{C}$, i.e. $H \equiv H(\vec{x}, \partial_{\vec{x}})$, where $\vec{x}$ are some coordinates

[3]Another way of saying this is that there are no exotic compact three-manifolds.

[4]Every Hilbert space has an orthonormal basis (or basis for short). Given the basis, Hilbert space can be recovered by 'completing' the basis, i.e. $\mathcal{H}$ consists of the set of all normalizable linear superpositions of states in the basis [9] (pp. 58-59). The set of coefficients in the aforementioned superposition is a complex number associated with each element of the basis; i.e. it is a *complex function* on the basis (a map from the basis to $\mathbb{C}$). A state in the Hilbert space is specified entirely by this set of coefficients. Therefore, a state in the Hilbert space is equivalent to a function on the basis.

Now, in a given theory, the basis can be inferred from the completeness relation, which, in general, takes the form $1 = \sum_{x \in \mathcal{C}} |x\rangle \langle x|$, where $\mathcal{C}$ will be called as 'configuration space'. The basis in that case is simply $\{|x\rangle : x \in \mathcal{C}\}$. From the discussion above, it follows that *Hilbert space is the set of all normalizable complex functions on* $\mathcal{C}$.

In quantum field theory, the basis consists of the states $|\phi(\boldsymbol{x})\rangle$, where $\phi(\boldsymbol{x})$ is any field configuration on a spatial hypersurface – that this is true follows from the well-known fact that the completeness relation in QFT is $1 = \int [d\phi(\boldsymbol{x})] \, |\phi(\boldsymbol{x})\rangle \langle \phi(\boldsymbol{x})|$ (see for e.g. [6], Sec. 9.1). (This then implies that, in QFT, $\mathcal{C}$ is the set of *all* field configurations on a spatial hypersurface.)

(usually infinitely many) on $\mathcal{C}$. The goal is then to determine the eigenvalues and eigenstates of H. Some of the states are single-particle states, and their eigenvalues are their measured masses. The hadron masses for example are, in principle, contained in the spectrum of the QCD Hamiltonian, though no-one has managed to extract them. Other states are multi-particle states, and their relative overlap is what we would call a scattering amplitude.

Notice that the elements of the Hilbert space are essentially defined in one dimension less than the spacetime dimension. However, relativistic covariance is guaranteed because the Hamiltonian satisfies the Poincaré algebra.

If one coordinatizes $\mathcal{C}$ with coordinates $\vec{y}$, instead of $\vec{x}$, then the dual Hamiltonian of the theory is $H\left(\vec{x}(\vec{y}), J \cdot \partial_{\vec{y}}\right)$ where $\vec{x}(\vec{y})$ is the change of variables and J is the Jacobian matrix. This means that there isn't a preferred coordinatization of $\mathcal{C}$. (The Jacobians for the transformations of $\vec{x}$ and $\partial_{\vec{x}}$ cancel out in the path integral [10].)

So what might the configuration space of 3+1 dimensional gravity be? It might be the set of all three-manifolds (including the empty manifold $\emptyset$, which serves as a proxy vacuum-state [11]), modulo diffeomorphism, with all admissible metric and matter fields on them. We could write this as $\mathcal{C} = \{\, |\, [\Sigma], \Phi(\Sigma)\,\rangle\,\}$ where $[\Sigma]$ stands for the equivalence class (under diffeomorphism) of an arbitrary three-manifold Σ, and $\Phi(\Sigma)$ stands collectively for the metric and matter fields on Σ. The new d.o.f. in this Hilbert space, compared to the standard theory of QG, is that $[\Sigma]$ is allowed to vary arbitrarily. The rationale for this choice of $\mathcal{C}$ is that gravity should be a theory not just of the metric on spacetime, but also of the spacetime itself. What one must note about $\mathcal{C}$ is that it is not the tensor product of the space of all manifolds with the space of all fields, because, to define the fields, one needs to specify the manifold. Therefore the two degrees of freedom are actually entangled.

Note that three-dimensional diffeomorphism is built into $\mathcal{C}$ as a gauge symmetry because the physical states depend only on the equivalence class under diffeomorphism. We expect to recover four-dimensional diffeomorphism symmetry by enforcing an extra constraint on $\mathcal{H}$ (namely the Hamiltonian constraint). This

is not unlike gauge theories, where four-dimensional gauge invariance arises from three-dimensional gauge invariance[5].

In contrast to the situation described above, in which $[\Sigma]$ can vary arbitrarily, the standard theory of QG is built on a globally hyperbolic spacetime M. This means that M is foliated by slices $\Sigma_t \subset M$, with $t \in \mathbb{R}$, i.e. $M = \bigcup_{t\in\mathbb{R}} \Sigma_t$, and the slices Σ_t are diffeomorphic to each other for all t [13]. That means that all the slices lie in the same class $[\Sigma_t]$. Therefore, the non-renormalizable model is a special case of the general model, where the class $[\Sigma_t]$ is fixed from the outset.

Do we expect the new degrees of freedom to restore renormalizability to gravity? That is a difficult question to answer without a calculational scheme, but there is no reason to rule it out. Clearly what one has to do is calculate previously divergent quantities and check if the extra d.o.f. cause the appropriate cancellations. How might we calculate in this theory?

Let us recall how one proceeds from the Hamiltonian formalism to the path integral formalism. We start with a matrix element $\langle\psi_1| e^{-2HT} |\psi_2\rangle$ and evaluate it by saturating with a complete set of states[6] $1 = \sum_{|\vec{x}\rangle\in\mathcal{C}} |\vec{x}\rangle \langle\vec{x}|$, repeatedly, from $t = -T$ to $t = +T$. The underlying degrees of freedom then acquire a time-dependence, i.e. the coordinates $\vec{x}$ of $\mathcal{C}$ now become $\vec{x}(t)$. In this sense, time is emergent. The path integral is then a sum over paths $\vec{x}(t)$, weighted appropriately. The path integral for our model in which $[\Sigma]$ is allowed to be arbitrary, will include a sum over histories of manifolds $[\Sigma(t)]$. (Note that an entire history of three-manifolds is equivalent to a four-manifold.) At each time, the three-manifold might have a different topology. There are topologies of two kinds: disconnected and multiply-connected. Consider the disconnected topologies for a moment. If there

[5] In the canonical quantization of gauge theories, the zeroth component of the gauge field is not physical and the Gauss law, $\sum_i \int d^3\boldsymbol{x} \frac{d\Phi_i^\lambda(\boldsymbol{x})}{d\lambda_a(\boldsymbol{y})} \Pi_i(\boldsymbol{x}) = 0$ (where Φ_i are all the physical field components, Π_i stands for their conjugate momenta and Φ_i^λ stands for the fields after a gauge transformation with gauge-transformation parameters $\lambda_a(\boldsymbol{x})$), enforces the invariance of the theory under three dimensional gauge transformations [12] (p. 232). However, once the path integral has been constructed, one finds that the zeroth component of the gauge field – which enters as a Lagrange multiplier – is on the same footing as the spatial components and that the path integral is actually invariant under the group of four-dimensional gauge transformations.

[6] In this informal discussion, we have glossed over the fact that we actually also need to saturate by $1 = \sum_{|\vec{p}\rangle\in\mathcal{C}^\star} |\vec{p}\rangle \langle\vec{p}|$, where $\mathcal{C}^\star$ is the dual 'momentum basis'.

was only one connected topological three-manifold Σ_0, the disconnected topologies are just $\bigcup_{i=1}^{n} \Sigma_0$, for any positive integer n. A particular history of manifolds $[\Sigma(t)]$ might then, very well, involve a transition between different n, i.e. the creation and annihilation of copies of Σ_0. Thus we are led to a many-body theory of spacetime, in which each connected copy of spacetime, Σ_0, can be created or destroyed like an elementary particle. Obviously an amplitude has to be associated with such events. From the past we know that this can, at least, be partially achieved by introducing certain auxiliary fields, which when integrated out, give a contribution that depends only on the topology of the four-manifold (we are referring to the work of E. Witten on Topological-QFT [14]). Also, as pointed out by said paper (in the final section), the scenario we are describing is really a three-brane scattering process. The open question is if the additional effect we've described is enough to restore renormalizability to gravitational amplitudes. We will not address this question here; instead we will pursue a different avenue and investigate a non-perturbative lattice formulation of the so-called non-renormalizable theory in Chapters 2.1 and 3.

1.2 The Bound States Conjecture

There was a suggestion in [4], motivated by the weak-gravity conjecture and black hole constructions, that bound states in quantum field theory (QFT) must have a minimum radius. Consider a bound state of radius R. Then $\Delta = mR$ (where m is the mass of heaviest elementary particle) is a dimensionless quantity and a function of the parameters, $\{\lambda\}$, in the theory, like the couplings and particle masses: $\Delta \equiv \Delta(\{\lambda\})$. The proposal of [4] is that $\Delta(\{\lambda\})$ is bounded below by some positive constant, i.e. $\Delta(\{\lambda\}) \geq \delta > 0$. The conjecture is non-trivial because, in a theory with scalars, say, one can imagine turning-up the scalar coupling indefinitely and squeezing any bound state to an arbitrarily small size. However, as this happens, the constituents become more energetic (momentum $p \sim R^{-1}$) and the process may become unstable when there is enough kinetic energy for particle production (this is like the mechanism involved in the Hagedorn limit [15]).

Solitons are known to possess a particle-like interpretation in QFT [16]. A soliton is an extended particle for which the question of its radius seems well posed. It can also be viewed as a bound state of the fundamental particles. Therefore, we found it natural to investigate the radius of solitons in the hope of answering the more general question of whether there indeed is a lower bound on the radius of a generic bound state.

Solitons are finite energy, non-dissipative solutions to the classical field equations – non-dissipative means that $\lim_{t\to\infty} \max_{\boldsymbol{x}} \mathcal{H}(t,\boldsymbol{x}) \neq 0$ [17] (Sec. 6.1), where $\mathcal{H}$ is the energy density. Intuitively, this means that the field stays lumped-up for all time.

Classically, the radius of a soliton, R_{cl}, is easy to define and compute: in line with [18], we will define it as the width of the energy density, normalized by the total energy:

$$R_{cl}^2 = \int d^3x\ |\boldsymbol{x}|^2 \mathcal{H}(\boldsymbol{x}) / \int d^3x\, \mathcal{H}(\boldsymbol{x}). \tag{1.1}$$

The interesting contribution to the radius is the quantum correction. To derive this, one needs a quantum theory of solitons and a method to compute matrix elements involving solitons in the initial and final states. The method of computing processes in which there is a single soliton, at rest, in the initial and final states, was well developed by several groups in the 70's, and generally, goes by the name of collective-coordinate-quantization [10] (reviewed in §2.2.3).

In the second project of this thesis, Chapter 4, we will develop the theory of quantum solitons and show how to calculate the quantum-corrected radius in the ϕ_2^4 model (we review classical ϕ_2^4 theory in §2.2.1), employing these old methods. Along the way we will give evidence that the sine-Gordon soliton is the Thirring fermion only at coupling $\beta^2 = 4\pi$.

Let us go through the main arguments of our second project. We recall that the configuration space of QFT in $\mathbb{R}^{d+1}$ is the set of field configurations on $\mathbb{R}^d$. (Let $\boldsymbol{x}$ denote positions in $\mathbb{R}^d$.) An elementary particle state of the QFT is a plane-wave impulse of the field. This can be made precise. For example, take the initial data $\phi_{cl}(\boldsymbol{x}) = \varepsilon\, e^{i\boldsymbol{p}.\boldsymbol{x}}$ and $\pi_{cl}(\boldsymbol{x}) = \varepsilon\, ip^0 e^{i\boldsymbol{p}.\boldsymbol{x}}$. Define an operator $O =$

$\exp i \int d^d\boldsymbol{x}\,(\pi\phi_{cl} - \phi\pi_{cl})$. This operator has the property that $O^{-1}\phi O = \phi + \phi_{cl}$ and $O^{-1}\pi O = \pi + \pi_{cl}$. Therefore it causes a shift by the classical configurations ϕ_{cl}, π_{cl}. In the limit that ε becomes infinitesimal, $\partial_\varepsilon O|_{\varepsilon=0} = a^\dagger_{\boldsymbol{p}}$. Therefore, $a^\dagger_{\boldsymbol{p}}$ creates a plane wave impulse.

Some QFTs contain more than just elementary particle states: solitons can also be cast as particle states. This is a simple generalization of the argument given before. Given initial data ϕ_{cl} and π_{cl} defining the soliton, define the operator $O = \exp i \int d^d\boldsymbol{x}(\pi\phi_{cl} - \phi\pi_{cl})$. O is simply the soliton creation operator [19]. Recall that single-particle states are classified by Wigner's method [6] (Sec. 2.5). In particular, massive states are classified according to their eigenvalues under spatial rotations $SO(d)$. A single-particle soliton state is no different – it can also be classified by Wigner's method. In the special case that the soliton is rotationally invariant, O is a scalar under rotations, so spin zero.

The states we obtain by application of O or $a^\dagger$ onto the vacuum (let us call these proxy-states) are not eigenstates of the Hamiltonian. Let us call eigenstates of the Hamiltonian 'exact-states'. The idea is that the proxy state is designed to have non-zero overlap with the exact state. Therefore, the exact state can be extracted by a limiting procedure: $|\text{exact}\rangle = \lim_{T\to\infty} e^{ET}e^{-HT}\,|\text{proxy}\rangle \,/\, \langle\text{exact}|\text{proxy}\rangle$ where E is the energy of the state. With this procedure in hand, one can study matrix elements between exact states. For example, given an exact single-particle state $|p^\mu\rangle$, consider $\langle p'|\,\mathcal{H}\,|p\rangle$. Using the limiting procedure, this can be written as a matrix element between proxy states: $\sim \langle 0|\,a_{\boldsymbol{p}'}e^{-HT}\,\mathcal{H}\,e^{-HT}a^\dagger_{\boldsymbol{p}}\,|0\rangle$. In the case of solitons, a and $a^\dagger$ will be replaced by $O^\dagger$ and O resp., but everything else is the same.

Since the classical radius is defined as the second moment of the energy density (see (1.1)), to define a quantum analogue, we will need to consider the form factor $\langle p'|\,\mathcal{H}(0)\,|p\rangle$. Taking derivatives of this w.r.t. to the momentum transfer $p' - p$ should give us moments of energy density, defined in a quantum way. In particular, taking two derivatives should give us the second moment, so we define the quantum radius, R, as $R^2 = M^{-2}\partial_{\ell^2}\,\langle k|\,\mathcal{H}(0)\,|k+\ell\rangle\,\Big|_{\ell=0}$ which we will show (in §4.5.1) gives us $R^2 = \frac{1}{2M^4}\,\langle k|\,\mathcal{H}(0)K^2\,|k\rangle$ in two dimensions, where K is the boost generator and

k^μ is the rest momentum. This is a matrix element between an initial and final soliton at rest. Therefore it can be directly evaluated by the method of collective-coordinate-quantization. The result can be organised in powers of $\hbar$; the leading term of order $\hbar^0$, we will find, recovers the classical definition (1.1). We then go on to calculate the term at $O(\hbar)$. The details are presented in the latter half of Chapter 4.

2 Overview

Contents

2.1 Causal Dynamical Triangulations

In this section we will review the model of CDT, mainly following [2].

CDT is a discretization of the gravitational path integral in quantum-gravity. Quantum-gravity in 3+1 dimensions, without any matter, is defined by the following path integral:

$$\langle h_2; \infty | h_1; -\infty \rangle = \int_{\substack{g(-\infty,\boldsymbol{x})=h_1(\boldsymbol{x}) \\ g(+\infty,\boldsymbol{x})=h_2(\boldsymbol{x}) \\ \sim\text{Diff}}} \prod_{\mu\leq\nu} [dg_{\mu\nu}(t,\boldsymbol{x})] \ \exp(i\, S_{\text{EH}}[g]), \tag{2.1}$$

in which the integral over metrics is modulo diffeomorphisms (i.e. two configurations related by a diffeomorphism $x^\mu \to x^\mu + \xi^\mu(x)$ are considered equivalent[1]). We assume that the underlying spacetime is globally hyperbolic: $M = \bigcup_{t\in\mathbb{R}} \Sigma_t$ and fixed. In (2.1), the induced metric on the past and future boundaries (at $t = \mp\infty$) has been fixed to the 3-metrics $h_1(\boldsymbol{x}) \equiv h_{1,ij}(\boldsymbol{x})$ and $h_2(\boldsymbol{x}) \equiv h_{2,ij}(\boldsymbol{x})$ respectively (where $i, j = 1, 2, 3$). The Einstein-Hilbert action is $S_{\text{EH}} = \frac{1}{16\pi G} \int d^4x \sqrt{|\det g|}(R - 2\Lambda)$, where R is the Ricci scalar, Λ is the cosmological constant and G is Newton's constant. (2.1) is the amplitude for a 3-metric $h_1(\boldsymbol{x})$ to propagate to a 3-metric $h_2(\boldsymbol{x})$.

CDT was proposed as an alternative to the earlier Dynamical Triangulations (DT) [20, 21] which is another way of discretizing the gravitational path integral – the main difference is that DT doesn't presuppose a time foliation. In CDT one integrates over all configurations (sometimes numerically and sometimes analytically). Therefore, calculations in CDT are supposed to give gravitational amplitudes non-perturbatively.

By numerically simulating CDT, one hopes to obtain non-perturbative information about QG, for example, whether 3+1 dimensional QG is non-perturbatively renormalizable: a possibility known as asymptotic safety [22]. The idea behind this proposal is that QG may have a fixed point (a point where all beta-functions vanish) at some non-zero coupling strength. Such a fixed point will be non-perturbative (because it is at non-zero coupling). Consider the number of operators whose

[1] One way of ensuring this is to insert four gauge-fixing delta-functions and the appropriate Jacobian factor associated with restricting the integral to this subspace, i.e. (2.1) is equivalent to

$$\int_{\substack{g(-\infty,\boldsymbol{x})=h_1(\boldsymbol{x}) \\ g(+\infty,\boldsymbol{x})=h_2(\boldsymbol{x})}} \prod_{\mu\leq\nu} [dg_{\mu\nu}(t,\boldsymbol{x})] \ \exp(i\, S_{\text{EH}}[g]) \ \delta(F_\mu(g)) \ \det_{\mu\nu,xy} \frac{\delta F_\mu(g^\xi(x))}{\delta \xi^\nu(y)},$$

where, for notational convenience, $g \equiv g_{\mu\nu}(x)$. $F_\mu(g)$ are the appropriate gauge-fixing functions, and g^ξ is the result of acting on g with the diffeomorphism generated by ξ.

couplings have non-negative mass dimension in the vicinity of this fixed point. If this number is finite and non-zero, then one obtains a renormalizable theory by setting all renormalized negative-mass-dimension couplings to zero. You might wonder why the same thing cannot be done around the 'free-fixed-point' (FFP) (the point with all renormalized couplings equal to zero); the reason is that, in the vicinity of the FFP, setting all couplings with negative mass dimension to zero, will result in a theory with only the cosmological constant term, which has no dynamics.

Briefly, we describe how the CDT discretization of (2.1) is constructed. First, one puts upper and lower bounds on time: $-T \leq t \leq T$ (eventually we will let $T \to \infty$ to recover the original expression). Next, time is discretized so that one considers only discrete values $t = a\,n$ ($n \in \mathbb{Z}$), where 'a' will play the role of the lattice spacing (we will eventually let $a \to 0$). So the spatial slices are discretely spaced in time: Σ_{-T}, Σ_{-T+a}, ..., Σ_{T-a}, Σ_T. $\Sigma_{\mp T}$ will be called the past and future boundary respectively.

Construct the 3-metric on each Σ_t in an invariant way – i.e. without coordinates – using 'triangulations', i.e. construct Σ_t by gluing together equilateral 3-simplices[2] (with edge length a) along common faces; and take the metric on the interior of each 3-simplex to be *flat*. This induces a metric on Σ_t since the length of any curve in Σ_t can be calculated as the sum of the lengths of the segments going through each simplex, calculated in the flat metric of each simplex. The curvature is concentrated on the edges of the simplices. To approximate a smooth 3-metric, take the limit $a \to 0$ – but, presently, hold off on this step, we will take $a \to 0$ later.

Then construct M and the 4-metric by gluing together neighbouring Σ_t using equilateral 4-simplices (with edge length a) and taking the interior of each 4-simplex to be flat. This is a CDT configuration. By considering all ways of triangulating the Σ_t's and all ways of connecting them together with 4-simplices, one obtains the CDT ensemble. Each element of the ensemble corresponds to a physically distinct metric configuration. The EH action can be discretized and written in

[2] A d-simplex is a triangle generalized to d dimensions. An equilateral 3-simplex is just a regular tetrahedron.

terms of the triangulation data, $\mathcal{T}$, using Regge calculus ([23], Sec. 2.2), giving $S_{\text{EH}}(\mathcal{T})$. Then the discretized version of (2.1) is

$$\sum_{\substack{\mathcal{T}:\partial_{\text{past}}\mathcal{T}=T_3\\ \partial_{\text{future}}\mathcal{T}=T_3'}} e^{iS_{\text{EH}}(\mathcal{T})}, \tag{2.2}$$

where the sum is over the CDT ensemble and the triangulations on the past and future boundaries are fixed to T_3 and T_3' respectively. Taking the limit $a \to 0$, while adjusting T_3 and T_3' to approximate the 3-metrics h_1 and h_2 respectively, and then taking the limit $T \to \infty$ should give the value of (2.1). Fortunately, the sum in (2.2) can be evaluated analytically for two-dimensional spacetimes. It is the 2-dimensional case that will concern us in this work. The 4-dimensional case requires numerical studies and it is still an active area of research (see [23], Sec. 7).

2.1.1 Two Dimensions

In 2 dimensions, the spatial slices are 1-dimensional. (We will continue to call spatial slices Σ_t and spacetime M.) We fix the topology of all Σ_t to be S^1. Therefore M has the topology of a cylinder. There is only one geometric invariant of a metric configuration, $h(x)$, in one-dimension: the volume: $L = \int dx\sqrt{h(x)}$. Therefore 1-metric configurations, modulo diffeomorphism, are equivalent to a length $L > 0$; and so, Hilbert space is the set of wavefunctions $\psi(L)$. In the discretized setup, this is reflected in the fact that a 1-manifold, Σ, constructed out of equal 1-simplices (which is just a line segment of length a) is specified entirely by the number of 1-simplices (and its total length is then: $a \times$ # of 1-simplices). Now, a 2-simplex is a triangle. So CDT configurations are formally defined as follows:

i. A sequence of concentric circles S_i, where the index i takes on integer values $i = 1, ..., t+1$. S_i is the spatial slice at time i. It is constructed out of equal 1-simplices, so each S_i consists of vertices $v \in S_i$ such that the distance between neighbouring vertices is a.

ii. Edges connecting all vertices $v \in S_i$, for $i \in [1, t]$, to at least one vertex $w \in S_{i+1}$ such that all faces are triangles. Each of these triangles is flat on the interior and has equal edge lengths a.

iii. A marked vertex in S_1 and S_{t+1} – this is purely for combinatoric convenience. What this means is that two graphs, which are the same otherwise, are considered distinct if their marks are at different locations.

This definition is illustrated in Fig. 2.1. The set of causal triangulations constructed

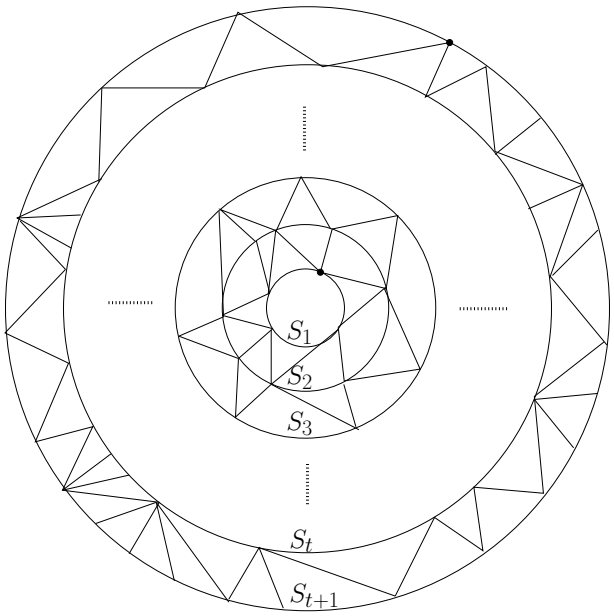

Figure 2.1: An element of $\mathcal{T}_t$. The marked vertices in S_1 and S_{t+1} are highlighted in bold.

according to (i)-(iii) will be called $\mathcal{T}_t$, and this is the CDT ensemble. We also define $\mathcal{T} := \bigcup_{t \in \mathbb{Z}^+} \mathcal{T}_t$.

Consider the following definitions. An edge connecting a vertex $v \in S_k$ to an adjacent vertex $w \in S_k$ is said to be horizontal. An edge is said to be forward (resp. backward) directed with respect to a vertex $v \in S_k$ if it connects v to a vertex in S_{k+1}(resp. S_{k-1}). A vertex $w \in S_k$ is said to be clockwise (resp. anti-clockwise) -adjacent to a vertex $v \in S_k$ if one meets w first as one travels from v clockwise (resp. anti-clockwise) along S_k. For a given $T \in \mathcal{T}_t$, define (see Fig. 2.2):

i. $e(v)$ as the horizontal edge connecting v to the vertex that is clockwise-adjacent to v. The map e is one to one and defined for all vertices in T.

ii. $f(v)$ as the forward directed edge w.r.t v which also bounds the same triangle bounded by $e(v)$. The map f is one to one and defined for all vertices in $\bigcup_{i\in[1,t]} S_i$.

iii. $\sigma_f(v)$ to be the number of forward-directed edges w.r.t. v, defined for all vertices in $\bigcup_{i\in[1,t]} S_i$.

iv. $\sigma_b(v)$ to be the number of backward-directed edges w.r.t. v, defined for all vertices in $\bigcup_{i\in[2,t+1]} S_i$.

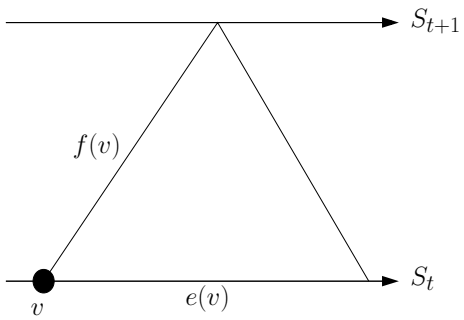

Figure 2.2: Definitions of $f(v)$ and $e(v)$. The arrows point in the clockwise direction.

The initial and final boundaries of a triangulation $T \in \mathcal{T}_t$ are defined as $\partial_1 T = S_1$ and $\partial_2 T = S_{t+1}$ respectively; they are referred to as the incoming and outgoing loops respectively.

2.1.2 The Cylinder Amplitude

So, what is (2.2) in two dimensions? To keep the 1-metric fixed on the boundaries we fix the length of the incoming and outgoing loop. The discretized EH action is $S_{\text{EH}} = \lambda\, a^2 \times \#$ of triangles. We've dropped the Ricci scalar term because it is a topological invariant (according to the Gauss-Bonnet theorem), and since the topology of M is fixed (to a cylinder) it only contributes an overall factor. The cosmological term equals $\lambda\, a^2 \times \#$ of triangles because each triangle has area $\sim a^2$. We've used λ for the cosmological constant, instead of Λ, because, later, we will

see that λ gets renormalized as $a \to 0$ – so we reserve λ for the bare coupling and Λ for the renormalized coupling.

We define $g = \exp(i\lambda a^2)$. Therefore (2.2) in 2-dimensions is

$$\tilde{G}(g, l_1, l_2; t) = \sum_{\substack{T \in \mathcal{T}_t : |\partial_1 T| = l_1 \\ |\partial_2 T| = l_2}} g^{|T|}. \tag{2.3}$$

In this expression, $|T|$ is the number of triangles in T, and $|\partial_1 T|$ and $|\partial_2 T|$ are the number of vertices on the incoming and outgoing loops respectively. This is called the cylinder-amplitude. We assume that it is analytic in a neighbourhood of $g = 0$. (2.3) gives the transition amplitude from an initial spatial universe of lattice length l_1 to a final spatial universe of lattice length l_2 in t time-steps. Taking the limit $a \to 0$ while keeping the physical lengths $L_1 = a\, l_1$, $L_2 = a\, l_2$ and $T = a\, t$ fixed, we will get an amplitude $\tilde{G}^s(\Lambda, L_1, L_2; T)$. Taking the limit $T \to \infty$ should then give the value of (2.1) in 2-dimensions.

We define the following generating function

$$G(g, x, y; t) := \sum_{l_1=0}^{\infty} \sum_{l_2=0}^{\infty} x^{l_1}\, y^{l_2}\, \tilde{G}(g, l_1, l_2; t) = \sum_{T \in \mathcal{T}_t} x^{|\partial_1 T|} y^{|\partial_2 T|} g^{|T|}.$$

We assume that G is analytic in a neighbourhood of $g = x = y = 0$. x and y will be referred to as the 'boundary cosmological constants' since they couple to volume of the boundaries. We can recover $\tilde{G}$ from G as follows:

$$\tilde{G}(g, l_1, l_2; t) = \oint_\gamma \frac{dx}{2\pi i x} \oint_\gamma \frac{dy}{2\pi i y}\, x^{-l_1}\, y^{-l_2}\, G(g, x, y; t), \tag{2.4}$$

where the contour γ encloses the neighbourhood of the origin in which G is analytic.

2.1.3 Bijection to Trees

It was shown in [24] that there is a bijection between $\mathcal{T}_t$ and $\mathcal{P}_{t+1}$ which is the space of planar rooted trees ('trees' from now on) of height $t+1$ with a marked vertex at height $t+1$. The height of a tree is the distance between the root and the furthest vertex, and the height of a vertex is its distance to the root. We use the terminology for neighbouring sites on trees as defined in Fig. 2.3. The bijection β maps $\mathcal{T}_t \ni T \to \tau \in \mathcal{P}_{t+1}$ as follows:

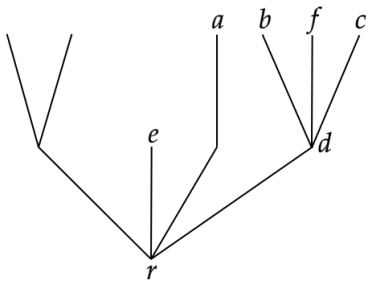

Figure 2.3: Tree terminology: r is the *root*; the vertex to the *left* of b is a; the vertex to the *right* of b is f; the *last child* of d is b; the *first child* of d is c; and e is a *leaf*.

I Introduce a root vertex r, of τ, in the centre of S_1 and add edges connecting it to each vertex in S_1.

II Delete $e(v)$ and $f(v)$ for all vertices $v \in T$.

III Assign the marked vertex in S_1 as the first child of the root vertex of τ.

IV Assign the marked vertex in S_{t+1} as the marked vertex in τ at height $t+1$.

Aside from the root vertex, τ shares all its vertices with T. Bar the root vertex, we may therefore refer interchangeably to the vertices of τ and T.

2.1.4 Generating Functions

By mapping $\mathcal{T}_t$ to $\mathcal{P}_{t+1}$ with the bijection β, we find that

$$G(g,x,y;t) = \sum_{\tau\in\mathcal{P}_{t+1}} g^{2|\tau|-2}(x/g)^{|\tau|_1}(y/g)^{|\tau|_{t+1}},$$

where $|\tau|$ is the number of vertices in τ and $|\tau|_i$ is the number of vertices at height i. We define $\mathcal{P}_{\leq t} = \bigcup_{i\in[0,t]} \mathcal{P}_i$ and the partition function of $\mathcal{P}_{\leq t}$ as

$$W(g,y;t) = \sum_{\tau\in\mathcal{P}_{\leq t}} \frac{1}{|\partial\tau|} g^{2|\tau|}(y/g)^{|\tau|_t},$$

where $|\partial\tau|$ is the number of vertices at the height of the tree. As Fig. 2.4 shows, a tree in $\mathcal{P}_{t+1}$ can be decomposed into sub-trees [25, 26] which lie in $\mathcal{P}_{\leq t}$. The number of sub-trees can be anywhere between one and infinity, and each contributes a factor of $\frac{x}{g}W(g,y;t)$. Therefore,

$$G(g,x,y,\xi;t) = y\frac{\partial}{\partial y}\sum_{n=1}^{\infty}\left(\frac{x}{g}W(g,y;t)\right)^n = y\partial_y\frac{1}{1-\frac{x}{g}W(g,y;t)}. \qquad (2.5)$$

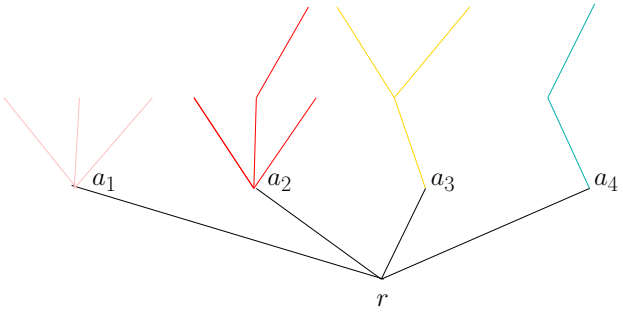

Figure 2.4: Decomposing a tree into sub-trees: $a_{1,2,3,4}$ are the roots of the sub-trees.

The operation $y\partial_y$ marks a vertex at height $t+1$, or, equivalently, marks the outgoing loop and removes the set of trees which are of height less than $t+1$. The model can be solved by finding recursion relations for W, to which we now turn.

The initial conditions are given by trees of height zero. So $W(g,y;0) = yg$. Following similar arguments as those that gave us (2.5), we obtain the following recursion $W(g,y;t+1) = g^2(1-W(g,y,t))^{-1}$ for $t \geq 0$. It is convenient to define $f_t(g,y) = g^{-2}W(g,y;t)$. f_t satisfies the initial condition $f_0(g,y) = y/g$ and the recursion relation

$$R(f_{t-1}, f_t) \equiv f_t(1-g^2 f_{t-1}) - 1 = 0, \tag{2.6}$$

where the argument (g,y) has been suppressed. From (2.5) we find that

$$G(g,x,y;t) = y\partial_y \frac{1}{1-gxf_t(g,y)}. \tag{2.7}$$

The solution to (2.6) with the initial condition is

$$f_t(g,y) = \frac{p_1^{-t} + c\, p_2^{-t}}{p_1^{-t-1} + c\, p_2^{-t-1}}, \tag{2.8}$$

with

$$c = -\frac{p_2(y-gp_1)}{p_1(y-gp_2)},$$

where $\{p_i\}_{i=1}^2$ are the two roots of $R(p,p) = 0$.

2.1.5 Scaling Limit and the Pure Gravity Phase

The grand-canonical partition function is determined by the fixed point of (2.6): $f_{t-1} = f_t = f_\infty$. The fixed point is obviously independent of the initial condition. So we will write $f(g) \equiv f_\infty(g)$. From (2.6), the fixed point $f(g)$ satisfies

$$P(f) \equiv f\,(1 - g^2 f) - 1 = 0. \tag{2.9}$$

Close to some critical value $g = g_c$, we expect $f(g)$ to exhibit the critical behaviour

$$f(g) = f_c - c(g_c - g)^\alpha + h.o.t.,$$

where c is a constant and α is fractional. For example, we can get a double-root of (2.9) at $g = g_c$ by requiring $P(f_c) = P'(f_c) = 0$. This gives us $\alpha = 1/2$ and $f_c = 2$, $g_c = 1/2$. The critical value g_c is actually the radius of convergence of $f(g)$ at $g = 0$. The critical point we've just identified lies in what is called the pure-gravity (PG) phase.

In any given phase, we expect to be able to take the scaling limit of observables. Consider $G(g, x, y; t)$. At the critical point, the radius of convergence in the x plane is $x_c = 1$ since the denominator of (2.7) vanishes: $1 - g_c x_c f_c = 0$, and the radius of convergence in the y plane is $(t+1)/t$, which in the limit $t \to \infty$ becomes $y_c = 1$. This follows because $f_t(g_c, y) = 2(ty - y - t)(ty - t - 1)^{-1}$ from (2.6). Therefore, around the PG critical point, we expand the couplings as so:

$$g = g_c(1 - \Lambda a^2/2), \quad x = 1 - aX, \quad y = 1 - aY, \tag{2.10}$$

and we take $T = a\,t$ fixed. Substituting these into observables and taking the limit $a \to 0$ will be how we take the scaling-limit – and what results is the 'continuum-observable'. These continuum observables are functions of Λ, X, Y and T, which are the continuum versions of the bulk, boundary cosmological constants and time respectively.

Substituting (2.10) in (2.8) and expanding in powers of a gives

$$f_{T/a}(g, y) = 2 + 2F(T, Y)\,a + \mathcal{O}(a^2), \tag{2.11}$$
$$F(T, Y) := -\Lambda^{\frac{1}{2}} \frac{-\Lambda^{\frac{1}{2}} + \Lambda^{\frac{1}{2}} e^{2\Lambda^{\frac{1}{2}} T} + Y e^{2\Lambda^{\frac{1}{2}} T} + Y}{\Lambda^{\frac{1}{2}} + \Lambda^{\frac{1}{2}} e^{2\Lambda^{\frac{1}{2}} T} + Y e^{2\Lambda^{\frac{1}{2}} T} - Y}.$$

Putting this in (2.7) and expanding in powers of a gives

$$G\left(g_c(1-\Lambda a^2/2), 1-aX, 1-aY; T/a\right) = \frac{1}{a^2} G^s(\Lambda, X, Y; T) + O(a^{-1}),$$
$$G^s(\Lambda, X, Y; T) := \frac{4\Lambda\, e^{2\Lambda^{\frac{1}{2}}T}}{\left(e^{2\Lambda^{\frac{1}{2}}T}(X+\Lambda^{\frac{1}{2}})(Y+\Lambda^{\frac{1}{2}}) - (X-\Lambda^{\frac{1}{2}})(Y-\Lambda^{\frac{1}{2}})\right)^2}. \quad (2.12)$$

$G^s(\Lambda, X, Y; T)$ is the continuum cylinder-amplitude. Similarly, we define the scaling limit of $\tilde{G}(\cdot)$ as

$$\tilde{G}^s(\Lambda, L, L'; T) = \lim_{a\to 0} \tilde{G}\left(g_c(1-\Lambda a^2/2), L/a, L'/a; T/a\right).$$

From (2.4), this can be expressed as

$$\tilde{G}^s(\Lambda, L, L'; T) = \int_{\gamma'} \frac{dX}{2\pi i} \int_{\gamma'} \frac{dY}{2\pi i}\, e^{XL} e^{YL'} G^s(\Lambda, X, Y; T), \quad (2.13)$$

where γ' is a path from $-i\infty$ to $+i\infty$ running to the right of all singularities of the integrand. Inverting this,

$$G^s(\Lambda, X, Y; T) = \int_0^\infty dL \int_0^\infty dL'\, e^{-XL} e^{-YL'} \tilde{G}^s(\Lambda, L, L'; T). \quad (2.14)$$

Using (2.12) in (2.13) finally gives

$$\tilde{G}^s(\Lambda, L_1, L_2; T) = \frac{\sqrt{\Lambda L_1 L_2}}{\sinh(\sqrt{\Lambda}T)} \times \exp\left(-\sqrt{\Lambda}(L_1+L_2)\coth(\sqrt{\Lambda}T)\right) I_1\left(2\frac{\sqrt{\Lambda L_1 L_2}}{\sinh(\sqrt{\Lambda}T)}\right) \quad (2.15)$$

2.1.6 The Hamiltonian

In the continuum limit, we expect that the Hilbert space is the set of wavefunctions $\psi(L)$ where L is the length of the spatial slices. So we expect that there exists a Hamiltonian H such that $\tilde{G}^s(\Lambda, L_1, L_2; T) = \langle L_2 | e^{-HT} | L_1 \rangle$, in which case $\partial_T \tilde{G}^s(\Lambda, L_1, L_2; T) = -H \tilde{G}^s(\Lambda, L_1, L_2; T)$. We will now find that there is indeed such a Hamiltonian.

Using (2.10), (2.11) in (2.7), we find

$$G^s(\Lambda, X, Y; T) = \partial_Y \left(\frac{-1}{X - F(T, Y)}\right). \quad (2.16)$$

Differentiating (2.16)

$$\partial_T G^s(\Lambda, X, Y, T) = \partial_Y \left(\frac{-\partial_T F(T,Y)}{(X - F(T,Y))^2} \right) = \partial_Y \left(\frac{\partial_T F(T,Y)}{\partial_Y F(T,Y)} G^s(\Lambda, X, Y; T) \right). \tag{2.17}$$

It can be shown that $F(T, Y)$ satisfies the following differential equation

$$\partial_T F - F^2 + \Lambda = 0,$$

with initial condition $F(0, Y) = -Y$, and the following composition rule

$$F(T, -F(T', Y)) = F(T + T', Y);$$

from which it follows that

$$\frac{\partial_T F(Y,T)}{\partial_Y F(Y;T)} = -\partial_T F(Y,T)|_{T=0} = \Lambda - Y^2.$$

From (2.17), we then get

$$\partial_T G^s(\Lambda, X, Y, T) = \partial_Y \left(\left(\Lambda - Y^2 \right) G^s(\Lambda, X, Y; T) \right). \tag{2.18}$$

Substituting (2.14) into (2.18) and integrating by parts shows that

$$H_{CDT} = -L \frac{\partial^2}{\partial L^2} + L\Lambda. \tag{2.19}$$

In [27], the authors showed that the Hamiltonian in Hořava-Lifshitz gravity is the same as H_{CDT}. Therefore, the scaling limit of CDT is H-L gravity.

The appropriate measure on the Hilbert space is $L^{-1}dL$, in which case (2.19) is self-adjoint. Consider now the large T limit of $\tilde{G}^s(\cdot)$, (2.15):

$$\tilde{G}^s(\Lambda, L_1, L_2; T \to \infty) = 4\Lambda L_1 L_2 \exp(-2T\Lambda^{\frac{1}{2}}) \exp(-\Lambda^{\frac{1}{2}}(L_1 + L_2)) + h.o.t.. \tag{2.20}$$

Since $\tilde{G}^s$ can be expressed as $\langle L_2 | e^{-H_{CDT}T} | L_1 \rangle$, we expect that in the large T limit, it projects onto the lowest energy eigenstate $H_{CDT}\psi_0(L) = 0 \implies \psi_0(L) = \exp(-\Lambda^{\frac{1}{2}}L)$. However, this doesn't happen because ψ_0 is not normalizable with the measure $L^{-1}dL$ and so doesn't contribute. Instead, $\tilde{G}^s$ projects onto the first excited state $H_{CDT}\psi_1(L) = 2\Lambda^{\frac{1}{2}}\psi_1(L) \implies \psi_1(L) = L\, e^{-\Lambda^{\frac{1}{2}}L}$, giving (2.20). The significance of ψ_0, however, is that it is the solution to the 'Wheeler-DeWitt equation': $H\psi = 0$, which determines the space of physical states in gravity.

2.1.7 Matter and the Hard-Dimer Model

CDT, as discussed so far, has been a discretization of QG with no matter fields. Discrete degrees of freedom can be coupled to CDT to imitate the coupling to matter – for instance, the Ising model on CDT [28], which is an unsolved problem. In contrast, the Hard-Dimer model on CDT (aka CDT+HD) is solvable and non-trivial.

The ensemble in CDT+HD consists of the set of hard-dimer configurations on causal triangulations. As shown in Fig. 2.5, a hard-dimer configuration consists of short rods (aka dimers), each lying across an edge of the triangulation (such an edge is said to be dual to a dimer), such that no two dimers are dual to edges of the same triangle. This last condition is called the 'hard-dimer rule'. This condition

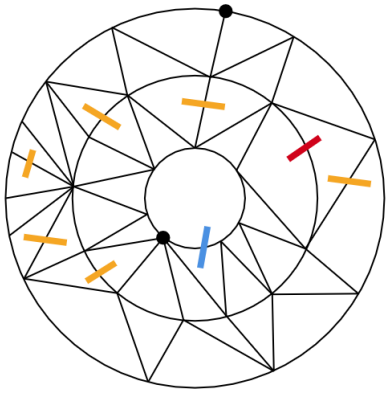

Figure 2.5: An allowed configuration of dimers is shown in orange. The red dimer is forbidden by the hard-dimer rule, and the blue dimer is forbidden by the boundary condition.

causes the dimers to interact with each other and the underlying geometry. The dimer configurations are subject to the boundary condition that there are no dimers dual to boundary edges (i.e. edges that lie in $\partial_1 T$ or $\partial_2 T$). A list of all instances of occurrence of a dimer on a causal triangulation is shown in Fig. 2.6. Each

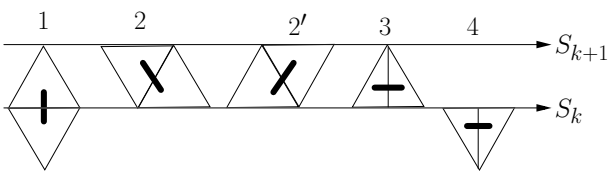

Figure 2.6: The types of dimers. The clockwise direction is indicated by the arrow.

dimer of type i is assigned a fugacity ξ_i. The partition function is defined as the sum over all triangulations, and dimer configurations, weighted by the triangle and dimer fugacities. We will define the relevant observables and solve this model in Chapter 3. We expect that the scaling limit of such a model gives a theory of some CFT coupled to Hořava-Lifshitz gravity.

2.2 Solitons

In this section, we will review solitons and the method of collective coordinate quantization. In a theory with some set of scalar fields $\vec{\phi}(x)$ and their conjugate momenta $\vec{\pi}(x)$, a soliton is initial data $\vec{\phi}(\boldsymbol{x})$ and $\vec{\pi}(\boldsymbol{x})$ such that the energy $H(\vec{\pi}, \vec{\phi})$ is finite, and the fields are non-dissipative [17] (Sec. 6.1): $\lim_{t\to\infty} \max_{\boldsymbol{x}} \mathcal{H}(t, \boldsymbol{x}) \neq 0$, where $\mathcal{H}$ is the energy density. Since they have finite energy, solitons are interpreted as particles. Scalar solitons in 4 dimensions were found by [29]. Solitons in 2 dimensions are well known: there is the kink in the ϕ^4 model [30] and the sine-Gordon soliton [17].

2.2.1 ϕ_2^4 model

We will deal in this section with the purely classical aspects of the ϕ_2^4 model. It is a theory of one real scalar field ϕ in 1+1 dimensions. The Lagrangian is [31]

$$\mathcal{L} = \frac{1}{2}(\partial_\mu \phi)^2 - \frac{1}{4\lambda^2}\phi^4 + \frac{1}{2}m^2\phi^2 - \frac{m^4\lambda^2}{4};$$

with $m^2 > 0$, the potential is a Mexican hat with two absolute minima of zero at $\phi = \pm\lambda m$. However, what we will do is to set $m = 1$ and work instead with the Lagrangian [30]

$$\mathcal{L} = \frac{1}{2}(\partial_\mu \phi)^2 - \frac{1}{4\lambda^2}\phi^4 + \frac{1}{2}\phi^2 - \frac{\lambda^2}{4}.$$

At any point it will be easy to restore factors of m using the fact that the mass dimensions of ϕ and λ are 0 and -1 resp.. The equation of motion (EOM) which follows is

$$\Box\phi + \lambda^{-2}\phi^3 - \phi = 0. \tag{2.21}$$

This admits a static soliton solution:

$$\phi_{cl}(x) = \lambda \tanh(x/\sqrt{2}).$$

The solution interpolates from one vacuum value $-\lambda$ at $x = -\infty$ to the other λ at $x = \infty$. The energy of a static solution is $\int dx\ (\phi'^2/2 + V(\phi))$ (where

$V = \phi^4/(4\lambda^2) - \phi^2/2 + \lambda^4/4)$. However, there is a virial relation[3][32] that ensures that $\int dx\ V = \int dx\ \phi'^2/2$. Therefore the energy is $\int dx\ \phi'^2$. This gives us the classical mass of the soliton:

$$M_0 = 2\sqrt{2}\lambda^2/3. \tag{2.22}$$

We also have

$$\int_{\infty}^{\infty} dx\, \phi'_{cl}(x)\phi_{cl}(x) = \phi_{cl}^2\Big|_{-\infty}^{\infty} = 0. \tag{2.23}$$

To establish the spectrum of perturbations, we expand around ϕ_{cl}: $\phi = \phi_{cl} + \Psi$. Using this in the EOM (2.21), the perturbation satisfies

$$\Box\Psi + \left(3\tanh^2\left(x/\sqrt{2}\right) - 1\right)\Psi = 0, \tag{2.24}$$

to linear order. The time dependence of Ψ is easy to solve for: $\Psi(t,x) = \exp(i\omega t)\psi(x)$. Then (2.24) becomes the Schrödinger equation

$$\psi'' + \left(\omega^2 + 1 - 3\tanh^2\left(x/\sqrt{2}\right)\right)\psi = 0.$$

If ω^2 is the 'energy' of this Schrödinger equation, then the potential is $3\tanh^2(x/\sqrt{2}) - 1$, which is plotted in Fig. 2.7. There exist two discrete eigenvalues

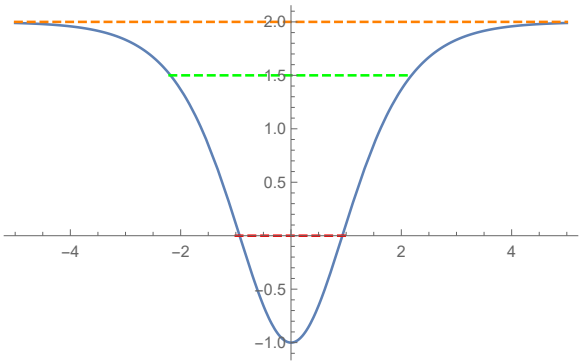

Figure 2.7: A plot of $(3\tanh^2(x/\sqrt{2}) - 1)$. Above the orange line there exist a continuum of scattering states. At the green and red line there exist bound states.

$\omega^2 = 0$ and $\omega^2 = 3/2$. Then there exist a continuum of eigenvalues $\omega^2 > 2$

[3]This follows from considering the dilatation $x \to \lambda x$ and using the fact that the energy is an extremum against variations in ϕ (in this case $\phi(x) \to \phi(\lambda x)$).

corresponding to modes which behave as free waves at $x = \pm\infty$. The normalized eigenfunctions are

$$\begin{aligned}
\psi_b &= \frac{\phi'_{cl}}{\sqrt{M_0}} \qquad \omega_b = 0, \\
\psi_a &= \sqrt{\frac{3}{2\sqrt{2}}}\frac{\sinh(x/\sqrt{2})}{\cosh^2(x/\sqrt{2})} \qquad \omega_a = \sqrt{3/2}, \\
\psi_k &= N_k^{-1}\exp(ikx)\left(3\tanh^2(x/\sqrt{2}) - 3\sqrt{2}ik\tanh(x/\sqrt{2}) - 1 - 2k^2\right), \\
\omega_k &= \sqrt{k^2+2},
\end{aligned}$$

where $k \in \mathbb{R}$ and N_k is a normalization factor. Note that $\psi_k^* = \psi_{-k}$. The asymptotic behaviour of ψ_k is

$$\psi_k = c\ \exp\left(ikx \pm i\arctan\left(\frac{3k}{\sqrt{2}-\sqrt{2}k^2}\right)\right), \quad x \to \mp\infty,$$

where c is a constant. We will now put the system in a large box of size L and require periodicity of the wavefunction $\psi(-L/2) = \psi(L/2)$. ψ_a and ψ_b are periodic as they stand. The condition of periodicity on $\psi_k(x)$ requires $e^{ikL+i\delta(k)} = 1$, where

$$\delta(k) := -2\left(\arctan\left(\sqrt{2}k\right) + \arctan\left(\frac{k}{\sqrt{2}}\right)\right).$$

This means that the allowed momenta k are discrete:

$$\begin{aligned}
k_m &= q_m - \delta(k_m)/L \\
&= q_m - \delta(q_m)/L + \mathcal{O}(L^{-2}),
\end{aligned} \tag{2.25}$$

where $q_m = 2\pi m/L$ and $m \in \mathbb{Z}$. We will denote ψ_{k_m} as ψ_m henceforth. Let us define the set $\mathcal{S} = \{b, a, \mathbb{Z}\}$. The set $\{\psi_n\}_{n\in\mathcal{S}}$ is complete and orthonormal and we will denote their eigenvalues as $\omega_{n\in\mathcal{S}}$.

We record a useful fact: for $m \in \mathbb{Z}$ we have

$$\psi_m(x)\psi_m^*(x') = \frac{e^{ik_m(x-x')}}{L}\left(1 + \frac{\sum_{l=0}^{3} k_m^l\, A_l(x,x')}{2(k_m^2+2)(2k_m^2+1)}\right) + \mathcal{O}(L^{-2}), \tag{2.26}$$

where

$$A_3(x,x') = 6i\sqrt{2}(\tau - \tau'), \tag{2.27}$$

$$A_2(x,x') = -6\tau^2 - 6\tau'^2 + 18\tau\tau' - 6, \tag{2.28}$$

$$A_1(x,x') = 3i\sqrt{2}(\tau - \tau')(3\tau\tau' + 1), \tag{2.29}$$

$$A_0(x,x') = (3\tau^2 - 1)(3\tau'^2 - 1) - 4, \tag{2.30}$$

with $\tau \equiv \tanh(x/\sqrt{2})$ and $\tau' \equiv \tanh(x'/\sqrt{2})$.

2.2.2 A Change of Variables in Quantum Mechanics

Let there be a quantum system with (an infinite number of) coordinates $\vec{q} = (q_1, q_2, ...)$. Let us consider a bijection $\vec{q} \to \vec{Q}(\vec{q})$ to new variables $\vec{Q} = (Q_1, Q_2, ...)$. We will define the Jacobian of this transformation as $J_{nm} = \partial Q_n / \partial q_m$. Note that the Jacobian is just a function of the coordinates so it commutes with $\vec{q}$ or $\vec{Q}$.

The inner product transforms as

$$\langle \psi_2 | \psi_1 \rangle = \int d\vec{q}\ \psi_2^*(\vec{q})\, \psi_1(\vec{q}) = \int d\vec{Q}\ J^{-1}\, \psi_2^*(\vec{q}(\vec{Q}))\, \psi_1(\vec{q}(\vec{Q})), \tag{2.31}$$

where $J = \det J_{nm}$, $d\vec{q} \equiv \prod_n dq_n$ and $d\vec{Q} \equiv \prod_n dQ_n$. Therefore states represented in terms of $\vec{Q}$ have an additional factor in the inner product. The would-be momentum operator $-i\partial/\partial Q_n$ is not Hermitian with this inner product. The fix for this is to define the momentum operator as $P_n := J^{1/2}(-i)\frac{\partial}{\partial Q_n} J^{-1/2}$ [10]. This is Hermitian:

$$\begin{aligned} &\int d\vec{Q}\ J^{-1}\, \psi_2^*(\vec{Q})\, J^{1/2}(-i)\frac{\partial J^{-1/2} \psi_1(\vec{Q})}{\partial Q_n} \\ &= \int d\vec{Q}\ J^{-1} \left(J^{1/2}(-i)\frac{\partial J^{-1/2}\, \psi_2(\vec{Q})}{\partial Q_n} \right)^* \psi_1(\vec{Q}). \end{aligned}$$

Note that the standard commutation relations $i[P_n, Q_m] = \delta_{nm}$ hold as a result of $i[p_n, q_m] = \delta_{nm}$ because $\vec{Q}$ commutes with J.

It is easy to show that $J = (\det g_{nm})^{-1/2}$ where

$$g_{nm} = \sum_l \frac{\partial q_l}{\partial Q_n} \frac{\partial q_l}{\partial Q_m}. \tag{2.32}$$

We will use this later in computing J for a specific theory.

The wavefunction in the $\vec{Q}$ basis is defined, as usual, as $\psi(\vec{Q}) = \langle \vec{Q} | \psi \rangle$. (2.31) then implies that the completeness relation is $1 = \int d\vec{Q}\ J^{-1} |\vec{Q}\rangle \langle \vec{Q}|$, which in turn implies that

$$\langle \vec{Q}_1 | \vec{Q}_2 \rangle = J\, \delta(\vec{Q}_1 - \vec{Q}_2).$$

Also, since the momentum eigenstates satisfy $\langle \vec{Q} | \vec{P} \rangle = J^{1/2} \exp(i\vec{P} \cdot \vec{Q})$, the completeness relation for the momentum eigenstates is $1 = \int d\vec{P}\, |\vec{P}\rangle \langle \vec{P}|$.

2.2.3 Collective-Coordinate Quantization

This section concerns the quantum aspects of solitons in the ϕ_2^4 model. The method we will discuss can be applied more generally however. The method goes by the name of collective coordinate quantization [10]. It consists of a change of variables from the usual field variables, to a soliton position variable and a perturbation field around the soliton. It is intended as a means to calculate transition amplitudes in which there is one soliton in the initial and final states.

We will refer to spatial positions as x and the position two-vector as x^μ. Recall that the configuration space of the theory is coordinatized by $\phi(x)$. We will now change variables $\beta : \phi(x) \to (X, \vec{a})$, where $\vec{a} \equiv (a_1, a_2, ...)$ stands for an infinite set of numbers. The domain of these variables is $a_n \in \mathbb{R}$ and $X \in \mathbb{R}$.

In the last section, we had the orthonormal set of functions $\{\psi_n\}_{n\in\mathcal{S}}$. In this section we will need their real counterparts. So we will form the set $\{\psi_b, \psi_a, \sqrt{2}\,\mathrm{Re}(\psi_m), \sqrt{2}\,\mathrm{Im}(\psi_m)\}$ (where $m \geq 0$) and define this as the set $\{\Psi_n\}_{n=0}^\infty$. We will let $\Psi_0 = \psi_b$. The wavefunctions $\{\Psi_n\}$ are complete, orthonormal and real. Their eigenvalues under $-\partial_x^2 + 3\tanh^2(x/\sqrt{2}) - 1$ will be called Ω_n^2.

Let us define the projection of ϕ onto the modes as follows

$$Q[\phi] := \int_{-\infty}^{\infty} M_0^{-1/2} \phi'_{cl}(x)\phi(x)\,dx,$$
$$Q_n[\phi] := \int_{-\infty}^{\infty} \Psi_n(x)\phi(x)\,dx, \qquad \text{for } n \geq 1.$$

Let $\phi_y(x) := \phi(x + y)$. Now, $X(\phi)$ is defined as the zero of $Q[\phi_y]$ in the y domain:

$$\int_{-\infty}^{\infty} \phi'_{cl}(x)\phi(x + X(\phi))\,dx = 0. \tag{2.33}$$

This is designed to extract the soliton position. For example, let $\phi(x) = \phi_{cl}(x - x_0)$ (this is the configuration of a soliton at x_0) then $Q[\phi_y] = \int \phi'_{cl}(x)\phi_{cl}(x + y - x_0)dx$ has a zero at $y = x_0$ because of (2.23). There is no proof that $Q[\phi_y]$ only has one such zero for each ϕ, but this is a global issue which will not be important when we work in perturbation theory [33] (pp. 36). We will define a_n by

$$a_n = Q_n[\phi_{X(\phi)} - \phi_{cl}].$$

This establishes the map β. We will now define

$$\chi(x) \equiv \sum_{n=1}^{\infty} a_n \Psi_n(x) = \phi_{X(\phi)}(x) - \phi_{cl}(x), \tag{2.34}$$

where the second equality follows because $Q[\phi_{X(\phi)} - \phi_{cl}] = Q[\phi_{X(\phi)}] = 0$ by definition. Recall that a change of variables should be a bijection. To show that β is injective, we just have to note that the inverse (from (2.34)) is

$$\phi(x) = \phi_{cl}(x - X) + \chi(x - X). \tag{2.35}$$

It is easy to see that the map is surjective. This completes the change of variables $\phi \rightarrow (X, \vec{a})$.

We will now express the Hamiltonian $H(\phi, \pi)$ in the new variables. First, ϕ can be straightforwardly substituted using (2.35). To re-express $\pi(x)$ we will have to use the chain rule. Recall that $\pi(x) \equiv -i\partial/\partial\phi(x)$. Now

$$\frac{\partial}{\partial\phi(x)} = \frac{\partial X}{\partial\phi(x)}\frac{\partial}{\partial X} + \sum_{n=1}^{\infty} \frac{\partial a_n}{\partial\phi(x)}\frac{\partial}{\partial a_n}. \tag{2.36}$$

Following the discussion in §2.2.2 we define $P = -iJ^{1/2}\partial_X J^{-1/2}$ and $\vec{p} = -iJ^{1/2}\partial_{\vec{a}} J^{-1/2}$. Let us also define

$$\bar{\pi}(x) = \sum_{n=1}^{\infty} \Psi_n(x) p_n. \tag{2.37}$$

Then

$$-i\sum_{n=1}^{\infty} \frac{\partial a_n}{\partial\phi(x)}\frac{\partial}{\partial a_n} = J^{-1/2}\int dy \frac{\partial\chi(y)}{\partial\phi(x)}\bar{\pi}(y)J^{1/2}. \tag{2.38}$$

From (2.34),

$$\frac{\partial\chi(y)}{\partial\phi(x)} = \delta(y + X - x) + \frac{\partial X}{\partial\phi(x)}(\chi'(y) + \phi'_{cl}(y)). \tag{2.39}$$

To compute $\partial X/\partial\phi(x)$, we take the functional derivative of (2.33) w.r.t. $\phi(x)$:

$$\begin{aligned} &\phi'_{cl}(x - X) + \frac{\partial X}{\partial\phi(x)}\int_{-\infty}^{\infty} \phi'_{cl}(y)\phi'(y + X)\, dy = 0 \\ \implies &\frac{\partial X}{\partial\phi(x)} = -\frac{\phi'_{cl}(x - X)}{\int \phi'_{cl}(y)(\chi'(y) + \phi'_{cl}(y))dy}. \end{aligned} \tag{2.40}$$

Then putting (2.40), (2.39), (2.38) in (2.36) we have

$$\pi(x) = J^{-1/2}\left(\bar{\pi}(x-X) - \frac{\phi'_{cl}(x-X)}{\int \phi'_{cl}(y)(\chi'(y)+\phi'_{cl}(y))dy}\left(P + \int \chi'(y)\bar{\pi}(y)dy\right)\right)J^{1/2}. \tag{2.41}$$

Note that $\bar{\pi}$ and χ (defined by (2.37) and (2.34)) satisfy constraints

$$Q[\bar{\pi}] = Q[\chi] = 0. \tag{2.42}$$

We also note that because $[p_n, a_n] = -i$, that

$$i[\bar{\pi}(x), \chi(y)] = \delta(x-y) - \frac{\phi'_{cl}(x)\phi'_{cl}(y)}{M_0}.$$

This follows from the completeness relation $M_0^{-1}\phi'_{cl}(x)\phi'_{cl}(y) + \sum_{n=1}^{\infty}\Psi_n(x)\Psi_n(y) = \delta(x-y)$. Note also that $[P, X] = -i$.

To compute the Jacobian in (2.41), we use (2.32). First we define the matrix $g_{..}$ as

$$\begin{aligned} g_{00} &= \int dx \frac{\partial\phi(x)}{\partial X}\frac{\partial\phi(x)}{\partial X} = \int dx\,(\phi'_{cl}(x)+\chi'(x))^2\,, \\ g_{n0} = g_{0n} &= \int dx \frac{\partial\phi(x)}{\partial X}\frac{\partial\phi(x)}{\partial a_n} = -\int dx\ \Psi_n(x)\chi'(x) \qquad n \geq 1, \\ g_{nm} &= \int dx \frac{\partial\phi(x)}{\partial a_n}\frac{\partial\phi(x)}{\partial a_m} = \delta_{nm} \qquad n, m \geq 1. \end{aligned}$$

The determinant is $\det g = g_{00} - \sum_{n=1}^{\infty} g_{0n}^2$. This gives

$$J = (\det g)^{-1/2} = \frac{\sqrt{M_0}}{\int dx(\phi'_{cl}+\chi')\phi'_{cl}}.$$

Using this result in (2.41), and by a series of commutations, we finally arrive at[4]

$$\pi(x) = \bar{\pi}(x-X) - \frac{1}{2}\left\{\frac{\phi'_{cl}(x-X)}{\int \phi'_{cl}(\chi'+\phi'_{cl})}, P + \int \chi'\bar{\pi}\right\}, \tag{2.43}$$

where $\{,\}$ denotes the anti-commutator. The dual Hamiltonian is simply gotten by substituting π and ϕ from (2.43) and (2.35) respectively, into $H(\phi,\pi)$. We will abuse notation by denoting the dual Hamiltonian $H(X,\chi,P,\bar{\pi})$ with the same symbol. Abusing notation again, we will also write $H(X,\vec{a},P,\vec{p})$ for the Hamiltonian expressed in the variables $P,\vec{p},X,\vec{a}$.

[4]It should be noted that $\int \chi'\bar{\pi} = \int \bar{\pi}\chi'$, and hence that the following formula matches that from [34].

2.2.4 The Path Integral

Ordering Convention

The transition from the operator formalism to the path integral involves some convention for the ordering of operators. For example, there is the convention of 'Weyl-ordering', which results in the so-called midpoint path-integral [10]. There is also the simpler 'left-right' ordering used by [6] (Sec. 9.1). We will utilise the latter convention. Let us briefly describe what it is. Recall from §2.2.2 that our theory has coordinate operators $\vec{Q}$, momentum operators $\vec{P}$, and the inner product (2.31). Consider a matrix element $\langle\psi_{out}|\, e^{-HT} O e^{-HT}\, |\psi_{in}\rangle$. Our convention will be that $H(\vec{Q},\vec{P})$ is ordered (by appropriate commutations) such that $\vec{Q}$ is to the left of $\vec{P}$. The operator $O \equiv O(\vec{P},\vec{Q})$ (where $\vec{P}$, $\vec{Q}$ live at time zero) is to be ordered such that $\vec{P}$ is to the left of $\vec{Q}$. Now by a series of insertions of $1 = \int J^{-1} d\vec{Q}\, |\vec{Q}\rangle\, \langle\vec{Q}|$ and $1 = \int d\vec{P}\, |\vec{P}\rangle\, \langle\vec{P}|$, and by using $\langle\vec{Q}|\vec{P}\rangle = J^{1/2} \exp(i\vec{P}\cdot\vec{Q})$, we obtain

$$\begin{aligned}
&\langle\psi_{out}|\, e^{-HT} O e^{-HT}\, |\psi_{in}\rangle \\
&= \lim_{N\to\infty} \int \prod_{k=-N}^{k=N} d\vec{Q}_k \prod_{k=-N}^{N-1} d\vec{P}_k \;\; \psi^*_{out}(\vec{Q}_N)\; \psi_{in}(\vec{Q}_{-N}) \\
&\quad \times O(\vec{P}_0,\vec{Q}_0)\, \exp \sum_{k=-N+1}^{N} \Big(i(\vec{Q}_k - \vec{Q}_{k-1})\cdot\vec{P}_{k-1} - H(\vec{Q}_k,\vec{P}_{k-1})\; T/N \Big)\,,
\end{aligned}$$

where $\vec{Q}_k \equiv \vec{Q}(kT/N)$, $\vec{P}_k \equiv \vec{P}(kT/N)$ and $\psi_{in/out}(\vec{Q}) = \langle\vec{Q}|\psi_{in/out}\rangle\, /\sqrt{J}$.

Soliton Path Integral

In what follows, we will assume that operators are ordered as described above. Now $|X,\vec{a}\rangle$ and $|P,\vec{p}\rangle$ are each a complete set of states for the Hilbert space. Following the steps from before, the matrix element $M = \langle\psi_{out}|\, e^{-HT} O(X,\vec{a},P,\vec{p}) e^{-HT}\, |\psi_{in}\rangle$ (where the arguments of O all live at time zero) becomes

$$\begin{aligned}
M = \int DX(t) D\vec{a}(t) DP(t) D\vec{p}(t)\;\; &\psi_{in}\left(X(-T),\vec{a}(-T)\right) \psi^*_{out}\left(X(T),\vec{a}(T)\right) \\
&O\left(P(0),\vec{p}(0),X(0),\vec{a}(0)\right) \exp \int_{-T}^{T} dt \left(iP\dot{X} + i\vec{p}\cdot\dot{\vec{a}} - H(X,\vec{a},P,\vec{p}) \right) \quad (2.44)
\end{aligned}$$

It will be more useful to use the variables $\chi(t,x)$, $\bar{\pi}(t,x)$. So (2.44) becomes

$$M = \int DXD\chi DPD\bar{\pi}\ \psi_{in}\left(X,\chi\right)\psi^{*}_{out}\left(X,\chi\right)\delta\left(Q[\chi]\right)\delta\left(Q[\bar{\pi}]\right)$$
$$O(P,\bar{\pi},X,\chi)\exp\int_{-T}^{T}dt\left(iP\dot{X}+i\int dx(\bar{\pi}\dot{\chi})-H(X,\chi,P,\bar{\pi})\right), \quad (2.45)$$

where we've left all the time arguments implicit. The delta-functions arise due to (2.42). We will in fact leave the delta-functions implicit from now on – they are always implied because χ and $\bar{\pi}$ are defined by (2.34) and (2.37) anyway.

2.3 Quantum Random Walks

A discrete-time Quantum Random Walk (QRW) on L is a model of the unitary dynamics of a particle, in discrete time ($t \in \{0, 1, 2, ...\}$), on a spatial lattice L. There is a fixed unitary operator U generating time translations: $t \to t + 1$. U is chosen to make the particle transition between neighbouring sites of the lattice. Therefore matrix elements of U^n can be expressed, in the path integral formulation, as a sum over paths, in discrete time, in which each step connects neighbouring sites. Therefore, these models are referred to as QRWs. The difference with the classical random walk (CRW) is that the CRW has a transition matrix with strictly positive entries and which isn't necessarily unitary.

In the theory of QRWs, the main object of study are matrix elements of U^n. There are several methods to compute U^n: the Fourier method [35], generating functions method [36], CMV method [37] and path counting [38] are some of these. See [39, 40] for work on the asymptotics of U^n for n large. The study of U^n is closely related to the spectrum of U; see [41] for a discussion of the relation between the spectral properties of U and the so called 'recurrence criterion' for walks and [42] for the connection with the phenomenon of 'localization'; see [43] for a mathematical discussion of the spectrum of U without any specific construction of U from a physical model. There have also been studies of QRWs on different lattices like $\mathbb{Z}^d$ [44] and the uniformly branching tree [45, 46].

QRWs exhibit ballistic spreading, i.e. the probability density $|\psi(t)|^2$ spreads-out at a rate linear in time, as opposed to CRWs which have diffusive spreading: $\sim \sqrt{t}$. Therefore, quantum search algorithms using QRWs offer a quadratic speed-up with respect to their classical counterparts [5, 47]. The 1D QRW has also been engineered in the lab [48].

The QRW on $\mathbb{Z}^+$ is a simple, solvable example which we will now review. Many of the statements we will make though are true for any unitary evolution operator U.

2.3.1 QRW on the half-line

(For a complex number z, the conjugate will be denoted by either z^* or $\bar{z}$.) As shown in Fig 2.8, the discrete half-line is defined as $\mathbb{H} = \{\text{root}\} \cup \mathbb{Z}^+$ (where $\mathbb{Z}^+ = \{1, 2, 3, ...\}$). We will write $v' > v$ if lattice site v' is further from the root

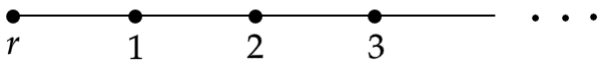

Figure 2.8: $\mathbb{H}$.

than site v. Also let $d(v', v)$ measure the shortest lattice distance between sites v and v'. The root will be called r henceforth.

The particle is allowed to sit at sites in $\mathbb{H}$. If the particle sits at any site but the root, then it has a spin $i \in \{1, 2\}$; if the particle sits at the root however, it has no spin. We define the configuration space as the collection of these possibilities: $\mathcal{C} = |r\rangle \bigcup_{\substack{n\in\mathbb{Z}^+ \\ i\in\{1,2\}}} |n, i\rangle$. We define these states to be orthonormal: $\langle\psi|\psi'\rangle = 0$ if $|\psi\rangle \neq |\psi'\rangle$ and $\langle\psi|\psi\rangle = 1$ for $|\psi\rangle, |\psi'\rangle \in \mathcal{C}$. The Hilbert space is defined as the L^2 completion of $\mathcal{C}$ over $\mathbb{C}$, i.e. the set of all normalizable superpositions (with complex coefficients) of states in $\mathcal{C}$. On this Hilbert space, we define a unitary operator $U := SC$. S and C are called the coin and shift operators respectively. We define them by their action on $\mathcal{C}$:

$$
\begin{aligned}
C|r\rangle &= |r\rangle, \\
C|n, i\rangle &= \sum_{j=1}^{2} c_{ij} |n, j\rangle; \\
S|r\rangle &= |1, 1\rangle, \\
S|1, 2\rangle &= |r\rangle, \\
S|n, 1\rangle &= |n + 1, 1\rangle \qquad \forall\, n \in \mathbb{Z}^+, \\
S|n, 2\rangle &= |n - 1, 2\rangle \qquad \forall\, n \in \mathbb{Z}^+ \setminus \{1\},
\end{aligned}
$$

where c_{ij} is a unitary 2×2 matrix called the 'coin-matrix'. A simple computation shows that S and C are unitary. Observe that U connects only neighbouring sites in one time step.

2.3.2 Generating Functions

As stated earlier, U is the time translation operator: $|\psi(t)\rangle = U^t |\psi\rangle$. To study the dynamics of the particle, consider the matrix element $\mu_t = \langle r| U^t |r\rangle$. It is convenient to define a generating function

$$\mu(z) = \sum_{t=0}^{\infty} z^t \mu_t = \langle r| (1 - zU)^{-1} |r\rangle .$$

This is called the return generating function. μ_t can be recovered from $\mu(z)$ via $\mu_t = (2\pi i)^{-1} \int_\gamma \mu(z) z^{-t-1} dz$ where γ is a small loop circling $z = 0$.

There is a related quantity called the first return generating function (for reasons we will explain shortly) $Q(z)$ which is defined as

$$Q(z) = \langle r| zU(1 - z\tilde{U})^{-1} |r\rangle = \sum_{t=1}^{\infty} z^t \langle r| U\tilde{U}^{t-1} |r\rangle \equiv \sum_{t=1}^{\infty} z^t Q_t, \tag{2.46}$$

where $\tilde{U} := (1 - |r\rangle \langle r|)U$. $\tilde{U}$ evolves the system according to U and then subtracts the projection onto the root state. There is a simple relation between the two: $\mu(z) = (1 - Q(z))^{-1}$ which can be proved as follows [41]:

$$\begin{aligned}
\mu(z)Q(z) &= \langle r| \frac{1}{1 - zU} |r\rangle \langle r| zU \frac{1}{1 - z\tilde{U}} |r\rangle \\
&= \langle r| \frac{1}{1 - zU} (1 - \tilde{U}U^{-1}) zU \frac{1}{1 - z\tilde{U}} |r\rangle \\
&= \langle r| \left(\frac{1}{1 - zU} - 1 \right) \frac{1}{1 - z\tilde{U}} - \frac{1}{1 - zU} \left(\frac{1}{1 - z\tilde{U}} - 1 \right) |r\rangle \\
&= \mu(z) - 1,
\end{aligned}$$

where we've used the fact that $\langle r| (1 - z\tilde{U}) |r\rangle = 1$.

We can write $Q_t = \langle r| U\tilde{U}^{t-1} |r\rangle$ as a sum over walks by inserting $1 = \sum_{\psi \in \mathcal{C}} |\psi\rangle \langle\psi|$ repeatedly between the $\tilde{U}$'s. For example

$$\begin{aligned}
Q_4 = \langle r| U\tilde{U}^3 |r\rangle &= \sum_{|\psi_{1,2,3}\rangle \in \mathcal{C}} \langle r| U |\psi_3\rangle \langle\psi_3| \tilde{U} |\psi_2\rangle \langle\psi_2| \tilde{U} |\psi_1\rangle \langle\psi_1| \tilde{U} |r\rangle \\
&= \langle r| U |1, 2\rangle \langle 1, 2| \tilde{U} |2, 1\rangle \langle 2, 1| \tilde{U} |1, 1\rangle \langle 1, 1| \tilde{U} |r\rangle \\
&= c_{22} c_{12} c_{11}.
\end{aligned}$$

In general we have

$$Q_n = \sum_{\substack{|\psi_{0,\ldots,n}\rangle \in \mathcal{C} \\ s.t. |\psi_0\rangle = |\psi_n\rangle = |r\rangle}} \langle\psi_n| U |\psi_{n-1}\rangle \prod_{i=1}^{n-1} \langle\psi_i| \tilde{U} |\psi_{i-1}\rangle . \tag{2.47}$$

Now, $\{|\psi_i\rangle\}_{i=0}^n$ can be thought of as the particle history. The histories contributing in (2.47) are such that $|\psi_0\rangle = |\psi_n\rangle = |r\rangle$ and $|\psi_i\rangle \neq |r\rangle$ for $0 < i < n$ since $\langle r| \tilde{U} |\psi\rangle = 0$ for any $|\psi\rangle \in \mathcal{C}$. In these histories, the particle starts at the root and doesn't return to the root till its last step. Hence these are referred to as first return walks. Therefore (2.47) can be written as

$$Q_t = \sum_{w \in \mathcal{L}_t(r)} P(w), \tag{2.48}$$

where $\mathcal{L}_t(r)$ is the set of first-return walks of length t, and $P(w)$ is the amplitude of walk w, both of which we will shortly define. Formally, a walk of length t is defined as a function $w(\tau)$ mapping integer times $\tau \in [0, t]$ to points on the lattice such that $d(w(\tau), w(\tau + 1)) = 1$ for all τ. We will write $|w|$ as shorthand for the length of a walk w.

We define T, the 'translation operator', that maps a walk w to a walk $w' = T(w)$ defined as $w'(\tau) = w(\tau) + 1$ for all $0 \leq \tau \leq |w|$, where $w(\tau) + 1$ is the unique vertex at distance $d(r, w(\tau)) + 1$ from the root.

$\mathcal{L}_t(r)$ is defined as those paths, w, s.t. $w(0) = w(t) =$ root and $w(\tau) \neq$ root when $0 < \tau < t$. Clearly $\mathcal{L}_t(r)$ only exists for t even. $P(w)$ is the product of the amplitudes of each step of the walk except the first:

$$P(w) = \prod_{t=1}^{|w|-1} p(w(t) \to w(t+1)),$$

where $p(w(t) \to w(t+1)) = 1$ if $w(t) = r$, otherwise $p(w(t) \to w(t+1)) = c_{nm}$ where

$$n = \begin{cases} 1 & w(t-1) < w(t), \\ 2 & w(t-1) > w(t), \end{cases}$$

$$m = \begin{cases} 1 & w(t+1) > w(t), \\ 2 & w(t+1) < w(t). \end{cases}$$

So, what we have is the original matrix element expressed as a sum over paths with an appropriate weighting $P(w)$. We will use this representation to write down an algebraic equation in $Q(z)$.

Define $\mathcal{L}_t(v)$ as the set of walks, w, of length t, s.t. $w(0) = w(t) = v \in \mathbb{H}$ and $w(\tau) > v$ for $0 < \tau < t$. These will be referred to as 'loops based at v'. Also define $\mathcal{L}(v) = \bigcup_{t=2}^{\infty} \mathcal{L}_t(v)$. Now, the set $\mathcal{L}(r)$ can be decomposed as follows:

$$\mathcal{L}(r) = \mathcal{L}_2(r) \bigcup_{n\geq 1} \mathcal{B}_n, \tag{2.49}$$

where $\mathcal{B}_n$ is the set of loops, based at r, in which the particle walks from r to 1, performs n loops based at 1, and then finally walks back to r. Let us define the partition function of $\mathcal{B}_n$ as

$$B_n(z) = \sum_{w\in\mathcal{B}_n} z^{|w|} P(w).$$

Similarly, due to (2.46), (2.48),

$$Q(z) = \sum_{w\in\mathcal{L}(r)} z^{|w|} P(w).$$

(2.49) implies that

$$Q(z) = c_{12}z^2 + \sum_{n=1}^{\infty} B_n. \tag{2.50}$$

For $n \geq 2$, consider a walk in $\mathcal{B}_n$. In this walk, the first loop based at 1 is followed by $n-1$ loops based at 1. The contribution that the first loop based at 1 makes to B_n is equal to $Q(z)$ because the translation operator provides an isomorphism $T : \mathcal{L}(r) \to \mathcal{L}(1)$ and because $P(w \in \mathcal{L}) = P(T(w))$. The contribution of the remaining $n-1$ loops equals $B_{n-1}(z)$ so we have

$$\begin{aligned} B_n(z) &= c_{21}Q(z)B_{n-1}(z) \qquad n \geq 2, \\ B_1(z) &= z^2 c_{11}c_{22}Q(z). \end{aligned}$$

From (2.50) it follows that

$$Q(z) = z^2 c_{12} + \frac{z^2 c_{11}c_{22}Q(z)}{1 - Q(z)c_{21}}. \tag{2.51}$$

So, we get a quadratic equation

$$c_{21}Q^2 + Q(z^2\Pi - 1) + z^2 c_{12} = 0, \tag{2.52}$$

where Π is the determinant of c_{ij}. This equation has the property that if $Q(z)$ is a solution, then $1/(Q(1/z^*))^*$ is also a solution. This follows from $\Pi c_{12}^* = c_{21}$ and $\Pi^* = \Pi^{-1}$ which in turn follow by unitarity of c_{ij}. Therefore, when z is a phase, the two roots of (2.52) are either both phases, or they both have the same phase with reciprocal magnitudes. Due to (2.46) and $Q_2 = c_{12}$, we have $Q(z) = c_{12}z^2 + O(z^4)$ near $z = 0$. This condition singles out one of the roots to (2.52) as the 'physical root'.

Recall that $\mu = \langle r| (1 - zU)^{-1} |r\rangle$. $\mu(z)$ therefore has singularities for those values of z for which $1 - zU$ is non-invertible. In other words, $\mu(z)$ has singularities when z^{-1} lies in the spectrum of U. Since U is unitary, the spectrum is a part of the complex unit circle. What kind of singularities does $\mu(z)$ have? The answer is that it has both poles and branch cuts on the unit circle. Since $\mu = (1 - Q)^{-1}$, μ and Q have the same branch cuts, and poles of μ occur when $Q = 1$. So, from (2.52), $\mu(z)$ has poles when

$$c_{21} + (z^2\Pi - 1) + z^2 c_{12} = 0. \tag{2.53}$$

When z is not a phase, we can show that $\mu(z) + \overline{\mu(\bar{z}^{-1})} = 1$: since z is not a phase, $\mu(z)$ is well-defined, so we can manipulate $(1 - zU)^{-1}$ as a convergent geometric series $\sum_{n=0}^{\infty}(zU)^n$, so

$$\begin{aligned}
\overline{\mu(\bar{z}^{-1})} &= \langle \text{root}| \frac{1}{1 - \bar{z}^{-1}U} |\text{root}\rangle^* \\
&= \langle \text{root}| \frac{1}{1 - z^{-1}U^{-1}} |\text{root}\rangle \\
&= \langle \text{root}| \frac{-zU}{1 - zU} |\text{root}\rangle = 1 - \mu(z),
\end{aligned}$$

where we've used that fact that $A^{\dagger -1} = A^{-1\dagger}$. For this reason, when z is not a phase $\overline{Q(\bar{z}^{-1})}^{-1} = Q(z)$. We also have that $\text{Re}(\mu(z)) > 1/2$ for $|z| < 1$, implying that $|Q(z)| < 1$ for $|z| < 1$. The fact that $\text{Re}(\mu(z)) > 1/2$ for $|z| < 1$ follows from

$$(1 - |z|^2)||(1 - zU)^{-1} |\text{root}\rangle ||^2 = 2\text{Re}(\mu(z)) - 1$$

(where $||a||$ is the Hilbert space norm). This can be shown as follows:

$$\begin{aligned} 2\mathrm{Re}(\mu(z)) - 1 &= \langle \mathrm{root}| \frac{1}{1-zU} + \frac{1}{1-\bar{z}U^{-1}} - 1 \, |\mathrm{root}\rangle \\ &= (1-|z|^2) \langle \mathrm{root}| \frac{1}{(1-zU)(1-\bar{z}U^{-1})} |\mathrm{root}\rangle \\ &= (1-|z|^2) || (1-zU)^{-1} |\mathrm{root}\rangle \, ||^2. \end{aligned}$$

On this basis, when does $Q(z)$ have branch cuts? From the fact that $|Q(z)| < 1$ when $|z| < 1$ and $\overline{Q(\bar{z}^{-1})}^{-1} = Q(z)$ for $|z| \neq 1$, we have that $|Q(z)| > 1$ for $|z| > 1$. Therefore, at those points $z_0 \in \mathbb{T}$ ($\mathbb{T}$ is shorthand for the complex unit circle) s.t $|Q(z_0)| \neq 1$, $Q(z_0 r)$ behaves discontinuously as r (a positive real) passes through $r = 1$: as $r \to 1^-$, $|Q(z_0 r)|$ tends to some number smaller than 1 and as $r \to 1^+$, $|Q(z_0 r)|$ tends to the reciprocal value. Therefore $Q(z)$ has branch cuts in those segments of the unit circle that $|Q(z)| \neq 1$. The behaviour of the roots of (2.52) near a branch point is shown in Fig 2.9. Taking the discriminant

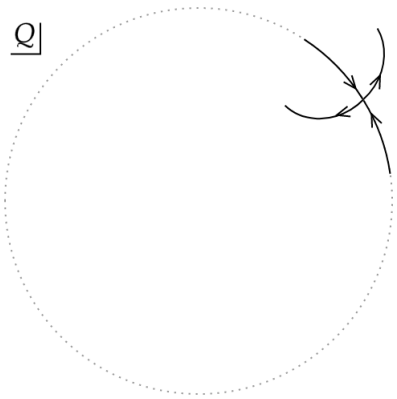

Figure 2.9: The complex Q plane. The dotted circle is the unit circle. The arrows indicate the flow of roots as z varies on the unit circle and passes through a branch point.

of (2.52) gives the location of the branch points:

$$1 - 2(c_{11}c_{22} + c_{12}c_{21})z^2 + \Pi^2 z^4 = 0. \tag{2.54}$$

For a randomly generated coin matrix C_1, the situation is shown in Fig 2.10. We extend the functions $\mu(z)$ and $Q(z)$ onto the branch cuts by setting $Q(z) = \lim_{r\to 1^-} Q(rz)$ and $\mu(z) = \lim_{r\to 1^-} \mu(rz)$ when $|z| = 1$.

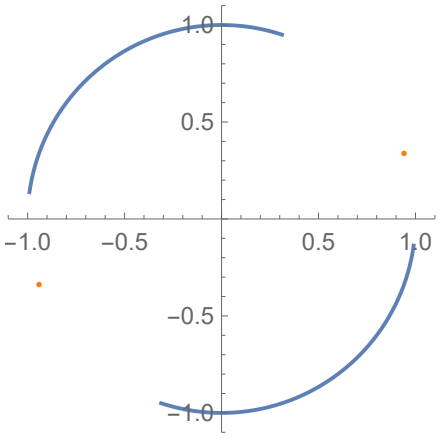

Figure 2.10: In blue and orange are the cuts and poles of $\mu(z)$ respectively.

In §2.3.4 we show that the poles originate from the bound state (aka pure-point) spectrum of U and the branch cuts from the scattering (aka absolutely-continuous (a.c.)) spectrum.

2.3.3 Condensation of Eigenvalues

To get a feeling for how the spectrum arises, we impose an infrared cut-off L on the spatial lattice and study the limit $L \to \infty$ [39]. On the boundary of the lattice we impose reflecting boundary conditions. To be specific, consider the following lattice: $\mathbb{H}_L = \text{root} \cup \{1, 2, ..., L\}$. We define this model so that the particle has no spin when it lies at the root or at L. The truncated configuration space is then $\mathcal{C}_L = |r\rangle \bigcup_{\substack{n\in\{1,..,L-1\}\\ i\in\{1,2\}}} |n,i\rangle \bigcup |L\rangle$. The time-evolution operator is defined as $U_L = S_L C_L$:

$$
\begin{aligned}
C_L\,|n,i\rangle &= \sum_{j=1}^{2} c_{ij}\,|n,j\rangle\,, \\
C_L\,|r\rangle &= |r\rangle\,, \\
C_L\,|L\rangle &= |L\rangle\,; \\
S_L\,|n,1\rangle &= |n+1,1\rangle \qquad \text{for} \;\; 1 \le n \le L-2, \\
S_L\,|n,2\rangle &= |n-1,2\rangle \qquad \text{for} \;\; 2 \le n \le L-1, \\
S_L\,|1,2\rangle &= |r\rangle\,, \\
S_L\,|r\rangle &= |1,1\rangle\,,
\end{aligned}
$$

$$S_L \left|L\right\rangle = \left|L-1,2\right\rangle,$$
$$S_L \left|L-1,1\right\rangle = \left|L\right\rangle.$$

U_L is a unitary operator of dimension $2L$. As $L \to \infty$, $U_L \to U$ in the 'strong operator topology' (i.e. $\lim_{L\to\infty} ||(U-U_L)x|| = 0$, for all x in the Hilbert space [49]).

Now consider $\mu_L(z) := \langle r| (1 - zU_L)^{-1} |r\rangle$ and $Q_L(z) := 1 - \mu_L^{-1}(z)$. Following the same argument that leads to (2.51), it can be shown that

$$Q_{L+1}(z) = z^2 c_{12} + \frac{z^2 c_{11} c_{22} Q_L(z)}{1 - Q_L(z) c_{21}}, \tag{2.55}$$
$$Q_1 = z^2. \tag{2.56}$$

In particular, the fixed point of this relation, $Q_{L+1} = Q_L = Q$, satisfies (2.51). $\mu_L(z)$ has poles when z^{-1} lies in the spectrum of U_L. Iterating (2.55) for μ_L starting from (2.56) shows that it is a meromorphic function with poles at $2L$ locations on the unit circle. As $L \to \infty$ the poles begin condensing on the circle. Figs. 2.11 and 2.12 show the eigenvalues of U_{40} and U_{80} with the same coin matrix C_1 used to generate Fig. 2.10. In the strict limit, the poles condense to form the two branch cuts of $\mu(z)$,

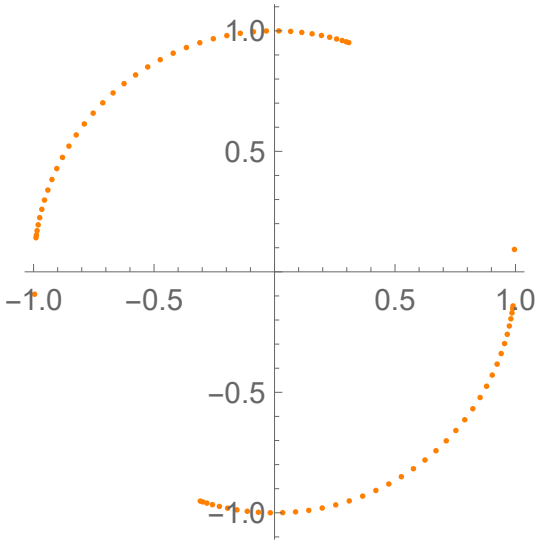

Figure 2.11: $L = 40$.

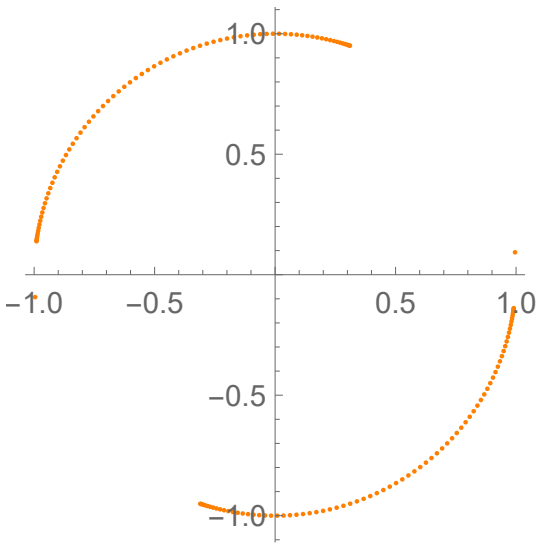

Figure 2.12: $L = 80$. Note the isolated eigenvalues slightly above and below the real axis.

while two poles remain isolated. These isolated poles of μ_L do not however converge to the poles of $\mu(z)$ as a comparison of Fig. 2.10 and 2.12 shows – the reason

for this is not clear, but we should point out that for two operators converging in the strong operator topology (as described above) there is no guarantee that the spectra coincide: Take for example the matrix A_n which is defined as zero everywhere except the (n,n) entry which is equal to 1. A_n converges, in the strong operator topology, to the zero matrix, as $n \to \infty$. However, the eigenvalues of the zero matrix are zero while the eigenvalues of A_n are $\{0,1\}$.

2.3.4 Spectrum of the QRW on $\mathbb{H}$

In this section we explicitly solve the eigenvalue equation $U|\lambda\rangle = \lambda|\lambda\rangle$ on the half-line $\mathbb{H}$. We first define eigenfunctions $a_n = \langle n,1|\lambda\rangle$ and $b_n = \langle n,2|\lambda\rangle$. We rescale $|\lambda\rangle$ so that $\langle r|\lambda\rangle = 1$. The eigenvalue equation written in terms of $\{a_n\}_{n=1}^{\infty}$ and $\{b_n\}_{n=1}^{\infty}$ reads

$$
\begin{aligned}
&1 = \lambda a_1,\\
&c_{12}a_1 + c_{22}b_1 = \lambda,\\
&\left.\begin{aligned} c_{11}a_n + c_{21}b_n &= \lambda a_{n+1},\\ c_{12}a_{n+1} + c_{22}b_{n+1} &= \lambda b_n. \end{aligned}\right\} \text{for } n \geq 1
\end{aligned}
$$

The solution to this set is unique and given by

$$
\begin{aligned}
\begin{pmatrix} a_n \\ b_n \end{pmatrix} &= \begin{pmatrix} c_{11}/\lambda & c_{21}/\lambda \\ -\frac{c_{12}c_{11}}{\lambda c_{22}} & \frac{\lambda}{c_{22}} - \frac{c_{12}c_{21}}{\lambda c_{22}} \end{pmatrix}^{n-1} \begin{pmatrix} 1/\lambda \\ \frac{\lambda}{c_{22}} - \frac{c_{12}}{\lambda c_{22}} \end{pmatrix};\\
\implies a_n &= \alpha_1\, p_1^n + \alpha_2\, p_2^n, \qquad (2.57)\\
\alpha_1 &= \frac{\Pi - c_{22}p_2\lambda + c_{21}\lambda^2}{c_{22}p_1(p_1-p_2)\lambda^2},\\
\alpha_2 &= \frac{\Pi - c_{22}p_1\lambda + c_{21}\lambda^2}{c_{22}p_2(p_2-p_1)\lambda^2},
\end{aligned}
$$

where $p_{1,2}$ are the roots of

$$
c_{22}\, p^2 - \left(\frac{\Pi}{\lambda} + \lambda\right) p + c_{11} = 0. \qquad (2.58)
$$

This equation has the property that if $p(\lambda)$ is a solution, then $\overline{p(\overline{\lambda}^{-1})}^{-1}$ is too, following from the fact that $c_{22}^{*}\Pi = c_{11}$. As λ varies on the unit circle, there are regions for which both $p_{1,2}$ are phases, and regions for which one root is inside the

unit circle and the other is outside; the behaviour of the roots as λ moves between these regions is qualitatively the same as in Fig. 2.9. When both $p_{1,2}$ are phases, the eigenstate (2.57) oscillates like a wave at large n. In the theory of Schrödinger equations, this would be called a scattering state (those states that behave as plane waves at large distances), but in this field they are usually called the absolutely continuous (a.c.) spectrum. As for Schrödinger equations, note that the scattering states are not normalizable (so strictly do not lie in the Hilbert space).

For all other λ, we have $|p_1| > 1$ and $|p_2| < 1$. This results in an eigenstate that grows exponentially at large n. These states do not have any interpretation and are not eigenfunctions of U. As λ varies in this region, however, it is possible that $\alpha_1 = 0$, leaving behind a state that is exponentially damped at large n. Such a state in Schrödinger equations is called a bound state. In this field, however, they are usually called the 'pure-point' (p.p.) or 'mass-point' spectrum. Setting $\alpha_1 = 0$ gives the condition for mass points:

$$\Pi - c_{22}\, p_2\, \lambda + c_{21}\lambda^2 = 0.$$

Rearranging for p_2 and substituting in (2.58) gives

$$c_{11}c_{22} + (c_{21} - 1)(c_{21}\lambda^2 + \Pi) = 0.$$

This is the same as (2.53) if z^{-1} is identified with λ, so we conclude that $\mu(z)$ has a pole when z^{-1} lies in the p.p. spectrum.

As Fig 2.13 shows, the regions in which there do and don't exist scattering states are separated by points at which $p_{1,2}$ collide (i.e. a double root). The condition for a double root is that the discriminant of (2.58) w.r.t p is zero:

$$\lambda^4 - 2(c_{11}c_{22} + c_{12}c_{21})\lambda^2 + \Pi^2 = 0.$$

If we identify z^{-1} with λ, then we notice that this is the same as equation (2.54). To complete the argument, we must show that when $|p(z^{-1})| \neq 1$, that $|Q(z)| = 1$

and conversely when $|p(z^{-1})| = 1$, that $|Q(z)| \neq 1$. We leave this as an exercise to the reader given that the exact relationship between Q and p is[5]

$$Q(z) = \frac{c_{22}p(z^{-1})z - z^2\Pi}{c_{21}}.$$

This finally shows that $Q(z)$ has branch cuts when z^{-1} lies in the a.c. spectrum.

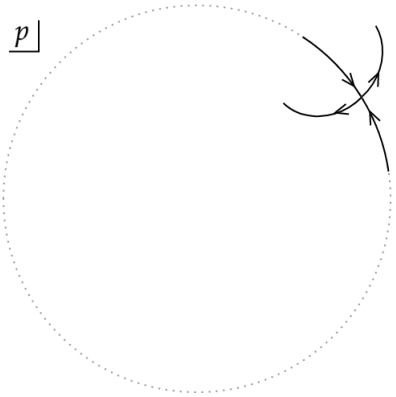

Figure 2.13: In the complex p plane, the flow of roots as λ varies on the unit circle and passes through a branch point is indicated by the arrows. In grey is the unit circle.

The collection of p.p. eigenvalues and a.c. eigenvalues is written as σ_{pp} and σ_{ac} respectively. The a.c. spectrum is said to be composed of 'bands' (where the support of σ_{ac} lies) separated by 'gaps'. Mass points can only occur in these gaps because mass points $\lambda \in \sigma_{pp}$ are characterized by $Q(\lambda^{-1}) = 1$ and gaps are characterized by $|Q(\lambda^{-1})| = 1$.

2.3.5 Induced Measure

We will show how $\langle r| U^n |r\rangle$ can be written as an integral w.r.t. a measure supported on the unit circle. Now

$$\mu_n = \langle r| U^n |r\rangle = (2\pi i)^{-1} \int_\gamma z^{-n-1}\mu(z)dz,$$

where γ is a small loop around the origin (see Fig 2.14). Due to the analytic structure of $\mu(z)$, γ can be deformed to the contour γ' shown in Fig. 2.15. We've

[5]This follows from solving $U|u\rangle = \lambda|u\rangle + |r\rangle$ for $|u\rangle$ and setting $\langle r|u\rangle = -\lambda^{-1}\mu(\lambda^{-1})$.

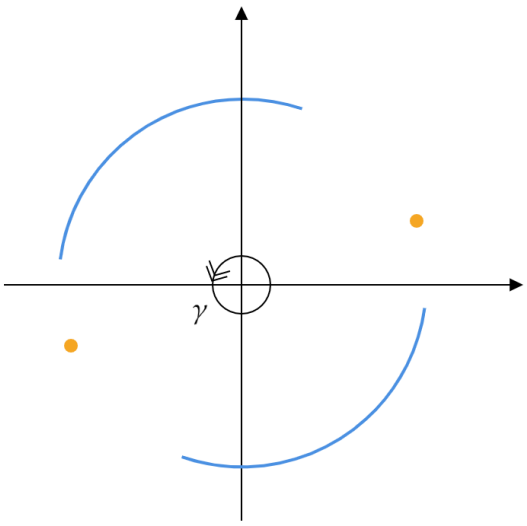

Figure 2.14: γ.

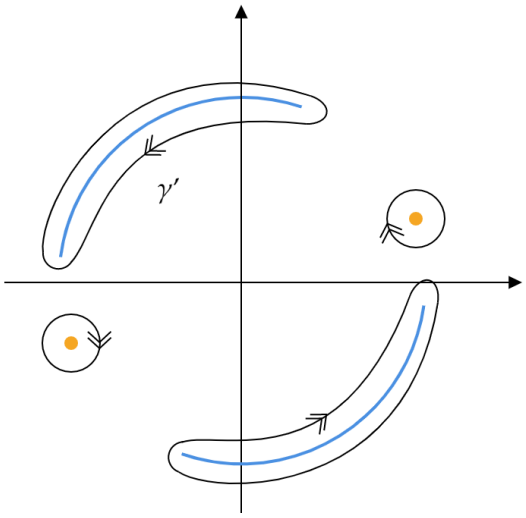

Figure 2.15: γ'. The blue bands are cuts of $\mu(z)$ and the orange points are poles of $\mu(z)$.

assumed here that the integral around the circle at infinity is zero since z^{-n-1} provides a large damping factor. Therefore

$$\mu_n = (2\pi i)^{-1} \int_c z^{-n-1} \text{disc}(\mu(z)) dz - \sum_{z^{-1} \in \sigma_{pp}} z^{-n-1} \text{Res}(\mu(z)),$$

where c is the union of branch cuts oriented in the clockwise direction, $\text{disc}(\mu(z))$ is the discontinuity across the cut: $\lim_{r\to 1^+} \mu(rz) - \lim_{r\to 1^-} \mu(rz)$ and σ_{pp} is the p.p. spectrum. Now since $\mu(z) + \overline{\mu(\bar{z}^{-1})} = 1$ when $|z| \neq 1$, the value of $\mu(z)$ on one side of the cut is $1 - \overline{\mu(z)}$ if its value on the other side of the cut is $\mu(z)$. Therefore

$$\text{disc}(\mu(z)) = 1 - \overline{\mu(z)} - \mu(z) = 1 - 2\text{Re}(\mu(z))$$

(recall that we defined $\mu(z) = \lim_{r\to 1^-} \mu(rz)$ for $|z| = 1$). Now let $z^{-1} = e^{i\theta} \in \sigma_{pp}$, and define

$$\nu(\theta) \equiv -\text{Res}(\mu(z)/z) = \lim_{r\to 1} (1-r)\mu(rz).$$

One then defines a measure (see [43] Sec. 1.1)

$$d\nu(\theta) = \underbrace{\left(2\text{Re}(\mu(e^{-i\theta})) - 1\right) \frac{d\theta}{2\pi}}_{\equiv d\nu_{ac}(\theta)} + \underbrace{\sum_{\theta_0:\ e^{i\theta_0} \in \sigma_{pp}} \nu(\theta_0)\delta(\theta - \theta_0) d\theta}_{\equiv d\nu_{pp}(\theta)} \tag{2.59}$$

such that

$$\mu_n = \int_0^{2\pi} e^{in\theta} d\nu(\theta). \tag{2.60}$$

2.3.6 Verblunsky Coefficients

One usually also defines the 'Schur function':

$$f(z) = \frac{\overline{Q(\bar{z})}}{z}.$$

The Schur function admits a continued fraction expansion [41]:

$$\begin{aligned} f &\equiv f_0, \\ f_j(z) &= \gamma_j + \frac{1-|\gamma_j|^2}{\gamma_j^* + 1/z f_{j+1}(z)} \qquad j = 0, 1, 2, ... \end{aligned} \tag{2.61}$$

$\{\gamma_j\}_{j=0}^{\infty}$ are called Verblunsky coefficients, satisfying $|\gamma_j| < 1$ for all j. Given the Verblunsky coefficients, one knows the Schur function exactly. Any sequence of Verblunsky coefficients s.t. $|\gamma_j| < 1$ gives a Schur function and, as shown in §2.3.5, a unique measure $d\nu(\theta)$. In the mathematics literature, one usually imposes some condition on the sequence of Verblunsky coefficients and computes the effect this has on the corresponding measure $d\nu(\theta)$. For example, there is the following result: *if the Verblunsky coefficient sequence is p-periodic then the associated measure has at most p bands* ([43] Chap. 11). This is easy to prove. The p-periodicity of the Verblunsky coefficients means that $\gamma_j = \gamma_{j+p}$ for all $j \geq 0$. Iterating (2.61) and expanding in a Taylor series, we have

$$\begin{aligned} f_0 &= \gamma_0 + \gamma_1(1-|\gamma_0|^2)z - (1-|\gamma_0|^2)(\overline{\gamma_0}\gamma_1^2 - \gamma_2 + \gamma_2|\gamma_1|^2)z^2 + O(z^3), \\ f_p &= \gamma_p + \gamma_{p+1}(1-|\gamma_p|^2)z - (1-|\gamma_p|^2)(\overline{\gamma_p}\gamma_{p+1}^2 - \gamma_{p+2} + \gamma_{p+2}|\gamma_{p+1}|^2)z^2 + O(z^3). \end{aligned}$$

Because of the periodicity of the Verblunsky coefficients, however, these two expansions are the same term by term, so $f_0(z) = f_p(z)$. Now iterating (2.61) p times allows f_0 to be written in terms of f_p. Then using $f_p = f_0$, one arrives at a quadratic equation for $f_0 \equiv f$, which takes the general form

$$\mathrm{pol}_p(z) f^2 + \mathrm{pol}_p(z) f + \mathrm{pol}_{p-1}(z) = 0, \tag{2.62}$$

where $\mathrm{pol}_p(z)$ represents any polynomial of order p in z. The endpoints of the bands of the measure occur when the discriminant of (2.62) is zero, which gives $\mathrm{pol}_{2p}(z) = 0$. This has at most $2p$ solutions which means that there are at most p bands. There is

another theorem that states that given two Verblunsky coefficient sequences $\{\alpha_j\}_{j=0}^{\infty}$ and $\{\beta_j\}_{j=0}^{\infty}$ s.t. $\alpha_j - \beta_j \xrightarrow[j\to\infty]{} 0$, then the a.c. spectrum corresponding to the two sequences is the same ([43] Sec. 4.3). This combined with the previous result, tells us that *for asymptotically p-periodic Verblunsky coefficients, the number of bands is at most p*. Later, in our model, §5.4, we will find an example of this.

2.3.7 Asymptotic return probabilities and localization

Consider μ_n for n large. Recall the integral representation (2.60) and the decomposition (2.59) $d\nu = d\nu_{ac} + d\nu_{pp}$. For large n, the dominant contribution to $\int e^{in\theta} d\nu_{ac}(\theta)$ comes from the regions near the edgepoints of the bands; let $\{e^{i\theta_i}\}_{i=1}^{N}$ be the collection of edgepoints of the bands. At an edgepoint, $\mathrm{Re}(\mu(e^{-i\theta_i})) = 1/2$, since $|Q(e^{-i\theta_i})| = 1$. An edgepoint is also a branch point of $\mu(z^{-1})$, so around an edgepoint we can expand μ as $2\,\mathrm{Re}(\mu(e^{-i\theta})) = 1 + C_i(\theta - \theta_i)^{1/2} + \text{h.o.t.}$ for some constants C_i. Therefore

$$\begin{aligned}\int e^{in\theta} d\nu_{ac}(\theta) &= \sum_{i=1}^{N} C_i e^{in\theta} (\theta - \theta_i)^{1/2} \frac{d\theta}{2\pi} + \text{h.o.t} \\ &= \sum_{i=1}^{N} \int C_i e^{in\theta_i} \Delta^{1/2} e^{in\Delta} \frac{d\Delta}{2\pi} + \text{h.o.t} \\ &= n^{-3/2} \sum_{i=1}^{N} c_i e^{in\theta_i} + \mathcal{O}(n^{-2}).\end{aligned}$$

In the second line we've defined $\Delta = \theta - \theta_i$ and in the last line we've rescaled $\Delta \to \Delta/n$. The c_i are some unknown constants. Let $\{e^{i\tilde{\theta}_i}\}_{i=1}^{M}$ be the set of mass points. Then, together with the contribution from $\int e^{in\theta} d\nu_{pp}(\theta)$

$$\mu_n = \sum_{i=1}^{M} \nu(\tilde{\theta}_i) e^{in\tilde{\theta}_i} + n^{-3/2} \sum_{i=1}^{N} c_i e^{in\theta_i} + \mathcal{O}(n^{-2}). \tag{2.63}$$

The root is said to be a localized state if $\limsup_{n\to\infty} |\langle r| U^n |r\rangle| \neq 0$, because then the particle always has a non-zero probability of being found at root. From (2.63), we see that this only happens when the p.p. spectrum is non-empty [42].

3

Dimers coupled to Causal Dynamical Triangulations

Contents

As we discussed in §2.1.7, CDT+HD is a model of discretized QG coupled to matter. In this chapter we will define and solve for various observables in CDT+HD and study their scaling limits.

3.1 Introduction

Models in which extra degrees of freedom (often called 'matter') are coupled to Dynamical Triangulations (DT) have been solved for many cases, showing that their scaling limit is equivalent to the corresponding flat-lattice CFT coupled to Liouville gravity.

Coupling matter to CDT is more difficult and only limited progress has been made. Numerical work [50–53] has established that the interaction between matter and geometry is weaker than for DT, and that CDT with gauge fields is a solvable, but topological, system [54]. The Ising model on CDT has been shown not to be magnetised at high enough temperature [28] but has otherwise resisted solution. It is known that the addition of curvature-squared [55] or extrinsic curvature terms [56] to the action does not change the universality class, and recently loop models have been investigated [57]. However by exploiting the bijection of the CDT with a tree ensemble [24], it is possible to make progress when the matter consists of hard-dimers [25, 58, 59]. It was shown that a restricted form of the hard-dimer model on CDT can be solved using a bijection with labelled trees; the model displays a transition away from the pure gravity phase of CDT, driven by the dimer interactions. A slightly less restricted HD model was analysed in [26] where a richer phase diagram was found. In this paper we show how to include all possible dimer types present on CDT in the bijection and lift all the restrictions bar one which is required to render the tree system local. We find that there are two tri-critical and two dense-dimer phases in addition to the pure gravity phase; the richness of the CDT+HD phase diagram arises from the ability to assign different dimer types.

The tree bijection enables us to calculate the disk and cylinder amplitudes by reducing the problem to one of solving a non-linear second order recurrence relation. In contrast to the earlier work, with more restrictive dimer ensembles, these relations appear not always to be linearizable by a judicious mapping of the problem; they are inherently non-linear and cannot be solved analytically in closed form. In the continuum limit however, the recurrence relations become a non-linear first or second order ordinary differential equation (ODE), which takes

a characteristic form in each phase of the model. The ODEs are vastly easier to solve than the recurrence relations and their solutions enable us to determine the continuum amplitudes and, in phases where it exists, a simple time translation operator (or Hamiltonian) acting on states labelled by the boundary length – in some phases, the Hamiltonian doesn't exist, but that is to be expected since the Hamiltonian should depend on the dimer degrees of freedom too.

The layout of this chapter is as follows. We define the *restricted* CDT+HD model in §3.2. We prove the bijection of CDT+HD with a labelled tree model in §3.3. We construct the cylinder amplitudes and their recurrence relations in §3.4. We map-out the phase diagram in §3.5. We take the scaling limit of the cylinder amplitudes and show that they satisfy various ODEs in §3.6. We derive the associated Hamiltonians in §3.7.

3.2 The restricted CDT+HD model

In this paper we generalise and extend the work of [26] by including dimers of type 4 (see Fig. 2.6). We will solve the CDT+HD model subject to a single restriction which renders the model solvable and is a relaxation of that imposed in [26]:

I. **Restriction:** If, for $v \in T$, $\sigma_b(v) > 1$ and $\sigma_f(v) = 1$, then $f(v)$ is not dual to a dimer.

Fig. 3.1 shows a dimer configuration which violates this restriction. We call a dimer

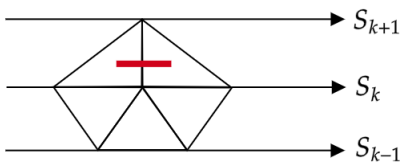

Figure 3.1: The dimer in red violates (I) since $\sigma_b = 2$ and $\sigma_f = 1$. S_i are spatial slices.

configuration satisfying the 'hard-dimer rule' (see §2.1.7), the boundary condition (see §2.1.7) and restriction (I) as admissible.

Let $\mathcal{D}_t$ denote the set of all triangulations in $\mathcal{T}_t$ decorated by all admissible dimer configurations. An element of $\mathcal{D}_t$ can be written as a pair (T, D), where $T \in \mathcal{T}_t$ and D is an admissible dimer configuration on T. Define $\mathcal{D} = \bigcup_{t\in\mathbb{Z}^+} \mathcal{D}_t$. The partition function of the set $\mathcal{D}_t$, which we call the cylinder-amplitude, is defined by

$$G(g, x, y; \xi_1, \xi_2, \xi_{2'}, \xi_3, \xi_4; t) = \sum_{(T,D)\in\mathcal{D}_t} x^{|\partial_1 T|} y^{|\partial_2 T|} g^{|T|} \xi_1^{|D|_1} \xi_2^{|D|_2} \xi_{2'}^{|D|_{2'}} \xi_3^{|D|_3} \xi_4^{|D|_4}, \quad (3.1)$$

where $|D|_i$ counts the number of dimers of type i in D. Each dimer of type i is weighted by a fugacity ξ_i, each triangle by a factor $g > 0$, each initial boundary edge by a factor $x > 0$, and each final boundary edge by a factor $y > 0$; if $g < g_c$, $x < x_c$, $y < y_c$, and the ξ_i are not too negative, then the series in (3.1) is convergent.

As pointed out in [25], the move in Fig. 3.2 converts a dimer of type $2'$ to one of type 2, without affecting the dimer configuration otherwise. Using the move, all

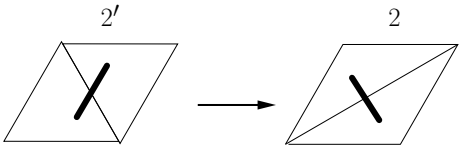

Figure 3.2: The move.

type $2'$ dimers can be converted to type 2, but we have to remember that those that have been converted have fugacity $\xi_{2'}$. Now, given a configuration D, with no type $2'$ dimers and n type 2 dimers, obtained in this way, it could have arisen from $\binom{n}{k}$ configurations with $n-k$ type 2 dimers and k type $2'$ dimers, which have weight $\xi_2^{n-k}\xi_{2'}^k$ each. Since this can happen for any $0 \le k \le n$, the total weight of D is $\sum_{k=0}^n \binom{n}{k} \xi_2^{n-k}\xi_{2'}^k = (\xi_2 + \xi_{2'})^n$. Applying this to (3.1), we get

$$G(g, x, y; \xi_1, \xi_2, \xi_{2'}, \xi_3, \xi_4; t) = G(g, x, y; \xi_1, (\xi_2 + \xi_{2'}), 0, \xi_3, \xi_4; t).$$

So without loss of generality we set $\xi_{2'} = 0$ and hereafter work with $G(g, x, y, \xi; t)$ where ξ stands for the set of dimer weights $\{\xi_1, \xi_2, \xi_3, \xi_4\}$. Similarly to (2.4), we define

$$\tilde{G}(g, l_1, l_2, \xi; t) = \oint_\gamma \frac{du}{2\pi i u} \oint_\gamma \frac{dv}{2\pi i v}\, u^{l_1}\, v^{l_2}\, G(g, x_c/u, y_c/v, \xi; t), \quad (3.2)$$

where the contour γ encloses the neighbourhood of the point at infinity in which G is analytic. x_c and y_c are the radius of convergence of $G(g, x, y, \xi; t)$ and appear to remove an overall divergent factor in the scaling limit.

3.3 Bijection to labelled trees

We define a labelled-tree as a pair (τ, l), of a tree, τ, in which each vertex, v, has a label $\ell(v)$ taking values

$$\begin{aligned}\ell(v) \equiv (p(v), q(v)) \in \mathcal{S} &= \{0,1,2,3\} \otimes \{0,4\} \setminus \{(1,4)\} \\ &= \{(0,0),(0,4),(1,0),(2,0),(2,4),(3,0),(3,4)\},\end{aligned}$$

i.e. $p(v) \in \{0,1,2,3\}$ and $q(v) \in \{0,4\}$ with the possibility $(p = 1, q = 4)$ excluded (see (viiia) later).

Consider an element $(T, D) \in \mathcal{D}_t$. Recall that T may be mapped to a tree $\tau = \beta(T)$ of height $t + 1$ (see §2.1.3). We denote by $\mathcal{RL}_{t+1}$, the set of labelled trees of height $t + 1$ obtained from $\mathcal{D}_t$ by applying β and then assigning the labelling to the tree as follows:

i. the root vertex is unlabelled;

ii. if $\sigma_b(v) = 1$ and this backward edge is dual to a dimer, $q(v) = 4$; otherwise $q(v) = 0$;

iii. if $e(v)$ is dual to a dimer, $p(v) = 1$;

iv. if $f(v)$ is dual to a dimer and $\sigma_f(v) > 1$, $p(v) = 2$;

v. if $f(v)$ is dual to a dimer and $\sigma_f(v) = 1$, $p(v) = 3$;

vi. if neither $f(v)$ nor $e(v)$ is dual to a dimer, $p(v) = 0$.

We denote this map by $\gamma : \mathcal{D}_t \to \mathcal{RL}_{t+1}$. The trees in $\mathcal{RL}_{t+1}$ do not have arbitrary labelling; the labelling is constrained by (see §A.1 for the derivation of these constraints)

vii. Boundary conditions: dimers dual to a boundary edge are not allowed:

(a) if $v \in \partial_1 T$, then $p(v) \in \{0, 2, 3\}$ and $q(v) = 0$;

(b) if $v \in \partial_2 T$, then $p(v) = 0$.

viii. Hard dimer rule:

(a) no vertex can have label $(1, 4)$;

(b) if a vertex v has label $p(v) = 3$, then the vertex on its left, w, satisfies $p(w) = 0$;

(c) if a vertex v has label $p(v) = 2$, then its first child w satisfies $p(w) \neq 1$ and $q(w) \neq 4$;

(d) if a vertex v has label $q(v) = 4$, then the vertex on its left, w, satisfies $p(w) \neq 1$ and $q(w) \neq 4$.

ix. Restriction (I): if vertex v is a last child then $p(v) \neq 3$.

x. Geometry:

(a) any vertex v with label $p(v) = 3$ is necessarily a leaf;

(b) any vertex v with label $p(v) = 2$ has at least one child;

(c) any vertex v with label $q(v) = 4$ is not a last child.

The proof that γ is a bijection is given in §A.1.

We define $\mathcal{L}_t^n$ to be the set of all labelled trees of height t, with the root labelled by $n = \ell(r) \in \mathcal{S}$ and satisfying all the above constraints (vii)-(x) *except* the initial boundary condition (viia). We also define the set $\mathcal{L}_{\leq t}^n = \bigcup_{i \in [0,t]} \mathcal{L}_i^n$.

All conditions on the labelling of a tree in $\mathcal{RL}_t$, except the restriction (ix), are consequences of the full hard dimer model; they arise either from the hard dimer rule, or from the geometry of $T \in \mathcal{T}_t$ and its associated tree. The restriction (ix) ensures that interactions in the labelled tree model are local (i.e. interactions are only between sibling vertices); otherwise, if v is a last child with $p(v) = 3$, then by the hard dimer rule (viiib), the label of the vertex on its left – which is not a sibling of v

– is constrained, thus generating a non-local interaction in the tree. The model can't be solved by the usual techniques if there are non-local interactions. Note that the model with no dimers of type 3, i.e. $\xi_3 = 0$, is not changed at all by the restriction.

Now consider the inversion operation $I : \mathcal{T}_t \to \mathcal{T}_t$ defined as $S_k(I(T)) := \mathcal{R}(S_{2+t-k}(T))$ with the connectivity of vertices unchanged, and where the $\mathcal{R}$ operation reverses the orientation of the circle S_k. Under I, the dimer types are mapped $1 \to 1$, $2 \to 2$ and $3 \leftrightarrow 4$, while the boundary fugacities are swapped $x \leftrightarrow y$. Under I, the restriction (ix) on $\beta(T)$ becomes the restriction that a vertex with label $q = 4$ in $\beta(I(T))$ is necessarily a leaf. Conversely, a vertex in $\beta(T)$ with label $q = 4$ that is *not* a leaf gets mapped to a vertex, in $\beta(I(T))$, that is a last child with label $p = 3$. It follows that while the full dimer model is invariant under I, this symmetry is broken by the restriction; this fact will be important later. A further corollary is that the unrestricted model with $\xi_4 = 0$ can in fact be solved by the methods of this paper, since it maps under I to our model with $\xi_3 = 0$, for which the restriction is empty.

3.4 Generating Functions

By mapping $\mathcal{D}_t$ to $\mathcal{RL}_{t+1}$ with the bijection γ we find that

$$G(g, x, y, \xi; t) = \sum_{(\tau,l)\in\mathcal{RL}_{t+1}} g^{2|\tau|-2}(x/g)^{|\tau|_1}(y/g)^{|\tau|_{t+1}} \prod_{v\in\tau\setminus r} \xi_{p(v)}\xi_{q(v)},$$

where $|\tau|$ is the number of vertices in τ, $|\tau|_i$ is the number of vertices at height i, and for convenience we define $\xi_0 \equiv 1$. We define the partition function of $\mathcal{L}^n_{\leq t}$ as

$$W^n(g, y, \xi; t) = \sum_{(\tau,l)\in\mathcal{L}^n_{\leq t}} \frac{1}{|\partial\tau|} g^{2|\tau|}(y/g)^{|\partial_2\tau|} \prod_{v\in\tau} \xi_{p(v)}\xi_{q(v)}.$$

As discussed in §2.1.4, any tree can be decomposed into sub-trees. By the dimer rule (viia), only labels $(0,0), (2,0), (3,0)$ are allowed for vertices on S_1. It follows that the subtrees of a tree in $\mathcal{RL}_{t+1}$ are elements of $\bigcup_{n\in\{(0,0),(2,0),(3,0)\}} \mathcal{L}^n_{\leq t}$. To the left of a sub-tree with root label $(3,0)$, there must be a sub-tree with root label $(0,0)$

due to (viiib). This includes the possibility of a sub-tree with root label $(3,0)$ being the left-most sub-tree and a sub-tree with root label $(0,0)$ being the right-most. By standard combinatoric arguments, it follows that

$$G(g,x,y,\xi;t) = y\frac{\partial}{\partial y}\frac{1+\left(\frac{x}{g}\right)^2 W^{(3,0)}W^{(0,0)}}{1-\left(\frac{x}{g}W^{(0,0)}+\frac{x}{g}W^{(2,0)}+\left(\frac{x}{g}\right)^2 W^{(3,0)}W^{(0,0)}\right)}, \tag{3.3}$$

where all W^n on the right-hand-side are evaluated at $(g,y,\xi;t)$. The operation $y\partial_y$ marks the exit loop and removes the set of trees which are of height less than t. The model can be solved by finding recursion relations for the W^n to which we now turn.

The initial conditions are given by trees of height zero. By the dimer rule (viib), only labels $(0,0)$ and $(0,4)$ are allowed on the final boundary, so

$$W^{(0,q)}(g,y,\xi;0) = yg\xi_q, \tag{3.4}$$

$$W^{(p\neq 0,q)}(g,y,\xi;0) = 0. \tag{3.5}$$

A vertex with label $(3,0)$ is necessarily a leaf (see (xa)). Therefore,

$$W^{(3,0)}(g,y,\xi;t+1) = g^2\xi_3, \qquad t\geq 0. \tag{3.6}$$

The W^n are not all independent. Since there are no restrictions on the children of a vertex with label $(1,0)$,

$$W^{(1,0)}(g,y,\xi;t+1) = \xi_1 W^{(0,0)}(g,y,\xi;t+1), \qquad t\geq 0. \tag{3.7}$$

Since the label $q(v)=4$ does not place any restrictions on the children of the vertex v, we have

$$W^{(p,4)}(g,y,\xi;t+1) = \xi_4 W^{(p,0)}(g,y,\xi;t+1), \qquad t\geq 0. \tag{3.8}$$

A tree in $\mathcal{L}^n_{\leq t+1}$ can be decomposed into sub-trees in $\bigcup_{n\in\mathcal{S}}\mathcal{L}^n_{\leq t}$ for $t\geq 0$. The restrictions do not allow the subtrees to appear in any order, as we will discuss now. To the left of a subtree with root label $(3,4)$ there must be another subtree – because of (ix) – and it must have root label $(0,0)$ due to (viiib), (viiid). Similarly, to the left of a subtree with root label $(3,0)$ there must be a subtree with root label $(0,0)$

or $(0,4)$, due to (viiib). To the left of a subtree with root label $(0,4)$ there must be a subtree with root label $(0,0)$, $(2,0)$ or $(3,0)$ due to (xc), (viiid). To the left of subtree with root label $(2,4)$ there must be a subtree with root label $(0,0)$, $(2,0)$ or $(3,0)$ due to (viiid). The label on the root of the subtrees to the left or right of a subtree with root label $(0,0)$, $(1,0)$ or $(2,0)$ are not constrained in contrast. This leads to

$$W^{(0,0)}(g,y,\xi;t+1) = \frac{g^2}{1-\left(W^{(1,0)}+W^{(0,0)}W^{(3,4)}+\frac{\left(W^{(0,0)}W^{(3,0)}+W^{(0,0)}+W^{(2,0)}\right)\left(1+W^{(0,4)}+W^{(2,4)}\right)}{1-W^{(0,4)}W^{(3,0)}}\right)}, \tag{3.9}$$

for $t \geq 0$ and where all W^n on the right-hand-side are evaluated at $(g,y,\xi;t)$. When decomposing $\mathcal{L}^{(2,0)}_{\leq t+1}$ into subtrees, the restriction (viiic) requires that the rightmost subtree must have root label $(0,0)$, $(2,0)$ or $(3,0)$. This leads to

$$W^{(2,0)}(g,y,\xi;t+1) = \frac{g^2\xi_2\left(\frac{W^{(0,0)}+W^{(2,0)}+W^{(0,0)}W^{(3,0)}}{1-W^{(0,4)}W^{(3,0)}}\right)}{1-\left(W^{(1,0)}+W^{(0,0)}W^{(3,4)}+\frac{\left(W^{(0,0)}W^{(3,0)}+W^{(0,0)}+W^{(2,0)}\right)\left(1+W^{(0,4)}+W^{(2,4)}\right)}{1-W^{(3,0)}W^{(0,4)}}\right)}, \tag{3.10}$$

for $t \geq 0$ and where all W^n on the right-hand-side are evaluated at $(g,y,\xi;t)$. Recursions for all other W^n follow from these two by using the relationships (3.6)-(3.8). It is convenient to define

$$f^1_t(g,y,\xi) = \frac{1}{g^2}W^{(0,0)}(g,y,\xi;t) \qquad t \geq 1,$$
$$f^2_t(g,y,\xi) = \frac{1}{\xi_2 g^2}W^{(2,0)}(g,y,\xi;t) \qquad t \geq 1.$$

Then applying (3.4)-(3.8), to (3.9), (3.10), we find that $f^i_t(g,y,\xi)$ satisfies the initial conditions (with the argument (g,y,ξ) suppressed for brevity)

$$f^1_1 = \frac{1}{1-gy-g^2y^2\xi_4}, \qquad f^2_1 = \frac{gy}{1-gy-g^2y^2\xi_4}, \tag{3.11}$$

and the recursion relations,

$$f^1_t = \mathcal{F}^1(f^1_{t-1},f^2_{t-1},g) \equiv \frac{1}{1-A_{t-1}}, \tag{3.12}$$
$$f^2_t = \mathcal{F}^2(f^1_{t-1},f^2_{t-1},g) \equiv \frac{1}{1-A_{t-1}}\left(\frac{g^2f^1_{t-1}+g^2\xi_2f^2_{t-1}+g^4\xi_3f^1_{t-1}}{1-g^4\xi_3\xi_4f^1_{t-1}}\right), \tag{3.13}$$
$$A_t = g^2\xi_1f^1_t+g^4\xi_4\xi_3f^1_t+\frac{g^2(g^2\xi_3f^1_t+f^1_t+\xi_2f^2_t)(1+g^2\xi_4f^1_t+g^2\xi_4\xi_2f^2_t)}{1-g^4\xi_3\xi_4f^1_t}. \tag{3.14}$$

Finally, from (3.3) we find that

$$G(g,x,y,\xi;t) = y\partial_y \frac{1+g^2x^2\xi_3 f_t^1}{1-g\,x(\xi_2\,f_t^2+(1+g\,x\,\xi_3)f_t^1)}, \tag{3.15}$$

where the f_t^i on the r.h.s. are evaluated at (g,y,ξ).

3.5 Phases and Critical Exponents

The grand-canonical partition function is the fixed point of the sequence generated by (3.11)-(3.14) i.e. $f_t^i = f_{t+1}^i = f_\infty^i, \forall i$. Define $f^i(g,\xi) \equiv f_\infty^i(g,y,\xi)$ (which is independent of the initial condition y). Eliminating f^2 from the coupled equations we find that $P(f^1,g,\xi)=0$ where $P(f^1,g,\xi)$ is quartic in f^1. Provided the dimer fugacities lie in the physical region above a limit surface (also called the critical surface), $\mathcal{S}(\xi)=0$, the dimer dynamics is not critical and does not significantly affect the geometry which remains that of pure gravity; so all points above the limit surface are in the PG phase. For fugacities below the limit surface, the model does not exist in the statistical mechanical sense. On the limit surface itself, the dimers can be critical and, as in [26], can then interact with the geometry strongly enough to drive it away from the pure gravity behaviour. In the rest of this section we discuss these properties in more detail.

3.5.1 Dimer phases

For a fixed set of fugacity values ξ in the physical region, the expansion (3.1) converges and $f^i(g,\xi)$ are analytic functions for $0<g<g_c(\xi)$. At $g=g_c(\xi)$, the physical root $f^i(g_c,\xi)\equiv f_c^i(\xi)$ is either a double root of P (if $\partial_{f^1}P=0$) or a triple root of P (if $\partial_{f^1}P=\partial_{f^1}^2P=0$) in which case the system is 'tri-critical' (a physical quadruple root never occurs). Close to $g=g_c(\xi)$ we expect $f^i(g,\xi)$ to exhibit the behaviour

$$\Delta f^i \equiv f^i(g,\xi)-f_c^i(\xi) = -\phi_c^i(\xi)(\Delta g)^\alpha + h.o.t.,$$

where $\Delta g = g_c(\xi)-g$. In the bulk of the physical region – which contains the pure gravity model $\xi_i=0,\forall i$ – there is a double root at $g=g_c(\xi)$; the dimers do not

interact strongly with the geometry and $\alpha = \frac{1}{2}$. On the boundary of the physical region (i.e. on the surface $\mathcal{S}(\xi) = 0$) the dimers interact strongly with the geometry and there is a triple root at $g = g_c(\xi)$ (tri-critical) which gives $\alpha = \frac{1}{3}$ generically.

The free energy of the system is given by [60]

$$\mu(\xi) = -\log g_c(\xi).$$

In the bulk of the physical region, $g_c(\xi)$ is a single real root of the discriminant of $P(f^1)$, so the dimer density is an analytic function of the fugacities. However $g_c(\xi)$ is a multiple root on the surface $\mathcal{S}(\xi_c) = 0$ where it is a non-analytic function of ξ:

$$g_c(\xi) = g_c(\xi_c) + C\,(\Delta\xi)^{1+\sigma} + h.o.t,$$

where $\Delta\xi$ is defined by $\{\xi_i = \xi_{ic} + \Delta\xi, \forall i\}$, C is a constant depending on ξ_c and 'h.o.t.' suppresses higher order terms in $\Delta\xi$. The dimer system is critical on the surface and we define σ, the dimer density exponent, through

$$\rho_{\text{dimer}} = \xi\,\partial_\xi \mu \sim (\Delta\xi)^\sigma.$$

In this model σ can take values $\frac{1}{2}$ or $-\frac{1}{3}$.

By considering the flow of roots we can see why ξ_c forms part of the limit surface $\mathcal{S}$. First consider the double root case. As a given fugacity ξ_i is decreased to ξ_{ic} while $\xi_{j\neq i}$ are held fixed at their ξ_c values, the physical root $g_c(\xi)$ meets another real root; then as ξ_i is decreased further, the two roots flow out into the complex plane and the statistical mechanical interpretation is lost. A similar argument applies for the triple-root case.

3.5.2 Phase conditions

To establish in detail the behaviour of $f^i(g, \xi)$ close to the critical surface, it is more convenient to study the relations (3.12), (3.13) directly. Differentiating we find that (from now on, we will usually suppress the ξ arguments)

$$(1 - \mathbb{T}^{ij})\frac{\partial f^j}{\partial g} = \frac{\partial \mathcal{F}^i}{\partial g},$$

where

$$\mathbb{T}^{ij} = \frac{\partial \mathcal{F}^i}{\partial f^j} \equiv \mathcal{F}^i_j$$

plays a special role in what follows. At the critical surface, $\mathbb{T}$ has at least one eigenvalue $\lambda_1 = \lambda_{1c} = 1$ and furthermore, by definition, no eigenvalue can reach 1 for $g < g_c(\xi)$. Defining

$$\mathcal{C}(\lambda) = \det(\lambda \mathbb{I} - \mathbb{T}) = \mathcal{F}^1_1 \mathcal{F}^2_2 - \mathcal{F}^1_2 \mathcal{F}^2_1 - \lambda(\mathcal{F}^1_1 + \mathcal{F}^2_2) + \lambda^2, \tag{3.16}$$

the criticality condition $\partial_{f^1} P(f^1_c, g_c, \xi) = 0$ is equivalent to $\mathcal{C}(1) = 0$ at $g = g_c(\xi)$, from which it follows that the second eigenvalue is

$$\lambda_{2c} = \mathcal{F}^1_1 + \mathcal{F}^2_2 - 1.$$

Provided $\mathcal{F}^1_1 \neq 1$, $\mathcal{F}^1_2 \neq 0$ the corresponding eigenvectors are

$$u_{1c} = \begin{pmatrix} \mathcal{F}^1_2 \\ 1 - \mathcal{F}^1_1 \end{pmatrix}, \qquad u_{2c} = \begin{pmatrix} \mathcal{F}^1_2 \\ \mathcal{F}^2_2 - 1 \end{pmatrix}, \tag{3.17}$$

and vectors orthogonal to u_{1c} and u_{2c}, which we denote $\bar{u}_{1c}$ and $\bar{u}_{2c}$ respectively, are

$$\bar{u}_{1c} = \begin{pmatrix} 1 - \mathcal{F}^1_1 \\ -\mathcal{F}^1_2 \end{pmatrix}, \qquad \bar{u}_{2c} = \begin{pmatrix} \mathcal{F}^2_2 - 1 \\ -\mathcal{F}^1_2 \end{pmatrix}. \tag{3.18}$$

Note that if $\lambda_{2c} = 1$ then $u_{2c} = u_{1c}$. In this case $\mathbb{T}$ is not diagonalizable but takes a Jordan normal form at $g = g_c(\xi)$; there is one regular eigenvector u_{1c} with eigenvalue $\lambda_1 = 1$, and a linearly independent vector u_{2c} satisfying

$$\mathbb{T} u_{2c} = u_{2c} + \epsilon\, u_{1c},$$

where ϵ is a function of the dimer fugacities ξ.

Now we expand (3.12) and (3.13) about the critical point by setting

$$\begin{aligned} f^i &= f^i_c + \phi^i, \\ g &= g_c - \Delta g, \end{aligned}$$

which gives

$$\begin{aligned} (1 - \mathbb{T})^{ij} \phi^j = -\Delta g \left(\frac{\partial \mathcal{F}^i}{\partial g} + \frac{\partial \mathbb{T}^{ij}}{\partial g} \phi^j \right) + \frac{1}{2} \mathcal{F}^i_{\ell k}\, \phi^\ell \phi^k \\ + \frac{1}{3!} \mathcal{F}^i_{k\ell m} \phi^k \phi^\ell \phi^m + O\left((\Delta g)^2, \phi^4 \right), \end{aligned} \tag{3.19}$$

and then decompose ϕ^i in the u_{1c}, u_{2c} basis. Various phases occur as some coefficients in (3.19) vanish which in turn causes different behaviour for ϕ^i. There are three cases (here $\phi_c > 0$, v^i_{1c} are constants that depend on the dimer fugacities):

i. Generic

$$\bar{u}^i_{2c}\frac{\partial \mathcal{F}^i}{\partial g} \neq 0, \quad \bar{u}^i_{2c}(u^\ell_{1c}\mathcal{F}^i_{\ell k}u^k_{1c}) \neq 0,$$

which leads to

$$\phi^i = -\phi_c(\Delta g)^{\frac{1}{2}}u^i_{1c} + v^i_{1c}\Delta g + O((\Delta g)^{3/2}). \tag{3.20}$$

ii. Tri-critical

$$\bar{u}^i_{2c}\frac{\partial \mathcal{F}^i}{\partial g} \neq 0, \quad \bar{u}^i_{2c}(u^\ell_{1c}\mathcal{F}^i_{\ell k}u^k_{1c}) = 0, \tag{3.21}$$

which leads to

$$\phi^i = -\phi_c(\Delta g)^{\frac{1}{3}}u^i_{1c} + v^i_{1c}(\Delta g)^{\frac{2}{3}} + O(\Delta g). \tag{3.22}$$

It can be shown that $\bar{u}^i_{2c}(u^\ell_{1c}\mathcal{F}^i_{\ell k}u^k_{1c}) = 0$ is equivalent to $\partial^2_{f^1}P(f^1_c, g_c, \xi) = 0$.

iii. Dense Dimer (so-called because it turns out that this phase has $\sigma < 0$)

$$\bar{u}^i_{2c}\frac{\partial \mathcal{F}^i}{\partial g} = 0, \quad \bar{u}^i_{2c}(u^\ell_{1c}\mathcal{F}^i_{\ell k}u^k_{1c}) = 0,$$

which leads to

$$\phi^i = -\phi_c(\Delta g)^{\frac{1}{2}}u^i_{1c} + v^i_{1c}\Delta g + O((\Delta g)^{3/2}). \tag{3.23}$$

It can be shown that $\bar{u}^i_{2c}\frac{\partial \mathcal{F}^i}{\partial g} = 0$ is equivalent to $\partial_g P(f^1_c, g_c, \xi) = 0$ and that $g_c(\xi)$ is a *triple* root of the discriminant at these points.

3.5.3 The Hausdorff dimensions

The exponents α and σ are not alone sufficient to characterise the phase diagram – we also need measures of the geometry. The global and local Hausdorff dimensions, d_H and d_h, are the simplest characterisation of the geometrical properties of these discretized systems. They measure the growth with height t of the spatial size of the triangulations.

The global Hausdorff dimension is determined through the large t behaviour of the two point function defined as (see [21] for details)

$$\tilde{\mathbb{G}}_{ij}(g,\xi;t) = \frac{1}{W^j(g,g,\xi;\infty)} \sum_{t'=t}^{\infty} \sum_{(\tau,l)\in\mathcal{L}^i_{t'+1}} \#^t_j(\tau) g^{2|\tau|} \prod_{v\in\tau} \xi_{p(v)}\xi_{q(v)}, \tag{3.24}$$

where $\#^t_j(\tau)$ is the number of vertices with label j, at height t, in τ. It is easy to show that this satisfies the composition law: $\sum_{k\in\mathcal{S}} \tilde{\mathbb{G}}_{ik}(g,\xi;t_1)\tilde{\mathbb{G}}_{kj}(g,\xi;t_2) = \tilde{\mathbb{G}}_{ij}(g,\xi;t_1+t_2)$. Using the same arguments which gave us the recursion relations for the generating functions in §3.4, we have $\tilde{\mathbb{G}}_{ij}(g,\xi;1) = \tilde{\mathbb{T}}_{ij}$, where

$$\tilde{\mathbb{T}}_{ij} := \lim_{t\to\infty} \frac{\partial W^i(g,g,\xi,t+1)}{\partial W^j(g,g,\xi,t)}.$$

This implies that $\tilde{\mathbb{G}}_{ij}(g,\xi;t) = (\tilde{\mathbb{T}}^t)_{ij}$. The eigenvalues of $\tilde{\mathbb{T}}$ determine the large t behaviour. Due to the simple proportionality relations (3.6)-(3.8), $\tilde{\mathbb{T}}$ has five zero eigenvalues and two non-trivial eigenvalues which coincide with those of $\mathbb{T}$. In other words, it is sufficient to consider the reduced two-point function defined as

$$\mathbb{G}_{ij}(g,\xi;t) = (\mathbb{T}^t)_{ij}.$$

As $t\to\infty$ and $g\uparrow g_c$, this takes the form

$$\mathbb{G}_{ij}(g,\xi;t) = G_{ij}\, e^{-m(g)t+\mathcal{O}(t^2)},$$

where G_{ij} is a constant, and the global Hausdorff dimension d_H is defined by

$$m(g) = c\,(\Delta g)^{\frac{1}{d_H}} + h.o.t..$$

On the other hand, the large t behaviour of $\mathbb{G}_{ij}$ is determined by the eigenvalues, λ, that take the value 1 at $g=g_c$ because $\mathbb{G}_{ij} = G_{ij}\lambda^t$ for large t, i.e. $m(g)\sim 1-\lambda(g)$. Defining the correlation exponent ν through

$$\Delta\lambda = 1-\lambda = b(\Delta g)^\nu + h.o.t.,$$

(where $b>0$ is a constant) we see that $d_H = \nu^{-1}$ [21]. The correlation function has a scaling limit for large times; letting $t = Ta^{-1}$, $\Delta g = \Lambda a^{\frac{1}{\nu}} = \Lambda a^{d_H}$ and taking $a\to 0$ we have

$$\mathbb{G}^s_{ij}(\Lambda,\xi;T) := \lim_{a\to 0} \mathbb{G}_{ij}(g_c - \Lambda a^{d_H},\xi;T/a) = G_{ij}\, e^{-b\Lambda^\nu T}. \tag{3.25}$$

For $g < g_c$, $\Delta\lambda_1 = 1 - \lambda_1 \neq 0$. Substituting in (3.16) shows that $\Delta\lambda_1$ satisfies

$$0 = \Delta\lambda^2 + \Delta\lambda\,(\lambda_{2c} - 1 + \mathcal{F}^i_{ij}\Delta f^j) + \partial_i\mathcal{C}(1)\,\Delta f^i + \frac{1}{2}\partial_i\partial_j\mathcal{C}(1)\Delta f^i\Delta f^j + O(\Delta g, (\Delta f)^3), \tag{3.26}$$

where $\partial_i\mathcal{C}(1) \equiv \partial\,\mathcal{C}(1)/\partial f^i$. On the critical surface (i.e. when $\mathcal{C}(1) = 0$) it is straightforward, using (3.17), (3.18), to show that

$$\partial_j\mathcal{C}(1) = (\mathcal{F}^1_2)^{-1}\bar{u}^i_{2c}(u^\ell_{1c}\mathcal{F}^i_{\ell j}),$$

so if the tri-critical condition (3.21) is satisfied, the term linear in Δf^j in (3.26) is actually the same order in Δg as the quadratic term. There are then four possible cases for $\Delta\lambda$ (in each case $b > 0$ is a different ξ-dependent constant):

i. Generic: the system is not tri-critical, and $\lambda_{2c} < 1$. In this case the dimers do not interact strongly enough with the geometry to affect its large scale properties and

$$\Delta\lambda = b(\Delta g)^{\frac{1}{2}} + h.o.t..$$

ii. Degenerate: the system is not tri-critical, *but* $\lambda_{2c} = 1$. We find

$$\Delta\lambda_{1,2} = \pm i\,b(\Delta g)^{\frac{1}{2}\alpha} + h.o.t.. \tag{3.27}$$

iii. Tri-critical I: the system is tri-critical, *and* $\lambda_{2c} = 1$. We find

$$\Delta\lambda_{1,2} = \omega_{1,2}(\Delta g)^{\frac{1}{3}} + h.o.t.,$$

where $\omega_{1,2}$ satisfy

$$0 = \omega^2 - \omega(\mathcal{F}^i_{ij}u^j_{1c}\phi_c) + \frac{1}{2}\partial_i\partial_j\mathcal{C}(1)\,\phi_c^2u^i_{1c}u^j_{1c} + \partial_i\mathcal{C}(1)v^i_{2c},$$

and direct calculation shows that

$$\omega_{1,2} = \frac{3}{2f^1_c}(1 \pm i/\sqrt{3}). \tag{3.28}$$

iv. Tri-critical II: the system is again tri-critical, but $\lambda_{2c} < 1$ which gives

$$\Delta\lambda = b\,(\Delta g)^{\frac{2}{3}} + h.o.t..$$

Next, we turn to the local Hausdorff dimension d_h which is yet another measure of the geometry and is defined as follows. First define the measures $\{\mu_{iN}\}_{i=1}^{2}$ on the space of labelled trees: $\mu_{iN}(\tau, l) := \frac{1}{f^i(N,\xi)} \prod_{v\in\tau\setminus r} \xi_{p(v)}\xi_{q(v)}$, where

$$f^i(N,\xi) := \oint_\gamma \frac{dg}{2\pi i\, g} g^{-2N} f^i(g,\xi),$$

in which γ is a small loop around the origin. The following limit exists $\mu_i := \lim_{N\to\infty} \mu_{iN}$ (see [26]). Only trees with $N+1$ vertices contribute to $f^i(N,\xi)$. Therefore $\mu_i(\tau, l)$ is only supported on infinite trees; in fact it is only trees with a single infinite-spine[1] (as opposed to two or more) which contribute to $\mu_i(\tau, l)$ as shown in [24] – the other infinite trees contribute to the subleading terms in μ_{iN} as $N \to \infty$. So let $\mathcal{A}$ denote the set of trees with a single infinite-spine and let $\mathcal{I}^1 := \{(\tau, l) \in \mathcal{L}_\infty^{(0,0)} : \tau \in \mathcal{A}\}$ and $\mathcal{I}^2 := \{(\tau, l) \in \mathcal{L}_\infty^{(2,0)} : \tau \in \mathcal{A}\}$.

For a given tree, τ, let $B_R(\tau)$ be the set of vertices in τ at or within radius R from the root; and let $|B_R(\tau)|$ denote the size of this set. Then define the expectation value of the number of vertices in a ball of radius R as

$$\langle |B_R| \rangle_{\mu_i} = \sum_{(\tau,l)\in\mathcal{I}^i} \mu_i(\tau, l) B_R(\tau).$$

Expanding in powers of R^{-1}, d_h is then defined as

$$\langle |B_R| \rangle_{\mu_i} = c_i\, R^{d_h}(1 + O(R^{-1})),$$

where c_i is some constant. The value of d_h, in practice, is determined by the structure of $\mathbb{T}$ and the second derivatives $\mathcal{F}^i_{jk}$ at $g = g_c$ and can be computed using the methods of the appendix of [26].

Dimer state	λ_{2c}	α	σ	ν	d_H	d_h
Tri-critical I	1	$\frac{1}{3}$	$\frac{1}{2}$	$\frac{1}{3}$	3	3
Dense-dimer I	1	$\frac{1}{2}$	$-\frac{1}{3}$	$\frac{1}{2}$	2	3
Tri-critical II	< 1	$\frac{1}{3}$	$\frac{1}{2}$	$\frac{2}{3}$	$\frac{3}{2}$	1
Dense-dimer II	< 1	$\frac{1}{2}$	$-\frac{1}{3}$	1	1	1
Pure-gravity	< 1	$\frac{1}{2}$	n/a	$\frac{1}{2}$	2	2

Table 3.1: Exponents and Hausdorff dimensions for the possible phases of the model.

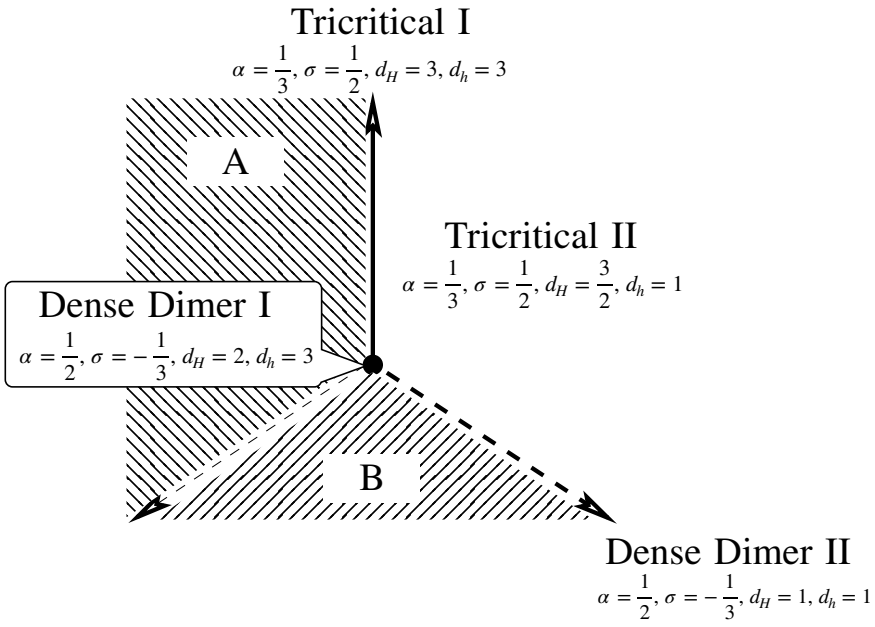

Figure 3.3: The space $\{\xi\}$, restricted to $\xi_1 = \xi_2 = \xi$, showing all the non pure-gravity phases of the model. Note that the shaded regions are not distinct phases.

3.5.4 The Phase Diagram

The full form of the limit surface $\mathcal{S}$ and the phase diagram for general ξ is complicated and not very informative. The regimes that occur in the model and the corresponding values of exponents and Hausdorff dimensions are listed in Table 3.1. Above the limit surface $\mathcal{S}$, the dimers are not critical and the system is in the regular Pure-Gravity phase. Restricting to $\xi_1 = \xi_2 = \xi$, the limit surface is two dimensional and is shown schematically in Fig 3.3. The relative richness of the phase diagram is a consequence of the structure of the CDT graphs enabling us to keep track of different orientations of dimers and assign different fugacities to them – something which cannot be done in the planar random graph case for example. We note the following:

[1] I.e. those trees with only one infinite self-avoiding path starting at the root.

a) The Tri-critical I (TCI) line lies in the plane $\xi_4 = 0$. The degenerate eigenvalues of $\mathbb{T}$ lead to the oscillatory behaviour superimposed on exponential decay of $\mathbb{G}_{ij}(g, \xi; t)$ (see (3.28)), and to $d_H = 3$ which violates the naive scaling prediction $d_H = \frac{3}{2}$. This phase was first identified in [25, 58] and the unexpected Hausdorff dimension in [26].

b) The Tri-critical II (TCII) phase occurs when $\xi_4 < 0$, and represents the generic tri-critical behaviour of the model with Hausdorff dimension $d_H = \frac{3}{2}$. It contains the point with all dimer fugacities equal $\xi_i \simeq -0.1646$ and also the point $\xi_{1,2,3} = 0$, $\xi_4 = -\frac{1}{3}$ for which the restriction (ix) has no effect; we will exploit this in the next section.

c) The Dense-dimer I (DDI) point terminates the TCI line (at $\xi \simeq -0.2267$, $\xi_3 \simeq -0.2781$, $\xi_4 = 0$) and the Dense-dimer II (DDII) line which emerges in the $\xi_4 < 0$ direction.

d) The dimer density exponent for the TC phases, $\sigma = 1/2$, is the same as that found in the model of dimers coupled to planar random graphs [60], and in earlier studies of dimers coupled to CDTs or trees [25, 26, 58]. The planar random graph result was a puzzle because it appears to contradict the KPZ formula [61]; inserting the value for the regular square lattice dimer model, $\sigma = -\frac{1}{6}$ [62], into the KPZ formula gives $\sigma = -\frac{1}{3}$. This phenomenon has been explained in terms of operator mixing between geometric and matter degrees of freedom by [63]. On the other hand, the DD phases do have $\sigma = -\frac{1}{3}$. It appears that with extra dimer fugacities available we can fine-tune so that the coefficient in the mixing vanishes thus revealing the $\sigma = -\frac{1}{3}$ behaviour.

e) In region A, both eigenvalues $\lambda_{1,2} = 1$ at $g = g_c$ but $\Delta\lambda$ is imaginary so the leading behaviour of $\mathbb{G}_{ij}$ is pure oscillatory (due to (3.27)) and d_H does not exist. We can understand why the surface, ξ_D, on which this occurs forms part of $\mathcal{S}$ by considering the flow of $\lambda_{1,2}$ as $g \uparrow g_c$. Holding dimer fugacities ξ_i fixed while varying g through g_c gives the flows shown in Fig. 3.4. For

$\xi_i < \xi_{iD}$, $|\lambda_{1,2}|$ exceeds 1 when $g < g_c$, resulting in exponential growth of correlation functions. As observed in [26] this phenomenon indicates failure of absolute convergence of the series (3.24).

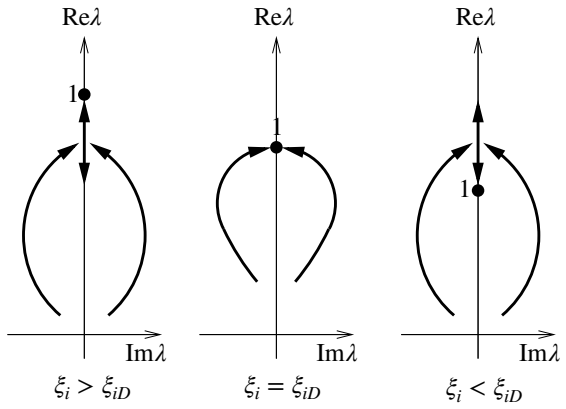

Figure 3.4: Flow of $\lambda_{1,2}$ as $g \uparrow g_c$. The arrows denote the direction of flow as g increases.

f) In region B small graphs dominate so there is no thermodynamic limit and the statistical mechanical interpretation fails.

3.6 Scaling limit of the Cylinder Amplitude

3.6.1 Introduction

We now return to the micro-canonical ensemble of surfaces with fixed temporal extent t. When g, x, y lie inside the joint region of convergence, Γ, of the series (3.1) for $G(g, x, y, \xi; t)$, graphs with large area (number of triangles) and long boundaries are exponentially suppressed. Only when the parameters lie on the boundary of Γ do large graphs contribute to the sum; so the continuum cylinder-amplitude is constructed by generalising the scaling limit (3.25) for the two point function $\mathbb{G}$ as follows. The scaling limit of $\tilde{G}(\cdot)$ is defined as (from now on we will suppress the ξ dependence in the amplitudes, but it remains implicitly through the values of x_c, y_c, f_c^i, g_c etc)

$$\tilde{G}^{s}(\Lambda, L, L'; T) = \lim_{a \to 0} \tilde{G}(g_c - \Lambda a^{d_H}, L/a^{\omega}, L'/a^{\omega}; T/a),$$

where the power $\omega > 0$ is determined as follows. Note that, by (3.2),

$$\tilde{G}^s(\Lambda, L, L'; T) = \lim_{a\to 0} \oint_\gamma \frac{du}{2\pi i u} \oint_\gamma \frac{dv}{2\pi i v}\, u^{L/a^\omega}\, v^{L'/a^\omega}\, G(g_c - \Lambda a^{d_H}, x_c/u, y_c/v; T/a).$$

Changing variables to X, Y defined by

$$\begin{aligned} u =& 1 + a^\omega X, \\ v =& 1 + a^\omega Y, \end{aligned}$$

we obtain[2]

$$\tilde{G}^s(\Lambda, L, L'; T) = \int_{\gamma'} \frac{dX}{2\pi i} \int_{\gamma'} \frac{dY}{2\pi i}\, e^{XL} e^{YL'} G^s(\Lambda, X, Y; T),$$

where γ' is a path from $-i\infty$ to $+i\infty$ running to the right of all singularities of the integrand, and

$$G^s(\Lambda, X, Y; T) = \lim_{a\to 0} a^{2\omega} G(g_c - \Lambda a^{d_H}, x_c(1 - a^\omega X), y_c(1 - a^\omega Y); T/a).$$

For this limit to be non-zero, the denominator in (3.15) must satisfy

$$1 - gx(\xi_2 f_t^2 + (1 + gx\xi_3) f_t^1) = O(a^\omega), \tag{3.30}$$

when expanded about $a = 0$ (we have assumed that the numerator in (3.15) is $O(1)$ which turns out to be the case). At infinite time f_t^i will converge to the fixed point of the evolution equations:

$$f_t^i \xrightarrow{t\to\infty} f^i(g, \xi) = f_c^i(\xi) - a^{\alpha d_H} \Lambda^\alpha \phi_c u_{1c}^i + a^{2d_H\alpha} v_{1c}^i + a^{3d_H\alpha} v_{2c}^i + h.o.t., \tag{3.31}$$

where the last equality follows from (3.20), (3.22), (3.23). However at large times f_t^i will retain memory of the initial conditions (3.11), so we generalize (3.31) away from $t = \infty$ as

$$f_{T/a}^i = f_c^i(\xi) + a^{\alpha d_H} \underbrace{\Lambda^\alpha \phi_c u_{1c}^i\, \rho(\Lambda, Y; T)}_{=: F^i(\Lambda, Y; T)} + a^{2\alpha d_H} v_1^i(\Lambda, Y; T) + a^{3d_H\alpha} v_2^i(\Lambda, Y; T) \tag{3.32}$$

$$+ h.o.t.$$

$$\equiv f_c^i(\xi) + \phi^i(\Lambda, Y; T). \tag{3.33}$$

[2]The inverse of this relation is given by the double Laplace transform:

$$G^s(\Lambda, X, Y; T) = \int_0^\infty dL \int_0^\infty dL'\, e^{-XL} e^{-YL'} \tilde{G}^s(\Lambda, L, L'; T). \tag{3.29}$$

Substituting (3.32) in (3.30), vanishing of the $O(1)$ coefficient in (3.30) determines x_c; and requiring that the $O(a^\omega)$ coefficient include $\rho(\Lambda, Y; T)$ fixes $\omega = d_H \alpha$.

Consider $F^i(\Lambda, Y; T)$ as defined in (3.32); using this in (3.15) we see that

$$G^s(\Lambda, X, Y; T) = -\frac{\partial}{\partial Y} \frac{c_0}{X - c_i F^i(\Lambda, Y; T)}, \tag{3.34}$$

where $c_0 > 0, c_{1,2}$ are constants. If we define the CDT graphs such that the outgoing loop is not marked, the cylinder amplitude, $\tilde{G}^s_U(\Lambda, L, L'; T)$, we get is

$$\tilde{G}^s_U(\Lambda, L, L'; T) = \tilde{G}^s(\Lambda, L, L'; T)/L'. \tag{3.35}$$

Its Laplace transform then gives

$$\begin{aligned} G^s_U(\Lambda, X, Y; T) &:= \int_0^\infty dL \int_0^\infty dL' \; e^{-XL} e^{-YL'} \tilde{G}^s_U(\Lambda, L, L'; T) \\ &= \int_Y^\infty G^s(\Lambda, X, Z; T)\, dZ \\ &= \frac{c_0}{X - F(\Lambda, Y; T)} - \frac{c_0}{X - F(\Lambda, \infty; T)}, \end{aligned} \tag{3.36}$$

where we've defined $F(\cdot) \equiv c_i F^i(\cdot)$ and used (3.35) to get the second line and (3.34) for the last line. In the pure CDT model, where $\xi_i = 0, \forall i$ and $c_0 = 1$, $\tilde{G}^s_U$ satisfies the composition law

$$\tilde{G}^s_U(\Lambda, L, L'; T + T') = \int_0^\infty \tilde{G}^s_U(\Lambda, L, I; T)\, \tilde{G}^s_U(\Lambda, I, L'; T')\, dI, \tag{3.37}$$

or, after a Laplace transform,

$$\begin{aligned} G^s_U(\Lambda, X, Y; T + T') &= \int_{\gamma'} \frac{dZ}{2\pi i} G^s_U(\Lambda, X, Z; T)\, G^s_U(\Lambda, -Z, Y; T') \\ &= \frac{1}{X - F(\Lambda, -F(\Lambda, Y; T'); T)} - \frac{1}{X - F(\Lambda, -F_\infty(\Lambda; T'); T)}, \end{aligned}$$

where we've used (3.36) in the last line and defined $F_\infty(\Lambda; T) \equiv F(\Lambda, \infty; T)$. It follows that

$$F(\Lambda, -F(\Lambda, Y; T'); T) = F(\Lambda, Y; T + T'), \tag{3.38}$$

and, taking $T' \to 0$, that $F(\Lambda, Y; 0) = -Y$. When type 1 dimers are present, the composition law, (3.37), does not have to be satisfied because the dimer configuration

on the intermediate boundary at T must be summed over as well. However, as we will see below, in some phases, the property (3.38) *is* still satisfied and then

$$G^s_U(\Lambda, X, Y; T+T') = c_0^{-1} \int_{\gamma'} \frac{dZ}{2\pi i}\, G^s_U(\Lambda, X, Z; T)\, G^s_U(\Lambda, -Z, Y; T'). \quad (3.39)$$

In these phases, the intermediate dimer configuration sum simply generates the c_0^{-1} prefactor.

We will also compute

$$W(\Lambda, Y) = \int_0^\infty -\frac{\partial F(\Lambda, Y, T)}{\partial Y}\, dT,$$

which is the CDT analogue of the disk amplitude for planar random graph models [58].

3.6.2 The differential equations

Now we show how differential equations satisfied by $\rho(T)$ can be obtained in the different phases. Substituting (3.33) into (3.12) and (3.13) and expanding in powers of a, we find (suppressing the argument of $\phi^i(\Lambda, Y; T)$)

$$\begin{aligned}(1-\mathbb{T})^{ij}\phi^j = &-a\frac{d\phi^i}{dT} - a^2\frac{d^2\phi^i}{2\,dT^2} - \Lambda a^{d_H}\left(\frac{\partial \mathcal{F}^i}{\partial g} + \frac{\partial \mathbb{T}^{ij}}{\partial g}\phi^j\right) + \frac{1}{2}\mathcal{F}^i_{\ell k}\,\phi^\ell\phi^k \\ &+ \frac{1}{3!}\mathcal{F}^i_{k\ell m}\phi^k\phi^\ell\phi^m + O\left(a^{2+\alpha d_H}, a^{d_H+2\alpha d_H}, a^{4\alpha d_H}\right). \end{aligned} \quad (3.40)$$

Substituting (3.32) for ϕ^i and expanding in powers of a, the terms of $O(a^{\alpha d_H+1})$ and $O(a^{\alpha d_H+2})$ lead to a differential equation for $\rho(T)$, $v_1^i(T)$ and $v_2^i(T)$. Actually, in phases where $\lambda_{2c} \neq 1$, it is sufficient just to consider the terms at $O(a^{\alpha d_H+1})$ – leading to a first-order ODE as (3.40) shows – but in phases where $\lambda_{2c} = 1$, the terms at $O(a^{\alpha d_H+1})$ and $O(a^{\alpha d_H+2})$ are both needed, leading to a second-order ODE. Eliminating $v_1^i(T)$ and $v_2^i(T)$ leads to a differential equation for $\rho(T)$. The constants of integration are fixed using the initial conditions (3.11), and provide the Y dependence of ρ. The conditions for the various phases (i)-(iii) and (iii), (iv) cause some coefficients in (3.40) to vanish, which in turn yields different behaviour for ρ. We find (in each case $b > 0$ is a different ξ-dependent constant)

a) Pure-gravity

$$\frac{1}{b\Lambda^{\frac{1}{2}}}\frac{\partial\rho}{\partial T} - \rho^2 + 1 = 0. \tag{3.41}$$

b) Tri-critical II

$$\frac{1}{b\Lambda^{\frac{2}{3}}}\frac{\partial\rho}{\partial T} + \rho^3 + 1 = 0. \tag{3.42}$$

c) Dense Dimer II

$$\frac{1}{b\Lambda}\frac{\partial\rho}{\partial T} + \rho^3 - \rho = 0. \tag{3.43}$$

d) Tri-critical I

$$\frac{1}{b^2\Lambda^{\frac{2}{3}}}\frac{\partial^2\rho}{\partial T^2} - \frac{3}{b\Lambda^{\frac{1}{3}}}\rho\frac{\partial\rho}{\partial T} + 1 + \rho^3 = 0.$$

e) Dense-dimer I

$$\frac{1}{b^2\Lambda}\frac{\partial^2\rho}{\partial T^2} - \frac{3}{b\Lambda^{\frac{1}{2}}}\rho\frac{\partial\rho}{\partial T} - \rho + \rho^3 = 0.$$

3.6.3 PG, TCII and DDII phases

In these phases, only one eigenvalue of $\mathbb{T}$ reaches 1 at the critical point so $\rho(T)$ is determined by a first order differential equation, and the two initial conditions (3.11) are in fact equivalent.

In the PG phase, solving (3.41), we find

$$F(\Lambda, Y; T) \equiv C\Lambda^{\frac{1}{2}}\rho(T) = C\Lambda^{\frac{1}{2}}\frac{C\Lambda^{\frac{1}{2}} - Y - (C\Lambda^{\frac{1}{2}} + Y)\exp 2b\Lambda^{\frac{1}{2}}T}{C\Lambda^{\frac{1}{2}} - Y + (C\Lambda^{\frac{1}{2}} + Y)\exp 2b\Lambda^{\frac{1}{2}}T}, \tag{3.44}$$

where $C = \phi_c c_i u^i_{1c}$. Re-defining $C^2\Lambda \to \Lambda$, $bC^{-1} \to b$, this leads to the disk amplitude

$$W(\Lambda, Y) = \frac{1}{\Lambda^{\frac{1}{2}} + Y},$$

and the cylinder amplitude

$$G^s(\Lambda, X, Y; T) = \frac{c_0\Lambda}{\Big((XY + \Lambda)\sinh b\Lambda^{\frac{1}{2}}T + (X + Y)\Lambda^{\frac{1}{2}}\cosh b\Lambda^{\frac{1}{2}}T\Big)^2}, \tag{3.45}$$

which are the well known amplitudes for the pure CDT model with no other degrees of freedom [2] and apply throughout the pure-gravity phase of the present model (we derived this formula by solving the discrete recurrence relations directly in §2.1.5,

which gave us (3.45) with $c_0 = 1$, see (2.12)). It is straightforward to check that $F(\Lambda, Y; T)$ implies the composition property (3.38) and therefore that G^s_U satisfies the composition law (3.39). This reflects the fact that the dimers, although present unless $\xi_i = 0, \forall i$ (where the discrete model can be solved exactly), are non-critical and generate no long distance correlations in the theory.

In the TCII phase, integrating (3.42), applying the initial conditions and re-defining $C^3\Lambda \to \Lambda$, $bC^{-1} \to b$, gives

$$\exp -3b\Lambda^{\frac{2}{3}}T = \prod_{i=1}^{3}\left(\frac{F(\Lambda, Y; T) + \beta_i\Lambda^{\frac{1}{3}}}{-Y + \beta_i\Lambda^{\frac{1}{3}}}\right)^{\beta_i}, \tag{3.46}$$

where $\beta = (1, e^{i\frac{2\pi}{3}}, e^{-i\frac{2\pi}{3}})$ are the cube roots of 1. While this relation cannot be solved in terms of elementary functions, it is easy to compute the disk amplitude

$$W(\Lambda, Y) = \frac{1}{3\Lambda^{\frac{1}{3}}}\frac{2\Lambda^{\frac{1}{3}} + Y}{\Lambda^{\frac{2}{3}} + Y\Lambda^{\frac{1}{3}} + Y^2},$$

and to check that $F(\Lambda, Y; T)$ still satisfies the composition property. Small and large T expansions are given in §A.2.

In this phase $\omega = d_H\alpha = \frac{1}{2}$ so a typical boundary length L scales as $T^{\frac{1}{2}}$ and the effect of the dimers is to compress the spatial direction rather than induce long range correlations in the temporal direction. An alternative way of seeing this is to observe that the model $\xi_{1,2,3} = 0$, $\xi_4 = -1/3$, lies in this phase – in which case there is no dimer configuration to take account of on the intermediate boundary in the composition law; however, the type 4 dimers correlate spatially adjacent vertices leading to the change in scaling behaviour from pure gravity. The tri-critical point of the 'natural' model, with all ξ_i equal, also lies in the TCII phase which, because of the form of F, cannot have G^s invariant under the inversion I; this cylinder function therefore cannot be representative of the tri-critical phase of the full unrestricted CDT+HD model for which G^s with all ξ_i equal must be I invariant.

In the DDII phase, integrating (3.43), applying the initial conditions and re-defining $C^2\Lambda \to \Lambda$, $bC^{-1} \to b$, gives

$$F(\Lambda, Y; T) = \Lambda^{\frac{1}{2}}\frac{-Y}{\sqrt{Y^2 + (\Lambda - Y^2)\exp -b\Lambda T}}, \tag{3.47}$$

from which

$$W(\Lambda, Y) = \frac{2}{Y(\Lambda^{\frac{1}{2}} + Y)}.$$

It is again straightforward to check that $F(\Lambda, Y; T)$ satisfies the composition property (3.38) and therefore that G^s_U satisfies the composition law. In common with TCII this phase has $\omega = d_H \alpha = \frac{1}{2}$ so a typical boundary length L scales as $T^{\frac{1}{2}}$ but the dimer density is large and again the effect of the dimers is to compress the spatial direction rather than induce long range correlations in the temporal direction.

3.6.4 The TCI and DDI phases

In these phases, both eigenvalues of $\mathbb{T}$ reach 1 at the critical point so $\rho(T)$ is determined by a second order differential equation, and there are two constants of integration to be determined from the initial conditions (3.11).

The TCI Phase

The solution for TCI takes the form

$$F(\Lambda, Y; T) \equiv C\Lambda^{\frac{1}{3}} \rho(T) = -C\Lambda^{\frac{1}{3}} \frac{\sum_{i=1}^{3} c_i \beta_i \exp \beta_i b \Lambda^{\frac{1}{3}} T}{\sum_{i=1}^{3} c_i \exp \beta_i b \Lambda^{\frac{1}{3}} T},$$

where, to ensure that F is real and has the correct behaviour as $T \to \infty$, we must have $c_i \neq 0$ and $c_2 = c_3^*$. Imposing the boundary conditions shows that F must diverge at $T = 0$, which implies that $\sum_i c_i = 0$, and that the $O(T^0)$ term is proportional to Y. After rescaling Λ and T by constants we obtain

$$F(\Lambda, Y; T) = -\Lambda^{\frac{1}{3}} \frac{\sum_{i=1}^{3} (A_c \beta_i Y + \beta_i^2 \Lambda^{\frac{1}{3}}) \beta_i \exp \beta_i \Lambda^{\frac{1}{3}} T}{\sum_{i=1}^{3} (A_c \beta_i Y + \beta_i^2 \Lambda^{\frac{1}{3}}) \exp \beta_i \Lambda^{\frac{1}{3}} T}, \tag{3.48}$$

and

$$W(\Lambda, Y) = \frac{1}{A_c^{-1} \Lambda^{\frac{1}{3}} + Y},$$

where A_c is a ξ-dependent constant encoding the asymmetry under the inversion operation I. We can also solve the discrete recurrence relations (3.11)-(3.14) in the TCI phase exactly, leading to the same conclusion – see §A.3. Note that $F(\Lambda, Y; T)$ does not have the composition property, and that the same result for $W(\Lambda, Y)$ has also been obtained using the classical limit of a multicritical matrix model [58].

Using (3.34), we find the cylinder function

$$G^s(\Lambda, X, Y; T) = \frac{c_0 A_c F'_\infty(\Lambda; T)}{\left((X - F_\infty(\Lambda; T))\,(A_c Y - F_\infty(\Lambda; T)) - F'_\infty(\Lambda; T)\right)^2}, \quad (3.49)$$

where prime is differentiation w.r.t T. Performing the inverse Laplace transform

$$\tilde{G}^s(\Lambda, L_1, A_c L_2; T) = \\ c_0 \exp((L_1 + L_2) F_\infty(\Lambda; T)) \sqrt{L_1 L_2 F'_\infty(\Lambda; T)}\, I_1\left(2\sqrt{L_1 L_2 F'_\infty(\Lambda; T)}\right) \quad (3.50)$$

where $I_1(x)$ is the modified Bessel function of the first kind. The r.h.s. is symmetric between L_1 and L_2; so $\tilde{G}^s$ is invariant under the inversion operator I for dimer fugacities such that $A_c = 1$.

Asymptotic Behaviour

Although the form of (3.50) applies to both PG and TCI phases, the physical behaviour is quite different. Taking $T \to 0$ for PG gives

$$\tilde{G}^s(\Lambda, L_1, L_2; 0) = L_1 \delta(L_1 - L_2),$$

which is a consequence of the composition law. For TCI, the pole in F_∞ leads to the small T behaviour

$$\tilde{G}_s \sim \exp\left(-2T^{-1}(L_1 + L_2 - \sqrt{2L_1 L_2})\right). \quad (3.51)$$

With L_1 fixed, the argument of the exponential above is maximum at $L_2 = L_1/2$ so, for small T, the length of the final boundary is forced to be half the length of the initial boundary. This slightly non-intuitive behaviour is driven by the negative dimer weights and demonstrates how the TCI phase does not satisfy the composition law.

Conversely, at large T

$$\tilde{G}^s \sim 3\Lambda^{2/3} L_1 L_2 e^{-3\Lambda^{1/3} T/2} \exp\left(-\Lambda^{1/3}(L_1 + L_2)\right) \\ \times \left(-\cos(\sqrt{3}\Lambda^{1/3} T/2) + \sqrt{3}\sin(\sqrt{3}\Lambda^{1/3} T/2)\right).$$

This has the same functional form of dependence on L_1, L_2 as PG, but oscillates at large T, whereas for PG it decays exponentially without oscillation and is always positive [2].

The average length of the final boundary of universes of temporal extent T with initial boundary length L_1 can be defined as [2]

$$\langle L_2\rangle_{L_1,T} = \frac{\int_0^\infty \tilde{G}^s(\Lambda, L_1, L, T)\, L\, dL}{\int_0^\infty \tilde{G}^s(\Lambda, L_1, L, T)\, dL}.$$

For small T, in the TCI phase

$$\langle L_2\rangle_{L_1,T} = L_1/2 + T + \text{h.o.t.},$$

which is consistent with the discussion above. For large T,

$$\begin{aligned}\langle L_2\rangle_{L_1,T} =& \frac{3}{2}\Lambda^{-1/3} + \\ & \frac{3}{4}e^{-3\Lambda^{1/3}T/2}\left(\left(3L_1 - 4\Lambda^{-1/3}\right)\sqrt{3}\sin(\frac{\sqrt{3}\Lambda^{1/3}T}{2}) - 3L_1\cos(\frac{\sqrt{3}\Lambda^{1/3}T}{2})\right) \\ & + h.o.t..\end{aligned}$$

So for late times it oscillates as it approaches $\frac{3}{2}\Lambda^{-1/3}$ exponentially, whereas the pure gravity case approaches a constant value exponentially without oscillations.

The DDI phase

The solution for DDI takes the form

$$F(\Lambda, Y; T) \equiv C\Lambda^{\frac{1}{2}}\rho(T) = -C\Lambda^{\frac{1}{2}}\frac{c_+ \exp b\Lambda^{\frac{1}{2}}T - c_- \exp -b\Lambda^{\frac{1}{2}}T}{1 + c_+ \exp b\Lambda^{\frac{1}{2}}T + c_- \exp -b\Lambda^{\frac{1}{2}}T};$$

and similar considerations to TCI lead to the disk amplitude

$$W(\Lambda, Y) = \frac{1}{\Lambda^{\frac{1}{2}} + Y},$$

and the cylinder amplitude

$$\begin{aligned}\tilde{G}^s(\Lambda, L_1, L_2; T) =& \sqrt{\Lambda L_1 L_2/2}\,\mathrm{csch}(\sqrt{\Lambda}T) \\ & \times \exp\left(-\sqrt{\Lambda}(L_1 + L_2)\coth(\sqrt{\Lambda}T)\right) I_1\left(\sqrt{2\Lambda L_1 L_2}\,\mathrm{csch}(\sqrt{\Lambda}T)\right).\end{aligned} \tag{3.52}$$

These are almost the same as in the PG phase – the only difference is that the argument of I_1 is $\sqrt{2}$ times smaller (see (2.15)). So the small T behaviour is the same as TCI (3.51) and no amount of rescaling in (3.52) can bring it into PG form. This in particular means that, again, the composition law does not hold.

Note that the DDI point lies at $\xi_4 = 0$; therefore the discrete recurrence relations in the DDI phase can be solved exactly, using the methods in §A.3, which, in the scaling limit, gives the same results as calculated above for the disk and cylinder functions.

3.7 Time evolution operators

We showed in §2.1.6 that there exists a Hamiltonian H, in the PG phase, such that $\partial_T \tilde{G}^s(\Lambda, L_1, L_2; T) = -H\tilde{G}^s(\Lambda, L_1, L_2; T)$. It turns out that this continues to be true in the TCII, DDII phases but not in the TCI, DDI phases. In the TCI, DDI phases, the lack of a Hamiltonian depending only on the length, L, is because the dimers cause strong correlations in the temporal direction, so the states in the continuum Hilbert space depend, not just on the length of the spatial universes, but also on some appropriate continuum dimer degree of freedom.

From (3.34) it follows that

$$\begin{aligned}\partial_T\, G^s(\Lambda, X, Y; T) &= -\,\partial_Y \left(\frac{c_0\, \partial_T F(\Lambda, Y; T)}{(X - F(\Lambda, Y; T))^2} \right) \\ &= \partial_Y \left(\frac{\partial_T F(\Lambda, Y; T)}{\partial_Y F(\Lambda, Y; T)} G^s(\Lambda, X, Y; T) \right).\end{aligned}$$

Assuming the composition property of F (3.38), (which holds in PG,TC2 and DD2), we obtain

$$\frac{\partial_T F(\Lambda, Y; T)}{\partial_Y F(\Lambda, Y; T)} = -\partial_T F(\Lambda, Y; T)|_{T=0}. \tag{3.53}$$

Evaluating this using (3.44)-(3.47) gives

$$\begin{aligned}\partial_T\, G^s(\Lambda, X, Y; T) &= \partial_Y \left(b(\Lambda - Y^2)\, G^s(\Lambda, X, Y; T \right), \\ \partial_T\, G^s(\Lambda, X, Y; T) &= \partial_Y \left(b(\Lambda - Y^3)\, G^s(\Lambda, X, Y; T) \right), \\ \partial_T G^s(\Lambda, X, Y; T) &= \partial_Y \left(b(\Lambda Y - Y^3)\, G^s(\Lambda, X, Y; T) \right),\end{aligned}$$

for pure-gravity [2], TCII, and DDII respectively. Substituting this in (3.29) and integrating by parts shows that

$$\begin{aligned} H_{PG} &= -L\partial_L^2 + L\Lambda, \\ H_{TCII} &= -L\partial_L^3 + L\Lambda, \\ H_{DDII} &= -L\partial_L^3 + L\Lambda\partial_L. \end{aligned}$$

Only the PG operator is self-adjoint (with the measure $L^{-1}dL$), the non-self-adjoint nature of the operators for TCII and DDII reflecting the negative dimer weights in the partition sum. For TCI and DDI the right hand side of (3.53) diverges which reflects the fact that the composition property does not hold and the sum over the intermediate dimer configuration must be taken fully into account. In fact one could take the converse point of view; namely that, because we expect the critical dimers to induce correlations in the T direction, $\partial_T F$ *must* diverge at $T = 0$. Of course the left hand side of (3.53) exists and is finite for $T > 0$ but it is T dependent so there is no time-independent evolution operator for these phases.

3.8 Discussion

In this work we have extended previous solutions of the hard dimer model on causal triangulations to allow all types of dimer on the graphs, and by removing all but one of the constraints imposed. The only constraint remaining in our work is – in the language of labelled trees – that it is forbidden for a last child to take label $p = 3$ (see (ix) in §3.3). This constraint is sufficient to render the tree model local, in the sense that there are no correlations between vertices at the same height that are not siblings, and hence exactly solvable. The model has a number of phases, depending upon the dimer weights ξ, which are all controlled by the quadratic and cubic critical points of a polynomial. The remaining question is whether our calculation is sufficiently general that, even if the last constraint were removed, no further critical point with distinct properties would appear.

The TCII and DDII phases obey the naive composition law because the dimers are correlated in the spatial direction but not strongly so in the T direction. As

the constraint affects spatially neighbouring dimers only, it seems unlikely that its removal will cause the correlations in the T direction to change; indeed our solution is exact for the $\xi_{1,2,3} = 0, \xi_4 = -1/3$, TCII model which is unaffected by the constraint. So we expect that the TCII phase will survive for some ξ, but that its boundaries will move; the same applies to the DDII phase as it appears on the boundary of TCII. However, $G^s(\Lambda, X, Y; T)$ can never be inversion symmetric because of (3.46) and (3.47); if the $\xi_3 = \xi_4$ tri-critical points lie in TCII in the unconstrained model, then $G^s(\Lambda, X, Y; T)$ must be modified.

The TCI and DDI phases have strong dimer-induced correlations in both temporal and spatial directions. This is reflected in the appearance of the second unit eigenvalue at criticality, isotropic scaling, and a cylinder function that does not obey the naive composition law. The appearance of the second eigenvalue should be robust against removal of the constraint. When $\xi_3 = \xi_4$, the full unconstrained model satisfies the inversion symmetry so $G^s(\Lambda, X, Y; T) = G^s(\Lambda, Y, X; T)$ which is satisfied by (3.49) whenever the asymmetry parameter $A_c = 1$. Provided a completely new phase does not appear, we expect that TCI does characterize the tri-critical physics of the full unconstrained but inversion-symmetric model.

On a fixed space-time lattice, the critical point of the hard dimer model corresponds to a conformal field theory with central charge $c = -\frac{22}{5}$ which also describes the Yang-Lee edge singularity [62]. On the other hand, the scaling limit of pure CDT is two-dimensional projectable Hořava-Lifshitz gravity as shown in [27]. We therefore expect that each scaling limit found here corresponds somehow to a CFT coupled to Hořava-Lifshitz gravity, and in particular that one of them is the Yang-Lee singularity. Now, when a lattice model whose critical dynamics is described by a CFT is coupled to DT, the matter exponents are shifted according to the KPZ formula [61], and the geometry of the gravity sector is changed. For $c > 1$ the interaction between matter and geometry is so strong that the space degenerates into a branched polymer structure. As c is decreased from one, the interaction becomes steadily weaker until at $c = -\infty$ matter exponents are unchanged from fixed lattice values and the space is smooth and flat and two-dimensional. Numerical evidence

suggests that the behaviour of CDT is rather different, with weaker interaction between matter and geometry, and in particular that $d_H = 2$ when $0 \leq c < 1$; at $c = -\infty$ we again expect to find that space is smooth flat and two-dimensional. The phase with the least back-reaction from the dimers onto the geometry is DDI. It has $d_H = 2$ as the pure gravity phase; the fact that the local Hausdorff dimension $d_h = 3$, rather than $d_h = 2$, is not observable in the scaling limit (but it is a signature that there is local interaction between dimers and geometry). The disk amplitude is the same as for pure gravity, and the cylinder amplitude alone, of the geometrical observables, betrays the presence of the dimers. As discussed in §3.5.4, the dimer exponent is shifted from its fixed lattice value, $\sigma = -\frac{1}{6}$, to $\sigma = -\frac{1}{3}$ as predicted by the KPZ formula. The fine tuning needed to get this rather than $\sigma = \frac{1}{2}$, as seen in TCI, precisely decouples the dimer degrees of freedom from the geometry and turns off the operator mixing discussed by [63]. These arguments all point to the scaling limit of the DDI phase being the Yang-Lee edge singularity coupled to CDT.

4

ϕ_2^4 Kink radius

Contents

4.1 Introduction

Given a particle state $|p^\mu\rangle$, a form factor is given by $\langle p'|\,\mathcal{O}\,|p\rangle$ for some operator $\mathcal{O}$. A form factor, when expanded in powers of the momentum transfer, $p' - p$, reveals information about the internal structure of the particle in question. With different operators $\mathcal{O}$, one can probe different aspects of the internal structure. This work arose from the question of whether there exists a lower bound on the radius of a generic bound-state in QFT [4].

As discussed in the introduction, §1.2, our goal will be to calculate the radius of the ϕ_2^4 kink by computing $\langle p'|\,T^{00}\,|p\rangle$, where $|p\rangle$ is the soliton state.

The layout of this chapter is as follows. In §4.2, §4.3, we discuss shift operators, soliton operators and soliton states. In §4.4 we comment on the similarity of these soliton operators with an old result of Mandelstam [64] in sine-Gordon theory. In §4.5, we calculate $\langle p'| T^{00} |p\rangle$ through to 1-loop order and extract the first quantum correction to the kink radius.

4.2 Shift Operators

Consider a QFT of one real scalar ϕ in $d+1$ dimensions; let x denote spacetime positions $(t, \boldsymbol{x})$. The orthonormal basis states of the Hilbert space are $|f\rangle_\phi$, which are eigenstates of ϕ: $\phi(\boldsymbol{x})\,|f\rangle_\phi = f(\boldsymbol{x})\,|f\rangle_\phi$. Similarly, there is a dual orthonormal basis $|g\rangle_\pi$ of eigenstates of π: $\pi(\boldsymbol{x})\,|g\rangle_\pi = g(\boldsymbol{x})\,|g\rangle_\pi$.

Let $B = \exp(-i\int \pi(\boldsymbol{x})g(\boldsymbol{x})d^d\boldsymbol{x})$; from the canonical commutation relations,

$$B^{-1}\phi(\boldsymbol{x})B = \phi(\boldsymbol{x}) + g(\boldsymbol{x}),$$

from which it follows that $B\,|f\rangle_\phi = c\,|f+g\rangle_\phi$; this in turn implies that

$${}_\phi\langle f|\exp(-i\int \pi(\boldsymbol{x})g(\boldsymbol{x})d^d\boldsymbol{x})\,|F\rangle = c^*\,F[f-g],$$

where $|F\rangle$ is a some state and $F[f] := {}_\phi\langle f|F\rangle$ (a functional). Taylor expanding the LHS and RHS in powers of g shows that $\pi(\boldsymbol{x})$ acts on functionals as $-i\delta/\delta f(\boldsymbol{x})$ and that $c = 1$. Therefore

$$\exp\left(-i\int \pi(\boldsymbol{x})g(\boldsymbol{x})d^d\boldsymbol{x}\right)|f\rangle_\phi = |f+g\rangle_\phi\,. \tag{4.1}$$

Similarly, one can show that

$$\exp\left(i\int \phi(\boldsymbol{x})g(\boldsymbol{x})d^d\boldsymbol{x}\right)|f\rangle_\pi = |f+g\rangle_\pi\,.$$

These are the so-called 'shift operators'. We will use them to define soliton operators.

4.3 Soliton States and Operators

Let spacetime be $d+1$ dimensional Minkowksi; let $\boldsymbol{x}$ denote spatial positions and x denote spacetime positions. Consider a real, interacting scalar field $\phi(\boldsymbol{x})$.

Let the classical equations of motion possess a soliton solution. This means that there exist initial data $\phi^{\boldsymbol{p}}_{cl}(\boldsymbol{x})$ and $\pi^{\boldsymbol{p}}_{cl}(\boldsymbol{x})$ such that the energy density doesn't dissipate under classical time evolution, where $\boldsymbol{p}$ here is the classical momentum of the soliton. The soliton creation operator (first written down by Cahill [19]) is

$$\mathcal{O}_{\boldsymbol{p}}(\boldsymbol{x}) = \exp\left(-i\int \pi(\boldsymbol{x}+\boldsymbol{a})\phi^{\boldsymbol{p}}_{cl}(\boldsymbol{a})d^d\boldsymbol{a} + i\int \phi(\boldsymbol{x}+\boldsymbol{a})\pi^{\boldsymbol{p}}_{cl}(\boldsymbol{a})d^d\boldsymbol{a}\right), \tag{4.2}$$

and the destruction operator is $\mathcal{O}_{\boldsymbol{p}}(\boldsymbol{x})^\dagger$. Note that the Baker-Campbell-Hausdorff formula allows (4.2) to be written as the product of exponentials times a constant.

If $\boldsymbol{p}=0$, we will drop the label $\boldsymbol{p}$ for ease. Now consider how $\mathcal{O}(\boldsymbol{x})$ transforms under a rotation $\boldsymbol{R}$. Let's assume that $\phi_{cl}(\boldsymbol{x})$ and $\pi_{cl}(\boldsymbol{x})$ are centered on $\boldsymbol{x}=0$ and are spherically symmetric. Then

$$U(\boldsymbol{R})\mathcal{O}(\boldsymbol{x})U^{-1}(\boldsymbol{R}) = \mathcal{O}(\boldsymbol{R}\boldsymbol{x}), \tag{4.3}$$

where $U(\Lambda, a^\mu)$ is the unitary operator acting on states, when there is a Poincaré transformation (Λ, a^μ). Similarly, for a translation $\boldsymbol{a}$,

$$U(\boldsymbol{a})\mathcal{O}(\boldsymbol{x})U^{-1}(\boldsymbol{a}) = \mathcal{O}(\boldsymbol{x}+\boldsymbol{a}). \tag{4.4}$$

As we said in the introduction, §1.2, an eigenstate of the Hamiltonian can be constructed by preparing a state at $t=0$ and time translating it to past Euclidean infinity. The state at $t=0$ can be thought of as a proxy to the exact state. Because time translation commutes with P_i and J_{ij} (the spatial-momentum and angular-momentum generators), the proxy state must already have good spatial-momentum and angular-momentum quantum numbers. Further, the exact state (if it contains several particles) inherits the exchange statistics of the proxy state. In conventional field theory (where one is interested in elementary particles), proxy states are Fock

states. Given a suitable proxy $|n,\sim\rangle$, the exact state $|n\rangle$ is[1]

$$|n\rangle = \lim_{T\to\infty} e^{ET} e^{-HT} |n,\sim\rangle \,/\, \langle n|n,\sim\rangle \,, \tag{4.5}$$

where E is the energy $H|n\rangle = E|n\rangle$. (4.5) projects the proxy state onto the lowest-energy exact-state (with non-vanishing overlap with the proxy-state) with the spatial-momentum and angular-momentum quantum numbers of the proxy-state. We should note that (4.5) avoids Haags theorem [65]. Haags theorem asserts that the proxy state cannot be unitarily related to the exact state; but because e^{-HT} is not unitary, this need not trouble us. The factor $\langle n|n,\sim\rangle^{-1}$ ensures $|n\rangle$ is normalized to unity. The factor e^{ET} amputates external legs.[2] Though (4.5) looks like it is in Euclidean signature, it is actually physical.[3]

Here, we are trying to construct a 1-particle soliton state. It is enough to construct the rest-state, from which the moving states can be obtained by a boost. Let $k^\mu = (M, 0, ..., 0)$ be the rest momentum and let $|k,\sim\rangle$ be the proxy to the rest-state. It is [19]

$$|k,\sim\rangle = \int d^d\boldsymbol{x}\ \mathcal{O}(\boldsymbol{x})\,|\Omega,\sim\rangle \,, \tag{4.6}$$

with

$$|\Omega,\sim\rangle = |\phi(\boldsymbol{x}) = \phi_0\rangle_\phi \,, \tag{4.7}$$

[1]This follows from inserting a complete set of energy eigenstates and picking out the state with lowest energy and non-vanishing overlap with $|n,\sim\rangle$.

[2]For a simple demonstration of this, imagine $|n,\sim\rangle$ was a Fock state. Then e^{ET} is equivalent to $e^{H_0 T}$ since H_0 is assumed to have the same spectrum as H ([6] Sec 3.1). Then the difference between H and H_0 will contain the difference between the bare mass (contained in H) and the exact mass (contained in H_0). These interaction vertices will then completely remove radiative corrections.

[3]As an example, consider ϕ^4 theory in 3+1 dimensions. Let $\langle m|n\rangle$ be a scattering amplitude, with $|n,\sim\rangle = \prod_{i=1}^n a^\dagger_{\boldsymbol{k}_i}|0\rangle$ and $|m,\sim\rangle = \prod_{j=1}^m a^\dagger_{\boldsymbol{p}_j}|0\rangle$. Using (4.5), we get

$$\langle m|n\rangle = C\int[d\phi]e^{-S[\phi]}\int\prod_{i=1}^n d^4x_i e^{i\boldsymbol{k}_i\boldsymbol{x}_i - E_{\boldsymbol{k}_i}x_i^0}\Box_{x_i}\phi(x_i)\int\prod_{j=1}^m d^4y_j e^{-i\boldsymbol{p}_j\boldsymbol{y}_j + E_{\boldsymbol{p}_j}y_j^0}\Box_{y_j}\phi(y_j),$$

where $C = \langle n|n,\sim\rangle^{-1}\langle m,\sim|m\rangle^{-1}$, $\Box_x \equiv (\partial^2_{x^0} + \boldsymbol{\nabla}^2_{\boldsymbol{x}} - m^2)$, $E_{\boldsymbol{k}} = \sqrt{\boldsymbol{k}^2+m^2}$ and $S = \int d^4x(\dot\phi^2 + (\boldsymbol{\nabla}\phi)^2 + m^2\phi^2)/2 + \lambda\phi^4$. Upto the factor C, you will recognise this as the amputated, Euclidean Greens function $G_E(k_1,...,k_n;-p_1,...,-p_m)$ with $k_i = (iE_{\boldsymbol{k}_i}, \boldsymbol{k}_i)$ and $p_j = (iE_{\boldsymbol{p}_j}, \boldsymbol{p}_j)$. The net result is that the external momenta are in Lorentz signature and that the loop-momenta (i.e. unfixed momenta) are in Euclidean signature, which is exactly the prescription used to calculate physical amplitudes. Further, the missing factors of i in the Feynman rules only affect the amplitude by an overall factor of i ([12] Sec. 4.8).

(in the notation of the previous section) where ϕ_0 is the minimum of the classical potential. $|\Omega, \sim\rangle$ is a proxy state to the true vacuum state, $|\Omega\rangle$, since it has zero spatial-momentum and angular-momentum quantum numbers.

From (4.3), (4.4), it follows that $|k, \sim\rangle$ has zero spatial and angular momentum. The exact state $|k\rangle$ is then

$$|k\rangle = \text{const.} \frac{\lim_{T\to\infty} e^{MT} e^{-HT} |k, \sim\rangle}{\langle k|k, \sim\rangle}, \tag{4.8}$$

where M is the pole-mass of the particle (i.e. renormalized and quantum corrected) and 'const.' allows for the possibility of adopting some different convention for the normalization of the particle state.

The moving state $|p\rangle$ is

$$|p\rangle = U(\Lambda) |k\rangle ,$$

where $\Lambda : k \to p$. Note that this definition is self-consistent: if we choose a different boost $\Lambda' : k \to p$, it will be related to Λ by a rotation and rotations leave $|k\rangle$ unchanged. It seems likely, though we can't prove it, that the moving state, $|p\rangle$, has the state

$$|p, \sim\rangle = \int d^d \boldsymbol{x}\ e^{i\boldsymbol{p}.\boldsymbol{x}} \mathcal{O}_{\boldsymbol{p}}(\boldsymbol{x}) |\Omega, \sim\rangle \tag{4.9}$$

as its proxy; i.e. that $|p\rangle$ can be obtained by applying the limiting procedure to (4.9). A similar phenomenon happens for elementary particle states – there one has to prove that $U(\Lambda) \lim_{T\to\infty} e^{E_p T} e^{-HT} a_p^\dagger |0\rangle = \text{const.} \times \lim_{T\to\infty} e^{E_{\Lambda p} T} e^{-HT} a_{\Lambda p}^\dagger |0\rangle$ where $E_p = \sqrt{\boldsymbol{p}^2 + m^2}$.

We note, as a consequence of the canonical commutation relations that the solitons operators cause a shift by the classical configurations:

$$\mathcal{O}_{\boldsymbol{p}}(\boldsymbol{x})^{-1} \phi(\boldsymbol{y}) \mathcal{O}_{\boldsymbol{p}}(\boldsymbol{x}) = \phi(\boldsymbol{y}) + \phi_{cl}^{\boldsymbol{p}}(\boldsymbol{y} - \boldsymbol{x}),$$
$$\mathcal{O}_{\boldsymbol{p}}(\boldsymbol{x})^{-1} \pi(\boldsymbol{y}) \mathcal{O}_{\boldsymbol{p}}(\boldsymbol{x}) = \pi(\boldsymbol{y}) + \pi_{cl}^{\boldsymbol{p}}(\boldsymbol{y} - \boldsymbol{x}).$$

The reason why the soliton operators take the form (4.2) is as follows. Consider the matrix element $\langle\psi_{out}|\, e^{-2HT}\mathcal{O}(\boldsymbol{x}_0)\,|\psi_{in}\rangle$. Transforming to the path integral, this is equal to

$$\int [d\phi][d\pi]\psi^*_{out}[\phi]\,\psi_{in}[\phi]\,e^{S'[\phi,\pi]}, \tag{4.10}$$

where

$$S' = S - i\int \pi(-T,\boldsymbol{x}_0+\boldsymbol{a})\phi_{cl}(\boldsymbol{a})d^d\boldsymbol{a} + i\int \phi(-T,\boldsymbol{x}_0+\boldsymbol{a})\pi_{cl}(\boldsymbol{a})d^d\boldsymbol{a}$$

and $S = \int_{-T}^{T} dt \int d^d\boldsymbol{x}\left(i\pi\dot{\phi} - \mathcal{H}(\pi,\phi)\right)$.

If we try evaluating (4.10) perturbatively, we will end up summing an infinite number of tree diagrams because the 'free' part of S' contains terms linear in the fields. These tree diagrams actually sum up to the classical background [66–68] which is determined by the equations of motion of S' ($\delta S'/\delta\phi = \delta S'/\delta\pi = 0$):

$$i\,\dot{\pi}(x) = i\,\delta(t+T)\pi_{cl}(\boldsymbol{x}-\boldsymbol{x}_0) - \frac{\partial\mathcal{H}}{\partial\phi(x)}, \tag{4.11}$$

$$i\,\dot{\phi}(x) = i\,\delta(t+T)\phi_{cl}(\boldsymbol{x}-\boldsymbol{x}_0) + \frac{\partial\mathcal{H}}{\partial\pi(x)}. \tag{4.12}$$

Note that the usual background $\phi = \pi = 0$ is not a solution. To build a solution, consider initial data $\phi(\boldsymbol{x}) = \pi(\boldsymbol{x}) = 0$ at a very early time slice. Then at $t = -T$ there is an abrupt jump to values $\phi_{cl}(\boldsymbol{x}-\boldsymbol{x}_0)$ and $\pi_{cl}(\boldsymbol{x}-\boldsymbol{x}_0)$ respectively and then there is standard evolution (i.e. governed by S). In other words, let $\phi_{cl}(t,\boldsymbol{x})$ and $\pi_{cl}(t,\boldsymbol{x})$ be the solutions to the *unsourced* EOM (i.e. the EOM derived from S) such that $\phi_{cl}(-T,\boldsymbol{x}) = \phi_{cl}(\boldsymbol{x})$ and $\pi_{cl}(-T,\boldsymbol{x}) = \pi_{cl}(\boldsymbol{x})$ is an initial condition. Then the solution to (4.11), (4.12) is

$$\phi(x) = \theta(t+T)\phi_{cl}(t,\boldsymbol{x}-\boldsymbol{x}_0),$$
$$\pi(x) = \theta(t+T)\pi_{cl}(t,\boldsymbol{x}-\boldsymbol{x}_0).$$

The step function here is the analogue of the sudden gauge jumps in t'Hooft's model [69] and indicate the creation of a soliton at $t = -T$.

4.4 Mandelstam's Operators

In this section, we will show that $\mathcal{O}_p(x)$, (4.2), written in the infinite-momentum-frame ($p \to \infty$) for sine-Gordon (SG) solitons is almost the same as Mandelstam's soliton creation operators [64]. In this section and the next, x is the spatial position and $x^\mu = (t, x)$ is the 2-vector.

sine-Gordon theory is a real scalar in 1+1 dimensions with Lagrangian

$$\mathcal{L} = \frac{1}{2}(\partial_\mu \phi)^2 + \frac{\mu^2}{\beta^2}\cos(\beta\phi) - \frac{\mu^2}{\beta^2}.$$

The basic soliton solution is time-independant and centered on $x = 0$:

$$g(x) = \frac{2\pi}{\beta} - \frac{4}{\beta}\arctan\exp\mu x.$$

This is a kink that interpolates from $2\pi/\beta$ at $x = -\infty$ to 0 at $x = \infty$. Now consider the boosted solution

$$g^{(v)}(t, x) := g(\gamma x + \gamma v t),$$

where $\gamma = (1 - v^2)^{-1/2}$. Correspondingly

$$\dot{g}^{(v)}(t, x) = \gamma v g'(\gamma x + \gamma v t).$$

Therefore the initial data for the moving soliton is $\phi_{cl}^{(v)}(x) = g(\gamma x)$ and $\pi_{cl}^{(v)}(x) = \gamma v g'(\gamma x)$. We will now pass to the infinite momentum frame. Consider the limits $v \to \pm 1$:

$$\phi_{cl}^{(\pm 1)}(x) = \lim_{v\to\pm 1} g(\gamma x) = \frac{2\pi}{\beta}\theta(-x),$$
$$\pi_{cl}^{(\pm 1)}(x) = \lim_{v\to\pm 1} \gamma v g'(\gamma x) = \mp\frac{2\pi}{\beta}\delta(x),$$

where θ is the step function. Now use this in (4.2) to get the soliton creation operator in this frame:

$$\mathcal{O}_\pm(x) = \exp i\int_{-\infty}^{\infty} da \left(\mp\frac{2\pi}{\beta}\delta(a)\phi(x+a) - \frac{2\pi}{\beta}\theta(-a)\pi(x+a)\right).$$

Mandelstam's operators [64] on the other hand are

$$\psi_\pm(x) = \exp i\left(\mp\frac{\beta}{2}\phi(x) - \frac{2\pi}{\beta}\int_{-\infty}^{x} da\,\dot{\phi}(a)\right). \tag{4.13}$$

Mandelstam proved that $\psi(x) = (\psi_+(x), \psi_-(x))^T$ is equivalent to the Thirring field for all β.

The only difference between $\mathcal{O}_\pm$ and $\psi_\pm$ is the factor of $2\pi/\beta$ with $\beta/2$ in front of ϕ. At $\beta^2 = 4\pi$, however, $2\pi/\beta = \beta/2$, so $\mathcal{O}_\pm = \psi_\pm$. By construction, $\mathcal{O}_\pm$ is the soliton operator for all β, so using Mandelstam's result, it follows that *only* at $\beta^2 = 4\pi$ is the SG soliton the same as the Thirring fermion. Our result is in agreement with Skyrme [70] (see eq. 31) who constructs a soliton operator that is identical to our $\mathcal{O}_\pm$, and that leads him to the same conclusion that the SG soliton is the Thirring fermion only when $\beta^2 = 4\pi$.

The classic result of Coleman [71] (and later others [72]) is that $e^{\pm i\beta\phi}$ in the SG model is equivalent to $\bar{\psi}(1 \pm \gamma_5)\psi$ in the Thirring model for all β (which actually follows from Mandelstam's (4.13) after some algebra). What the Coleman/Mandelstam results show is that there *is* a duality between the SG and Thirring models *for all* β, specifically between the operator $\psi_\pm$ in (4.13) and the Thirring field; what our result shows, however, is that $\psi_\pm$ doesn't describe the SG *soliton*, except at $\beta^2 = 4\pi$.

4.5 ϕ_2^4

The Hamiltonian of the $1+1$ dimensional ϕ^4 model is

$$H(\pi,\phi) = \int \frac{1}{2}\left(\pi^2 + \phi'^2 - (m^2+\delta_{m^2})\phi^2 + \frac{\lambda^2}{2}(m^2+\delta_{m^2})^2 + \frac{\phi^4}{2\lambda^2}\right)dx + C$$

(note the unusual coupling λ^{-2} instead of λ). λ has mass dimension -1. m stands for the renormalized mass parameter. We now set $m = 1$ and work instead with

$$H(\pi,\phi) = \int \frac{1}{2}\left(\pi^2 + \phi'^2 - (1+\delta_{m^2})\phi^2 + \frac{\lambda^2}{2}(1+\delta_{m^2})^2 + \frac{\phi^4}{2\lambda^2}\right)dx + C; \tag{4.14}$$

at the end it will be quite easy to restore factors of m on the basis of dimension counting. The reason we set $m = 1$ is so that we can import the 'Feynman rules' that [30] calculated with $m = 1$. The mass counterterm is

$$\delta_{m^2} = \frac{3}{4\pi\lambda^2}\int \frac{dk}{\sqrt{k^2+2}}. \tag{4.15}$$

C is a constant that has to be adjusted so that $H\,|\Omega\rangle = 0$, where $|\Omega\rangle$ is the vacuum. Therefore

$$C = -\langle\Omega|\,\frac{1}{2}\int dx\left(\pi^2+\phi'^2-(1+\delta_{m^2})\phi^2+\frac{\lambda^2}{2}(1+\delta_{m^2})^2+\frac{\phi^4}{2\lambda^2}\right)|\Omega\rangle\,.$$

Its value will be calculated in §B.3. We should note that

$$\phi_{cl}\propto\lambda, \qquad M_0\propto\lambda^2, \qquad \delta_{m^2}\propto\lambda^{-2},$$

where $M_0 = 2\sqrt{2}\lambda^2/3$ is the classical mass of the kink (see (2.22)). The pole-mass of the kink will be denoted by M.

4.5.1 Form Factors

The one-particle normalization conditions that we adopt are ([73] Sec. 2.4.1)

$$\langle k|k'\rangle = 4\pi k^0\,\delta(k-k'), \tag{4.16}$$

$$U(\Lambda)\,|k\rangle = |\Lambda k\rangle\,. \tag{4.17}$$

This means that the mass dimension of $|k\rangle$ is 0. Consider

$$\Gamma^{\mu\nu}(k,k') := \langle k|\,T^{\mu\nu}(0,0)\,|k'\rangle\,,$$

where $T^{\mu\nu}(t,x)$ is the energy-momentum tensor. The mass dimension of Γ is +2. By a standard set of manipulations[4] [6] (Sec. 10.6), one can show that

$$\Gamma^{\mu\nu}(k,k') = \frac{1}{2}\left(F_1(l^2)(k+k')^\mu(k+k')^\nu + F_5(l^2)\left(\eta^{\mu\nu}-l^{-2}l^\mu l^\nu\right)\right), \tag{4.18}$$

[4]The covariance of $T^{\mu\nu}$ implies that $\Gamma^{\mu\nu}(k,k')$ can be constructed from the tensor structures $k^\mu k^\nu$, $k^\mu k'^\nu$, $k'^\mu k^\nu$, $k'^\mu k'^\nu$ and $\eta^{\mu\nu}$; $\partial_\mu T^{\mu\nu} = \partial_\nu T^{\mu\nu} = 0$ implies $l_\mu\Gamma^{\mu\nu} = l_\nu\Gamma^{\mu\nu} = 0$; $T^{\mu\nu\dagger} = T^{\nu\mu}$ implies $\Gamma^{\mu\nu}(k,k')^* = \Gamma^{\nu\mu}(k',k)$ which in turn implies F_1, F_5 are real; the momentum operator is $\hat{P}^\mu = \int dx\,T^{0\mu}(t,x)$, so $k^\mu = 2\pi\Gamma^{0\mu}(k,k)$, which implies $F_1(0) = 1$, $F_5(0) = 0$.

where $l^\mu \equiv (k-k')^\mu$. F_1 and F_5 are undetermined, real functions of l^2 and M, but the M dependence is rarely displayed. At $l^2 = 0$, they satisfy $F_1(0) = 1$ and $F_5(0) = 0$. They are the so-called form factors and they encode everything non-trivial about $\Gamma^{\mu\nu}$.

The radius of the particle is related to the first derivatives of the form factors, $F_1'(0)$ and $F_5'(0)$. The form factors depend only on the momentum difference, so we can conveniently choose $k^\mu = (M, 0)$, $k'^\mu = (\sqrt{M^2+q^2}, q)$ and expand in powers of q. The momentum transfer satisfies $l^2 = -q^2 + \mathcal{O}(q^4)$. We define the radius, R, as

$$R^2 = \frac{1}{M^2}\partial_{-q^2}\Gamma^{00}(k,k')\Big|_{q=0}. \tag{4.19}$$

The rationale for this choice is that to leading order in $\hbar$ (i.e. classically), it gives $R^2 = \int dx\, x^2\mathcal{H}_{cl}(x)/\int dx\,\mathcal{H}_{cl}(x)$ (see (4.38) later) which, as discussed in §1.2, is reasonable. Let Λ be the Lorentz transformation that takes $k \to k'$ and expand the corresponding operator $U(\Lambda)$ in powers[5] of q:

$$U(\Lambda) = 1 - \frac{iq}{M}K - \frac{q^2}{2M^2}K^2 + \mathcal{O}(q^3), \tag{4.20}$$

where K is the boost generator:

$$K = \int dx\; x\, T^{00}(0,x). \tag{4.21}$$

Using (4.17), (4.20) in (4.19) shows that

$$R^2 = \frac{1}{2M^4}\left\langle k\right|\mathcal{H}(0,0)K^2\left|k\right\rangle, \tag{4.22}$$

where the energy density $\mathcal{H}(t,x) = T^{00}(t,x)$. Expanding (4.18) also shows that $R^2 = (F_5'(0) - 2 + 4M^2F_1'(0))/(2M^2)$ in terms of the form factors.

4.5.2 Evaluation

We will compute R^2 in powers of λ^{-1} and our goal will be to determine the sub-leading term. We should note that the expansion in powers of λ^{-1} is equivalent

[5]This follows from $U = \exp(i\omega_{10}K)$ where $\omega_{\mu\nu} = \eta_{\mu\rho}\omega^\rho_\nu$ and ω^μ_ν is determined from $\Lambda^\mu_\nu = \delta^\mu_\nu + \omega^\mu_\nu + O(\omega^2)$ – which gives $\omega_{10} = -q/M$.

to the expansion in powers of $\hbar$ ([74] Sec. 1.1), so what we are working out is the first quantum correction to R. Using (4.21) in (4.22) gives

$$R^2 = \frac{1}{2M^4}\int x\,x'\,\langle k|\,\mathcal{H}(0,0)\mathcal{H}(0,x)\mathcal{H}(0,x')\,|k\rangle\,dx\,dx'. \tag{4.23}$$

Let

$$O \equiv \frac{1}{2M^4}\int x\,x'\,\mathcal{H}(0,0)\mathcal{H}(0,x)\mathcal{H}(0,x')dx\,dx';$$

applying (4.6), (4.8) to (4.23), we then have[6]

$$R^2 = \frac{\lim_{T\to\infty} e^{2MT}\int \langle\Omega,\sim|\,\mathcal{O}^\dagger(y)e^{-HT}Oe^{-HT}\mathcal{O}(z)\,|\Omega,\sim\rangle\,dz\,dy}{\langle k|k\rangle^{-1}\lim_{T\to\infty} e^{2MT}\int \langle\Omega,\sim|\,\mathcal{O}^\dagger(y)e^{-2HT}\mathcal{O}(z)\,|\Omega,\sim\rangle\,dz\,dy}. \tag{4.24}$$

To evaluate this, we will work in a spatial box of size L and then let $L\to\infty$. The factor of $\langle k|k\rangle$ in (4.24) is fixed since (4.16) reads $\langle k|k\rangle = 2ML$ in a box of size L. Now, since $\pi_{cl}=0$, the soliton operator is $\mathcal{O}(x)=\exp(-i\int da\;\phi_{cl}(a)\pi(x+a))$; using (4.1), (4.7), we then have $\mathcal{O}(x)\,|\Omega,\sim\rangle = |\phi_{cl}(\cdot-x)\rangle_\phi$ (which is the configuration of a soliton centered on x). When we make the change of variables from ϕ to X and χ, the state $|\phi_{cl}(\cdot-x)\rangle_\phi$ is easily seen to correspond to $|X=x,\chi=0\rangle$ (which we will denote as $|x,0\rangle$). Therefore, we have

$$R^2 = \frac{\lim_{T\to\infty} e^{2MT}\int \langle y,0|\,e^{-HT}Oe^{-HT}\,|z,0\rangle\,dz\,dy}{\frac{1}{2ML}\lim_{T\to\infty} e^{2MT}\int \langle y,0|\,e^{-2HT}\,|z,0\rangle\,dz\,dy}. \tag{4.25}$$

In §B.1, we present the intermediate steps that allow (4.25) to be written as

$$R^2 = \left(\int[d\chi][d\bar\pi]e^{S[\bar\pi,\chi]}\int dx\,dx'\,dx''\,(x-x'')\,(x'-x'')\;\tilde{\mathcal{H}}(x'')\,\tilde{\mathcal{H}}(x)\,\tilde{\mathcal{H}}(x')\right) \tag{4.26}$$

$$\times\left(M^3\int[d\chi][d\bar\pi]e^{S[\bar\pi,\chi]}\right)^{-1}, \tag{4.27}$$

where

$$\tilde{\mathcal{H}}(x) := a(x)+b(x)+c(x)+\mathcal{O}(\lambda^{-1}); \tag{4.28}$$

$$a\propto\lambda^2,\qquad b\propto\lambda,\qquad c\propto\lambda^0; \tag{4.29}$$

$$\begin{aligned} a(x) &:= \frac{1}{2}\left(\phi_{cl}'^2-\phi_{cl}^2+\frac{\phi_{cl}^4}{2\lambda^2}+\frac{\lambda^2}{2}\right),\\ b(x) &:= (\phi_{cl}'\chi)', \\ c(x) &:= \frac{1}{2}\left(\bar\pi^2+\chi'^2-\chi^2+\frac{3}{\lambda^2}\phi_{cl}^2\chi^2-\delta_{m^2}(\phi_{cl}^2-\lambda^2)\right)+C_0(x) \end{aligned} \tag{4.30}$$

[6] The denominator of (4.24) follows from applying (4.6), (4.8) to $\langle k|k\rangle$ and eliminating the common factor of $|\langle k|k,\sim\rangle|^2$ between this and R^2.

($C_0(x)$ is defined in §B.1), and

$$S = S_{free} + S_{int} + \mathcal{O}(\lambda^{-2}); \tag{4.31}$$

$$S_{free} \propto \lambda^0, \qquad S_{int} \propto \lambda^{-1}; \tag{4.32}$$

$$S_{free} = \int d^2x \left(i\bar{\pi}\dot{\chi} - \frac{1}{2}\bar{\pi}^2 - \frac{1}{2}\chi'^2 + \frac{1}{2}\chi^2 - \frac{3}{2\lambda^2}\phi_{cl}^2\chi^2 \right), \tag{4.33}$$

$$S_{int} = \int d^2x \left(-\frac{\phi_{cl}\chi^3}{\lambda^2} + \delta_{m^2}\phi_{cl}\chi \right). \tag{4.34}$$

To calculate (4.26)-(4.27), we expand in powers of S_{int}, which leaves us with moments of the free action: $\langle \chi^n \bar{\pi}^m \rangle \equiv \int [d\chi][d\bar{\pi}] \chi^n \bar{\pi}^m e^{S_{free}[\bar{\pi},\chi]}$. The moments can in turn be built from the propagators $\langle \bar{\pi}\chi \rangle$, $\langle \chi\chi \rangle$ and $\langle \bar{\pi}\bar{\pi} \rangle$. These propagators are given explicitly in §B.2. Expanding (4.26)-(4.27) in powers of λ^{-1} using (4.28)-(4.34), we find

$$R^2 = M^{-3}(\eta + \gamma + \mathcal{O}(\lambda^3)); \qquad \eta \propto \lambda^6, \qquad \gamma \propto \lambda^4; \tag{4.35}$$

$$\eta := \int a_1 a_2 a_3 \, d\mu, \tag{4.36}$$

$$\gamma := \int d\mu \Big(a_1 a_2 \langle S_{int}\, b_3 \rangle + a_1 \langle b_2 b_3 \rangle + \langle c_1 \rangle a_2 a_3 + \text{cyclic permutations of 1,2,3} \Big). \tag{4.37}$$

$a_{1,2,3}$ here stands for $a(x''), a(x), a(x')$ respectively and the same goes for $b_{1,2,3}$ and $c_{1,2,3}$. The measure stands for $d\mu \equiv dx\, dx'\, dx''(x - x'')(x' - x'')$.

$a(x)$ is actually the classical energy density, so $M_0 = \int a(x)dx = 2\sqrt{2}\lambda^2/3$ and $\int x\, a(x)dx = 0$. Therefore the contribution from η gives the classical term

$$R^2 = \frac{a_{(2)}}{M_0} + O(\lambda^{-1}), \tag{4.38}$$

where

$$a_{(2)} \equiv \int x^2 a(x) = \frac{\sqrt{2}m\lambda^2}{9} \left(\pi^2 - 6 \right).$$

We note that (4.38) agrees with (1.1).

The quantum correction γ evaluates to

$$\gamma = c_{(2)} M_0^2 + 2c_{(0)} M_0\, a_{(2)} - 2M_0^2 \int \langle S_{int}\, \chi(x) \rangle\, \phi'_{cl}(x)\, x\, dx, \tag{4.39}$$

where $c_{(0)} \equiv \int \langle c(x) \rangle dx$ and $c_{(2)} \equiv \int \langle c(x) \rangle x^2 dx$. In deriving this we've integrated by parts and used the fact that $\phi'_{cl}(x)$ is exponentially damped at large $|x|$, and used the fact that

$$\int d\mu \, (a_1 \langle b_2 b_3 \rangle + \text{cyclic permutations of 1,2,3}) = 0$$

because

a) $\int b = \int (\phi'_{cl} \chi)' = 0$ since ϕ'_{cl} is exponentially damped at large $|x|$,

b) $\int x\, b = \int x (\phi'_{cl} \chi)' = [x \phi'_{cl} \chi]_{-\infty}^{\infty} + \int \phi'_{cl} \chi = 0$ because of the constraint on χ (see (2.42)).

In evaluating $\langle c(x) \rangle$, we notice that $c(x)$ contains the product of two fields at the same point. To regulate the divergences associated with this, we need to 'point-split' the arguments:

$$c(x) = \lim_{x' \to x} c_{ps}(x, x'),$$

where (with all operators at time zero)

$$c_{ps}(x,x') = \frac{1}{2} \left(\bar{\pi}(x) \bar{\pi}(x') + \left(\partial_x \partial_{x'} + 3\lambda^{-2} \phi_{cl}^2(x) - 1 \right) \chi(x) \chi(x') + \delta_{m^2} \left(\lambda^2 - \phi_{cl}^2(x) \right) \right)$$

$$+ C_{0,ps}(x,x').$$

$C_{0,ps}(x,x')$ is the point split version of $C_0(x)$ and it is defined and calculated in §B.3. Using the propagators defined in §B.2, and (B.8), we get

$$\begin{aligned} \langle c_{ps}(x,x') \rangle = & \frac{1}{2} \left(\partial^2 + \partial_x \partial_{x'} + 3\lambda^{-2} \phi_{cl}^2(x) - 1 \right) G^s(0;x,x') + \frac{1}{2} \Delta^s(0;x,x') \\ & + \frac{1}{2} (\lambda^2 - \phi_{cl}^2(x)) \left(\delta_{m^2} - 3\lambda^{-2} \tilde{G}(0;x,x') \right), \end{aligned} \tag{4.40}$$

where $G^s(t;x,x') \equiv G(t;x,x') - \tilde{G}(t;x,x')$, $\Delta^s(t;x,x') \equiv \Delta(t;x,x') - \tilde{\Delta}(t;x,x')$ (these subtracted propagators are worked out in §B.4) and ∂^2 is two derivatives w.r.t. to the first argument of G^s. It can be checked using (4.15), (B.9), that $\delta_{m^2} = 3\lambda^{-2} \tilde{G}(0;x,x)$, so that the last term in (4.40) can be dropped. Using (B.11)-(B.13), and isolating the discrete mode, we get

$$\langle c_{ps}(x,x') \rangle = c^P(x,x') + c^C(x,x'),$$

where

$$c^P(x,x') = \frac{1}{4}\sqrt{\frac{2}{3}}\left(\partial_x\partial_{x'} + 3\lambda^{-2}\phi_{cl}^2(x) + \frac{1}{2}\right)\psi_a(x)\psi_a(x'),$$
$$c^C(x,x') = \int dk \frac{(\partial_x\partial_{x'} + 3\lambda^{-2}\phi_{cl}^2(x) + 1 + k^2)\left(e^{ik(x-x')}\sum_{l=0}^3 k^l A_l(x,x')\right)}{16\pi(k^2+2)^{3/2}(2k^2+1)}$$

(with $A_l(x,x')$ defined in (2.27)-(2.30)). c^P is finite when $x' \to x$:

$$c^P(x,x) = \frac{\sqrt{3}}{32}\left(-9\cosh\left(\sqrt{2}x\right) + 2\cosh\left(2\sqrt{2}x\right) + 9\right)\operatorname{sech}^6\left(\frac{x}{\sqrt{2}}\right).$$

c^C can be written as

$$c^C(x,x') = \sum_{l=0}^{5} B_l(x,x')\mathcal{K}_l(x,x'),$$

where

$$\mathcal{K}_l(x,x') \equiv \int \frac{k^l\,dk}{16\pi}\frac{e^{ik(x-x')}}{(k^2+2)^{3/2}(2k^2+1)}, \tag{4.41}$$

and, using (2.27)-(2.30),

$$B_5(x,x') = 12i\operatorname{sech}^2\left(\frac{x}{\sqrt{2}}\right)(x-x') + \mathcal{O}\left((x-x')^2\right),$$
$$B_4(x,x') = \mathcal{O}(x-x'),$$
$$B_3(x,x') = \mathcal{O}(x-x'),$$
$$B_2(x,x') = 3\operatorname{sech}^2\left(\frac{x}{\sqrt{2}}\right)\left(1 - 9\tanh^2\left(\frac{x}{\sqrt{2}}\right)\right) + \mathcal{O}(x-x'),$$
$$B_1(x,x') = \mathcal{O}(x-x'),$$
$$B_0(x,x') = -3\operatorname{sech}^2\left(\frac{x}{\sqrt{2}}\right)\left(1 + 15\tanh^4\left(\frac{x}{\sqrt{2}}\right)\right) + \mathcal{O}(x-x').$$

For $l = 0,1,2,3$, $\mathcal{K}_l$ is finite when $x' \to x$:

$$\mathcal{K}_3(x,x) = \mathcal{K}_1(x,x) = 0,$$
$$\mathcal{K}_2(x,x) = \frac{9-\sqrt{3}\pi}{216\pi},$$
$$\mathcal{K}_0(x,x) = \frac{4\sqrt{3}\pi - 9}{432\pi}.$$

For $l = 4, 5$, we have[7]

$$\mathcal{K}_4(x,x') = -\frac{\log|x-x'|}{16\pi}\left(1+\mathcal{O}(x-x')\right),$$
$$\mathcal{K}_5(x,x') = \frac{i}{16\pi(x-x')} + \mathcal{O}(1).$$

Putting this all together,

$$\langle c(x)\rangle = c^P(x,x) + \sum_{l=0,2} B_l(x,x)\mathcal{K}_l(x,x) + \lim_{x'\to x}\sum_{l=4,5} B_l(x,x')\mathcal{K}_l(x,x')$$
$$= \frac{\operatorname{sech}^6\left(\frac{x}{\sqrt{2}}\right)}{96\pi}\left((-72-9\sqrt{3}\pi)\cosh(\sqrt{2}x) + (2\sqrt{3}\pi-9)\cosh(2\sqrt{2}x) + 27 + 9\sqrt{3}\pi\right).$$

This gives

$$c_{(0)} = \frac{1}{2\sqrt{6}} - \frac{3}{\pi\sqrt{2}}, \qquad c_{(2)} = \frac{\pi\left(14\sqrt{3}+\pi\left(\sqrt{3}\pi-18\right)\right)-18}{36\sqrt{2}\pi}.$$

The exact mass of the kink is given by[8]

$$M = \int_{-\infty}^{\infty} dx(a(x) + \langle c(x)\rangle) + \mathcal{O}(\lambda^{-1}) = M_0 + c_{(0)} + \mathcal{O}(\lambda^{-1}).$$

Restoring factors of m, this gives $M = 2\sqrt{2}m^3\lambda^2/3 + m/(2\sqrt{6}) - 3m/(\pi\sqrt{2}) + \mathcal{O}(\lambda^{-1})$ in agreement with the canonical result [31, 75, 76].

[7] To show this, we expand $(2k^2+1)^{-1}$, in (4.41), in powers of $(k^2+2)^{-1}$, and induce powers of k using $-i\partial_x$:

$$\mathcal{K}_l(x,x') = \frac{(-i\partial_x)^l}{32\pi}\int dk\, e^{ik(x-x')}\left\{\frac{1}{(k^2+2)^{5/2}} + \mathcal{O}\left(\frac{1}{(k^2+2)^{7/2}}\right)\right\}.$$

For $l = 4, 5$, the sub-leading terms give a finite contribution when $x' \to x$, so we will not be interested in these; the leading term, on the other hand, is divergent when $x' \to x$ and can be evaluated using $\int dk\, e^{ikx}(k^2+2)^{-5/2} = \frac{x^2}{3}K_2(\sqrt{2}|x|)$, where K_n is the modified Bessel function of the second kind.

[8] This follows from $M = \langle k|k\rangle^{-1}\langle k|H|k\rangle$ and using all the steps that led from (4.22) to (4.35)-(4.37).

The final term in (4.39) is evaluated as follows

$$
\begin{aligned}
&-2M_0^2 \int \langle S_{int}\,\chi(x)\rangle\,\phi'_{cl}(x)\,x\,dx \\
&= 6M_0^2\lambda^{-2}\int x\,dt\,dy\,dx\,\phi'_{cl}(x)\phi_{cl}(y)G^s(0;y,y)G(t;y,x) \\
&= 3M_0^2\lambda^{-2}\int_{-\infty}^{\infty} x\,dy\,dx\,\phi'_{cl}(x)\phi_{cl}(y)\left(\frac{\psi_a(y)^2}{\sqrt{6}}+\int\frac{dk}{8\pi}\frac{\sum_{l=0}^3 k^l A_l(y,y)}{(k^2+2)^{3/2}(2k^2+1)}\right) \\
&\times\left(\frac{\psi_a(y)\psi_a(x)}{3/2}+\int\frac{dk}{2\pi}\frac{e^{ik(y-x)}}{k^2+2}\left(1+\frac{\sum_{l=0}^3 k^l A_l(y,x)}{2(k^2+2)(2k^2+1)}\right)\right) \\
&= \frac{M_0^2(-9-8\sqrt{3}\pi+\sqrt{3}\pi^3)}{18\sqrt{2}\pi}.
\end{aligned}
$$

We should note that point splitting the arguments in the correlation function $\langle S_{int}\chi\rangle$ above does not change the result because all the momentum integrals are convergent.

The loop-corrected radius

Putting this all together and restoring factors of m, we finally get

$$
mR = \sqrt{\frac{1}{6}(\pi^2-6)} + (m\lambda)^{-2}\underbrace{\frac{\sqrt{3}\pi\,(2+\pi^2)-72}{8\pi\sqrt{6\,(\pi^2-6)}}}_{\approx -0.06} + \mathcal{O}(m\lambda)^{-3}.
$$

If $\bar{\lambda} \equiv (m\lambda)^{-1}$, we expect that the two terms above are the first of a series, $mR = \sum_{n=0}^{\infty} c_n \bar{\lambda}^n$, with radius of convergence $\bar{\lambda}_c$. The supposed bound $mR \geq \delta > 0$ can now be checked. As Fig. 4.1 shows, as the force increases (i.e. when λ reduces, or $\bar{\lambda}$ increases), the radius decreases because of the negative quantum correction. So it appears that, to this order in $\bar{\lambda}$, the soliton *can* be made smaller by increasing the scalar force. The question of whether this persists for larger $\bar{\lambda}$ depends on the higher order coefficients, c_i, for $i > 2$.

4.6 Outlook

Further work is required to assess the 'bounds states conjecture' as proposed by [4]. Our calculation shows that the first quantum correction to the radius of the ϕ_2^4 kink is negative. We leave to future work the question of what the higher order quantum corrections are, and how they modify the behaviour of the radius as a function of the coupling constant.

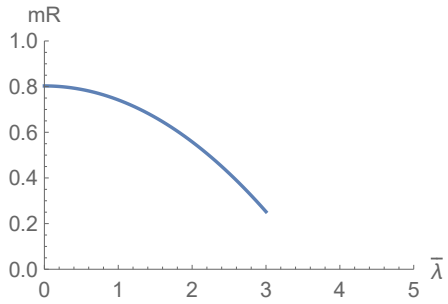

Figure 4.1: mR as a function of $\bar{\lambda}$. This behaviour holds in a vicinity of $\bar{\lambda} = 0$.

We wonder if it is possible to recast the theory in terms of the soliton operators, resulting in a dual theory in which the soliton field is the 'fundamental field'. Deriving the duality would require techniques similar to those reviewed in §2.2.3 – the difference is that the transformations won't be 'point-canonical' (i.e. purely a transformation of field variables)[9]. If this can be done, multi-soliton matrix elements will become calculationally accessible and even pair creation of solitons (an effect that is known to be hard to calculate ([77] Sec. 1.4)). What we are after is similar to what Mandelstam achieved for sine-Gordon theory [64].

'Dualities' have been a hot topic since Maldacena's discovery of AdS/CFT. The typical scenario in a 'duality' is that the amplitudes in theory $\mathcal{A}$ are the same as *some* amplitude in theory $\mathcal{B}$ – knowing which usually proceeds via a 'dictionary' which relates variables in $\mathcal{A}$ to those in $\mathcal{B}$. It is obviously desirable, where possible, to prove a duality from first principles. What this means is to, either, assume or motivate the dictionary, and then to show that the Hamiltonian of $\mathcal{B}$ can be derived by a change of variables from the Hamiltonian of $\mathcal{A}$. In this sense, Mandelstam's proof of the duality between SG and Thirring models is the first of such proofs.

[9] Because the soliton operator is a mix of ϕ and π.

5

Quantum Random Walk on a Cayley Tree

Contents

In §2.3, we discussed the model of a QRW on the half-line. In this chapter, we consider a QRW on a lattice known as the 3-Cayley tree. A q-Cayley tree is a uniformly branching tree, of branching degree q, with a distinguished root vertex. Figs. 5.1 and 5.2 show the 3-Cayley and 4-Cayley trees for example. In this sense, the half-line is a 2-Cayley tree. In this chapter we will focus on the 3-Cayley tree, calling it tree for short.

The layout of this chapter is as follows. In §5.1 we define the model; in §5.2 we derive equations for the generating functions; in §5.3 we solve these equations numerically to establish properties of the spectrum; in §5.4 we introduce a simple coin matrix that allows tractable computations; in §5.5 we invert $U - \lambda$ which leads us to solve the 'perturbed eigenvalue equation': $U|u\rangle = \lambda|u\rangle + |r\rangle$.

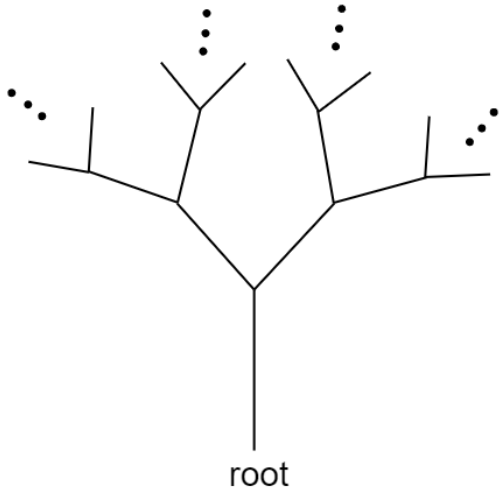

Figure 5.1: The 3-Cayley tree. The ellipses suppress the infinitely repeating pattern.

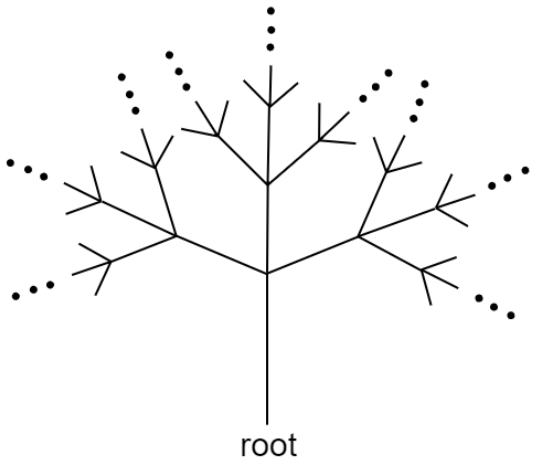

Figure 5.2: The 4-Cayley tree.

5.1 Setup

To be concrete, our tree is an infinite, rooted tree such that the root has degree 1 and all other vertices have degree 3, and we make the following definitions (see Fig. 5.3):

- Let $\mathcal{T}$ be the collection of the vertices of the tree.
- r is the root vertex and r' is the unique vertex neighbouring r.
- For vertices v and v', $d(v, v')$ measures the shortest lattice distance between them. A vertex v will be said to be at radius R if $d(r, v) = R$.
- For vertices v and v', $v > v'$ will mean that v is further from the root than v'.
- Given a vertex v, we define $L(v)$, ($R(v)$ and $D(v)$ resp.) as the vertex branching left (right and down resp.). Note that these are defined only for $v \in \mathcal{T}\backslash r$.

The allowed states of the particle are as follows: when the particle sits at any site but the root, it has a spin $i \in \{1, 2, 3\}$. When the particle sits at the root, however, it has no spin. Therefore configuration space (i.e. the set of basis states) is $\mathcal{C} = |r\rangle \bigcup_{\substack{v\in\mathcal{T}\backslash r \\ i\in\{1,2,3\}}} |v, i\rangle$. The states in $\mathcal{C}$ are defined to be orthonormal. Hilbert space

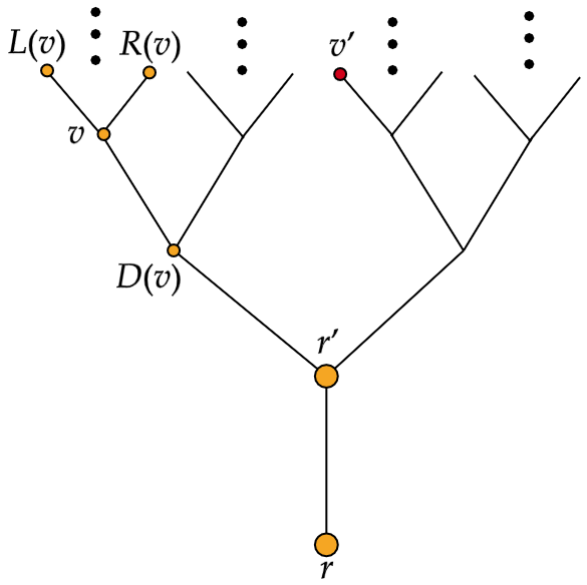

Figure 5.3: Tree Terminology: for an arbitrary vertex v, we have displayed the definitions of $L(v)$, $R(v)$ and $D(v)$.

is the set of all normalizable superpositions of states in $\mathcal{C}$. To define the unitary time evolution operator we first define the coin operator C:

$$C\left|r\right\rangle = \left|r\right\rangle,$$
$$C\left|v,i\right\rangle = \sum_{j=1}^{3} c_{ij}\left|v,j\right\rangle,$$

where c_{ij} is a 3×3 unitary matrix referred to as the coin matrix. Next we define 'shift operators'. To do this we introduce different 'labellings' of the tree. There are in fact six different ways of labelling $\mathcal{T}$ that we will be interested in. The different ways of labelling $\mathcal{T}$ will be called 12, 13, 21, 23, 31 and 32 which together make the set $\mathbb{L} = \{12, 13, 21, 23, 31, 32\}$. The labelling of type ij is defined as follows: we introduce a function $l(r)$ that assigns a label from the set $S = \{1, 2, 3\}$ to the root r and functions $l_L(v)$, $l_R(v)$ and $l_D(v)$ that assign to a vertex $v \in \mathcal{T}\backslash r$, a label from the set S. The labelling of type ij satisfies

- $l(r) = i$.
- $l_L(r') = i$, $l_R(r') = S\backslash\{i, j\}$ and $l_D(r') = j$.
- $l_L(L(v)) = l_L(v)$, $l_R(L(v)) = l_D(v)$ and $l_D(L(v)) = l_R(v)$, $\forall v \in \mathcal{T}\backslash r$.

- $l_L(R(v)) = l_R(v)$, $l_R(R(v)) = l_L(v)$ and $l_D(R(v)) = l_D(v)$, $\forall v \in \mathcal{T}\backslash r$.

It is convenient to represent this like in Fig. 5.4.

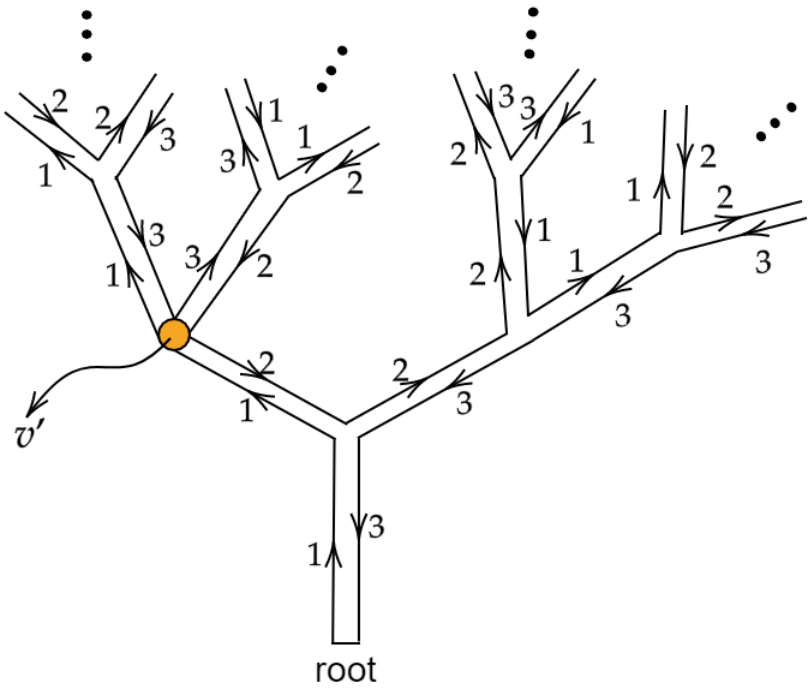

Figure 5.4: Labelling of type 13. This diagram is to be read as follows: for a vertex $v \in \mathcal{T}\backslash r$, $l_L(v)$ (resp. $l_R(v)$ and $l_D(v)$) is given by the label of the arrow pointing out of v towards $L(v)$ (resp. $R(v)$ and $D(v)$); $l(r)$ on the other hand is the label of the arrow pointing out of the root. For example, for the vertex v' shown in orange, $l_L(v') = 1$, $l_R(v') = 3$ and $l_D(v') = 2$.

We will say that (ijk) is the local labelling around a vertex $v \in \mathcal{T}\backslash r$ iff $l_L(v) = i$, $l_R(v) = j$ and $l_D(v) = k$. Vertices of local labelling (123) (resp. (132), (213), (231), (312) and (321)) will be called vertices of type 1 (resp. 2, 3, 4, 5 and 6), see Fig 5.5.

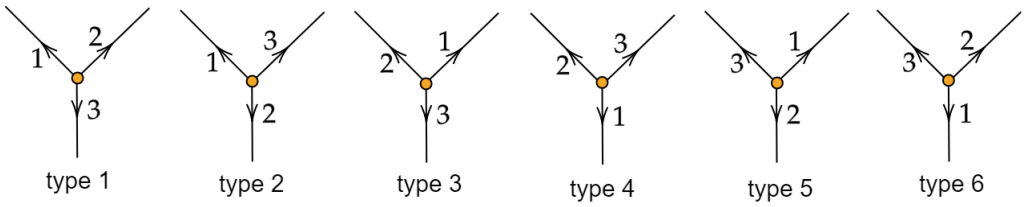

Figure 5.5: The orange vertex is said to be of type $i \in \{1, 2, 3, 4, 5, 6\}$ if it falls into one of the categories above.

Any vertex $v \in \mathcal{T}\backslash r$ can be uniquely written as a sequence of L and R acting

on r'. Let S_v denote that sequence. For example, the vertex v' in Fig. 5.3 can be written as $v' = L \circ L \circ R(r')$, so $S_{v'} = LLR$. For the vertex r', we have $S_{r'} = \mathrm{id}$.

For each type of labelling $\alpha \in \mathbb{L}$, we have a different shift operator S_α. The time evolution operators are defined as $U_\alpha = S_\alpha C$. To specify S_{ij}, we define its action on all basis states: $S_{ij}\left|r\right\rangle = \left|r', i\right\rangle$, $S_{ij}\left|r', j\right\rangle = \left|r\right\rangle$; and for all other states $\left|v, i\right\rangle \neq \left|r', j\right\rangle$, we have $S_{ij}\left|v, i\right\rangle = \left|v', i\right\rangle$ where $v' = L(v)$ if $l_L(v) = i$, $v' = R(v)$ if $l_R(v) = i$ or $v' = D(v)$ if $l_D(v) = i$ (see [46] for a different set of shift operators that one can define on the Cayley tree).

We define return and first-return generating functions

$$\mu_\alpha(z) = \left\langle r\right| \left(1 - zU_\alpha\right)^{-1} \left|r\right\rangle = \sum_{t=0}^{\infty} (\mu_\alpha)_t z^t,$$
$$Q_\alpha(z) = \left\langle r\right| zU_\alpha(1 - z\tilde{U}_\alpha)^{-1} \left|r\right\rangle = \sum_{t=2}^{\infty} (Q_\alpha)_t z^t,$$

respectively, where $\tilde{U}_\alpha := (1 - \left|r\right\rangle \left\langle r\right|)U_\alpha$. Like before, they are related by $\mu_\alpha(z) = (1 - Q_\alpha(z))^{-1}$. We will now show that $Q_\alpha(z)$ satisfy a set of polynomial equations.

5.2 Generating functions

As in §2.3.2, $Q_\alpha(z)$ can be written as a sum over walks:

$$Q_\alpha(z) = \sum_{w \in \mathcal{L}(r)} z^{|w|} P_\alpha(w), \tag{5.1}$$

where $\mathcal{L}(r)$ is the set of walks s.t. $w(0) = w(|w|) = r$ and $w(\tau) > r$ when $0 < \tau < |w|$. $P_\alpha(w)$ is the amplitude of walk w. It is product of the amplitudes of each step except the first:

$$P_\alpha(w) = \prod_{t=1}^{|w|-1} p_\alpha\left(w(t) \to w(t+1)\right),$$

where $p_\alpha\left(w(t) \to w(t+1)\right) = 1$ if $w(t) = r$, otherwise $p\left(w(t) \to w(t+1)\right) = c_{nm}$, where

$$n = \begin{cases} l_L(v(t-1)), & \text{if } L(v(t-1)) = v(t) \\ l_R(v(t-1)), & \text{if } R(v(t-1)) = v(t) \\ l_D(v(t-1)), & \text{if } D(v(t-1)) = v(t) \end{cases}$$

$$m = \begin{cases} l_L(v(t)), & \text{if } L(v(t)) = v(t+1) \\ l_R(v(t)), & \text{if } R(v(t)) = v(t+1) \\ l_D(v(t)), & \text{if } D(v(t)) = v(t+1) \end{cases}$$

Clearly, the assignment of amplitudes depends on the labelling scheme α.

Let $\mathcal{L}_t(v)$ denote the set of walks w of length t such that $w(0) = w(t) = v$ and $w(\tau) > v$ for $0 < \tau < t$. These will be refereed to as 'loops based at v'. Also define $\mathcal{L}(v) = \bigcup\limits_{t \geq 2} \mathcal{L}_t(v)$. The set of all loops based at r can be decomposed as follows

$$\mathcal{L}(r) = \mathcal{L}_2(r) \bigcup_{n \geq 1} \left(\mathcal{B}_n^L \bigcup \mathcal{B}_n^R \right). \tag{5.2}$$

$\mathcal{B}_n^L$ (resp. $\mathcal{B}_n^R$) is the set of loops based at r in which the particle walks from r to r', performs a loop based at r' – with the condition that the first step is to $L(r')$ (resp. $R(r')$) – then performs a further $n-1$ loops based at r' and then finally walks back to r. Define

$$B_\alpha^L(n) = \sum_{w \in \mathcal{B}_n^L} z^{|w|} P_\alpha(w),$$
$$B_\alpha^R(n) = \sum_{w \in \mathcal{B}_n^R} z^{|w|} P_\alpha(w).$$

We will now write down relations for $B_{13}^L(n)$ and $B_{13}^R(n)$. Consider a walk in $\mathcal{B}_n^L$. In this walk, the first loop based at r' lies in the set $\mathcal{W} \equiv \{w : w \in \mathcal{L}(r'),\ w(1) = L(r')\}$. However $\mathcal{W}$ is isomorphic to $\mathcal{L}(r)$ via $w'(t) = S_{w(t)}(L(r'))$ where $w \in \mathcal{L}(r)$ and $w' \in \mathcal{W}$; furthermore $P_{13}(w') = P_{12}(w)$. Therefore the contribution of the first loop to $B_{13}^L(n)$ is equal to $Q_{12}(z)$. Now, the second loop can have a first step to either $L(r')$ or $R(r')$. If the second loop has a first step to $L(r')$ then the total contribution of all steps but those of the first loop is $B_{13}^L(n-1)$. Conversely if the second loop has first step to $R(r')$ then the total contribution of all steps but those of the first loop is $B_{13}^R(n-1)$. Therefore we have

$$B_{13}^L(n) = Q_{12}(z) c_{11} \left(\frac{c_{22}}{c_{12}} B_{13}^R(n-1) + \frac{c_{21}}{c_{11}} B_{13}^L(n-1) \right). \tag{5.3}$$

A similar argument leads to

$$\begin{aligned} B^R_{13}(n) &= Q_{23}(z)c_{12}\left(\frac{c_{32}}{c_{12}}B^R_{13}(n-1)+\frac{c_{31}}{c_{11}}B^L_{13}(n-1)\right), \\ B^L_{13}(1) &= z^2 c_{11}c_{23}Q_{12}(z), \\ B^R_{13}(1) &= z^2 c_{12}c_{33}Q_{23}(z). \end{aligned} \tag{5.4}$$

Due to (5.2), (5.1), $Q_{13}(z)$ can be constructed from these generating functions straightforwardly

$$Q_{13}(z) = z^2 c_{13} + \sum_{n=1}^{\infty}\left(B^L_{13}(n)+B^R_{13}(n)\right). \tag{5.5}$$

Solving the recursion relations (5.3), (5.4) and substituting in (5.5) finally gives

$$Q_{13} = A(Q_{12},Q_{23}) \equiv \frac{z^2\left(-Q_{12}\Pi c^*_{32}-Q_{23}\Pi c^*_{21}+c_{13}+Q_{12}Q_{23}\Pi\right)}{Q_{23}Q_{12}\Pi c^*_{13}-c_{21}Q_{12}-c_{32}Q_{23}+1}, \tag{5.6}$$

where $\Pi \equiv \det c_{ij}$ and we've used the fact that $\Pi c^*_{ij}(-)^{i+j} = \det(M(c_{ij}))$ where $M(c_{ij})$ is the minor of c obtained by omitting c_{ij}. Repeating the procedure for the other generating functions we get

$$Q_{12} = B(Q_{13},Q_{32}) \equiv \frac{z^2\left(-Q_{13}\Pi c^*_{23}-Q_{32}\Pi c^*_{31}+c_{12}+Q_{13}Q_{32}\Pi\right)}{Q_{32}Q_{13}\Pi c^*_{12}-c_{31}Q_{13}-c_{23}Q_{32}+1}, \tag{5.7}$$

$$Q_{23} = C(Q_{21},Q_{13}) \equiv \frac{z^2\left(-Q_{13}\Pi c^*_{12}-Q_{21}\Pi c^*_{31}+c_{23}+Q_{13}Q_{21}\Pi\right)}{Q_{21}Q_{13}\Pi c^*_{23}-c_{31}Q_{13}-c_{12}Q_{21}+1}, \tag{5.8}$$

$$Q_{32} = D(Q_{31},Q_{12}) \equiv \frac{z^2\left(-Q_{12}\Pi c^*_{13}-Q_{31}\Pi c^*_{21}+c_{32}+Q_{12}Q_{31}\Pi\right)}{Q_{31}Q_{12}\Pi c^*_{32}-c_{21}Q_{12}-c_{13}Q_{31}+1}, \tag{5.9}$$

$$Q_{21} = E(Q_{23},Q_{31}) \equiv \frac{z^2\left(-Q_{23}\Pi c^*_{13}-Q_{31}\Pi c^*_{32}+c_{21}+Q_{23}Q_{31}\Pi\right)}{Q_{31}Q_{23}\Pi c^*_{21}-c_{32}Q_{23}-c_{13}Q_{31}+1}, \tag{5.10}$$

$$Q_{31} = F(Q_{32},Q_{21}) \equiv \frac{z^2\left(-Q_{21}\Pi c^*_{23}-Q_{32}\Pi c^*_{12}+c_{31}+Q_{21}Q_{32}\Pi\right)}{Q_{32}Q_{21}\Pi c^*_{31}-c_{12}Q_{21}-c_{23}Q_{32}+1}. \tag{5.11}$$

(5.6)-(5.11) have the property that if $\{Q_\alpha(z)\}_{\alpha\in\mathbb{L}}$ is a solution then $\{\overline{Q_\alpha(\bar{z}^{-1})}^{-1}\}_{\alpha\in\mathbb{L}}$ is too. For any given z there are several solutions for Q_α. The 'physical root' (or 'physical branch', or even 'physical sheet') of these equations is that which behaves around $z=0$ as $Q_\alpha(z) = c_\alpha z^2 + O(z^4)$ since $(Q_\alpha)_2 = c_\alpha$.

(5.6)-(5.11) can be reduced to a single equation as follows. First eliminate Q_{13} and Q_{31}:

$$\begin{aligned}
Q_{12} &= B(A(Q_{12}, Q_{23}), Q_{32}) \longrightarrow Q_{23} = G(Q_{12}, Q_{32}), \\
Q_{23} &= C(Q_{21}, A(Q_{12}, Q_{23})) \longrightarrow Q_{12} = H(Q_{23}, Q_{21}), \\
Q_{32} &= D(F(Q_{32}, Q_{21}), Q_{12}) \longrightarrow Q_{21} = I(Q_{32}, Q_{12}), \\
Q_{21} &= E(Q_{23}, F(Q_{32}, Q_{21})) \longrightarrow Q_{32} = J(Q_{21}, Q_{23}).
\end{aligned}$$

Then eliminate Q_{23} and Q_{21}:

$$\begin{aligned}
Q_{12} &= H(G(Q_{12}, Q_{32}), I(Q_{32}, Q_{12})), \\
Q_{32} &= J(I(Q_{32}, Q_{12}), G(Q_{12}, Q_{32})).
\end{aligned}$$

Each of the equations above can be rearranged as a polynomial and we find that they both factorize. One of the factors in each equation contains the physical branch – we can check which by substituting $Q_\alpha = c_\alpha z^2 + O(z^4)$ and computing if it becomes identically zero to $\mathcal{O}(z^4)$. We find that each of these surviving factors are of order $Q_{12}^2 Q_{32}^2$. Eliminating these for Q_{32} results in an eight-order polynomial equation, too large to display – we will refer to this as the master polynomial. Using numerical techniques, we are able to solve this polynomial and establish the behaviour of the generating functions.

5.3 Spectrum

As discussed in §2.3, z lies on a branch cut of $Q_\alpha(z)$ when z^{-1} lies in the a.c. spectrum of U_α; and $Q_\alpha(z) = 1$ when z^{-1} lies in the p.p. spectrum of U_α.

Our first observation is that $Q_\alpha(z)$ has the same branch cuts for all α. For a typical coin matrix (generated randomly), Fig. 5.6 is a schematic of the analytic structure of $Q_{32}(z)$. It is a curious fact that for all the random coin matrices that we studied numerically, we never observed a spectrum with more than six bands. This apparent upper bound may be related to the branching ratio of the tree, though we have no result in this direction. We attempted to conjecture a relationship by

numerically computing the number of bands of the 4-Cayley tree, but this was not possible because the master polynomial is harder to come by here.

There has been work in the past on determining regions of $U(3)$ (unitary 3×3 matrices) such that coin matrices in these regions give rise to spectra that are purely absolutely continuous or pure point only and in understanding the transition between such regions [46]. In this vein, see [45] for a fairly general condition on the coin matrix that guarantees the absence of mass points.

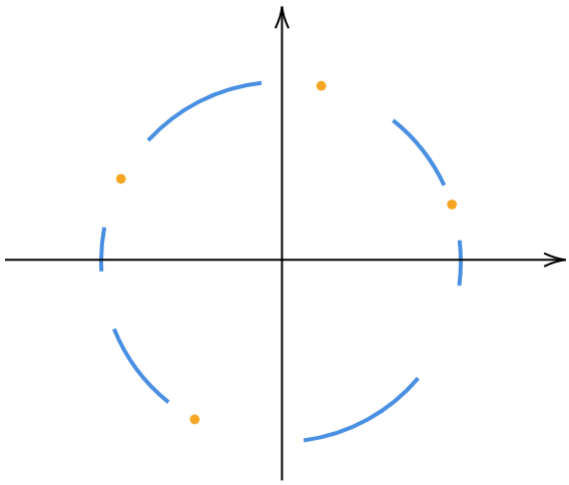

Figure 5.6: In blue are the cuts of Q_{32}, and in orange are points where $Q_{32} = 1$.

5.4 Symmetric coin matrix

In this section we introduce a coin matrix simple enough to allow tractable computations. Let

$$c = \begin{pmatrix} c_{11} & c_{13} & c_{13} \\ c_{13} & c_{11} & c_{13} \\ c_{13} & c_{13} & c_{11}. \end{pmatrix}$$

Then $Q = Q_{13} = Q_{12} = Q_{21} = Q_{23} = Q_{31} = Q_{32}$ satisfies

$$Q = z^2 \frac{Q^2\Pi - 2Q\Pi c_{13}^* + c_{13}}{Q^2\Pi c_{13}^* - 2Qc_{13} + 1}. \tag{5.12}$$

An example of such a coin matrix is

$$c = \begin{pmatrix} -1/3 & 2/3 & 2/3 \\ 2/3 & -1/3 & 2/3 \\ 2/3 & 2/3 & -1/3 \end{pmatrix}, \qquad \det c = 1, \tag{5.13}$$

which we will adopt henceforth for explicit calculations. (5.12) describes a three-sheeted Riemann surface. The physical sheet has no points where $Q = 1$ (so the p.p. spectrum is empty) and it has four branch points $\pm z_0$ and $\pm z_0^{-1}$ on the circle (with the understanding that z_0 lies in the first quadrant) that are the roots of

$$-72 + 88z_0^2 - 23z_0^4 + 88z_0^6 - 72z_0^8 = 0. \tag{5.14}$$

The situation is depicted in Fig 5.7.

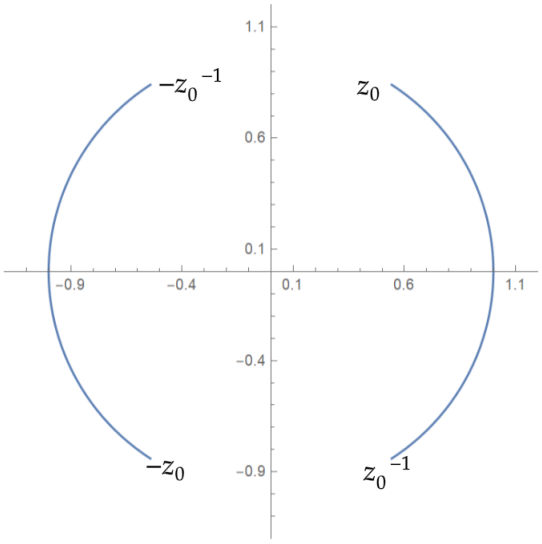

Figure 5.7: The cuts of $Q(z)$ and their edgepoints.

This model is also interesting because it has asymptotically periodic Verblunsky coefficients. A numerical computation shows that the Verblunsky coefficients $\{\gamma_n\}$ approach $\{\gamma, 0, -\gamma, 0, ...\}$ as $n \to \infty$, where the ellipses suppress the repeating pattern, with $\gamma = 0.5427....$ Substituting this sequence in (2.62) and setting the discriminant to zero gives $(1 + z^2)^2 - 4z^2\gamma^2 = 0$. This must have solutions $\pm z_0$, $\pm z_0^{-1}$ since the a.c. spectra must agree (as discussed in §2.3.5). This requires

$$\gamma = \frac{z_0 + z_0^{-1}}{2},$$

which agrees with the numerical result.

5.5 The spectrum a different way

For convenience we define $Q \equiv Q_{13}$, $\mu \equiv \mu_{13}$, $U \equiv U_{13}$ and $\tilde{U} \equiv \tilde{U}_{13}$. In this section we will compute the state

$$|u\rangle = (U - \lambda)^{-1} |r\rangle . \tag{5.15}$$

We will vary λ on the unit circle and enquire when (5.15) breaks down. When λ lies in the spectrum, $|u\rangle$ will be non-normalizable. This will allow us, in principle, to compute the spectrum a different way.

Now, we can rewrite (5.15) as

$$U |u\rangle = \lambda |u\rangle + |r\rangle . \tag{5.16}$$

Therefore this is almost the same as the eigenvalue equation except for a 'source term' $|r\rangle$ which will contribute only at the root. Define the wavefunctions $u_r = \langle r|u\rangle$, $a_v = \langle v, 1|u\rangle$, $b_v = \langle v, 2|u\rangle$ and $c_v = \langle v, 3|u\rangle$ for $v \in \mathcal{T}\backslash r$. Notice that $\langle r|u\rangle = -\lambda^{-1}\mu(\lambda^{-1})$, though we will not use this relation. In terms of the wavefunctions, (5.16) reads

$$u_r = \lambda a_{r'}, \tag{5.17}$$

$$c_{13}a_{r'} + c_{23}b_{r'} + c_{33}c_{r'} = \lambda u_r + 1, \tag{5.18}$$

$$c_{11}a_{r'} + c_{21}b_{r'} + c_{31}c_{r'} = \lambda a_{L(r')}, \tag{5.19}$$

$$c_{12}a_{L(r')} + c_{22}b_{L(r')} + c_{32}c_{L(r')} = \lambda b_{r'}, \tag{5.20}$$

for the vertices closest to the root. What we notice is that there don't seem to be enough equations to propagate the wavefunction out from the origin uniquely. For example, even if u_r is given, (5.17) and (5.18) are not enough to determine $a_{r'}, b_{r'}$ and $c_{r'}$. Similarly, even if $a_{r'}, b_{r'}$ and $c_{r'}$ are given, (5.19) and (5.20) are not enough to determine $a_{L(r')}, b_{L(r')}$ and $c_{L(r')}$. The general phenomenon is that there are only two equations on the wavefunction at a point at radius $r+1$ in terms of the wavefunctions

at radius r: given a vertex v at radius r of type 1, and the neighbouring vertex $v' = L(v)$ at radius $r+1$ of type 2 for example, those two equations are

$$\begin{aligned} c_{11}a_v + c_{21}b_v + c_{31}c_v &= \lambda a_{v'}, \\ c_{12}a_{v'} + c_{22}b_{v'} + c_{32}c_{v'} &= \lambda b_v. \end{aligned} \tag{5.21}$$

However there is a way out: there are extra equations so that given the wavefunction at radius r, the wavefunction at radius $r+1$ can be uniquely determined. For example let v' be a vertex of type 2. Then we have

$$b_{v'} = (c_{13}a_{v'} + c_{23}b_{v'} + c_{33}c_{v'})Q_{32}(\lambda^{-1}), \tag{5.22}$$

$$c_{v'} = (c_{11}a_{v'} + c_{21}b_{v'} + c_{31}c_{v'})Q_{13}(\lambda^{-1}). \tag{5.23}$$

There are similar equations that can be written for vertices of other types. We prove (5.22) and (5.23) in App. C. Since v' in (5.21) is of type 2, we combine (5.22), (5.23) with (5.21), allowing us to determine $\{a_{v'}, b_{v'}, c_{v'}\}$ in terms of $\{a_v, b_v, c_v\}$:

$$\begin{pmatrix} a_{v'} \\ b_{v'} \\ c_{v'} \end{pmatrix} = \underbrace{\lambda^{-1} \begin{pmatrix} c_{11} & c_{21} & c_{31} \\ c_{11}B_2 & c_{21}B_2 & c_{31}B_2 \\ c_{11}A_2 & c_{21}A_2 & c_{31}A_2 \end{pmatrix}}_{\equiv T_{1L}} \begin{pmatrix} a_v \\ b_v \\ c_v \end{pmatrix}, \tag{5.24}$$

$$A_2 = \frac{c_{11}Q_{13}(\lambda^{-1}) + \Pi c_{32}^* Q_{32}(\lambda^{-1})Q_{13}(\lambda^{-1})}{1 - c_{31}Q_{13}(\lambda^{-1}) - c_{23}Q_{32}(\lambda^{-1}) + c_{12}^*\Pi Q_{32}(\lambda^{-1})Q_{13}(\lambda^{-1})},$$

$$B_2 = \frac{c_{13}Q_{32}(\lambda^{-1}) + c_{22}^*\Pi Q_{13}(\lambda^{-1})Q_{32}(\lambda^{-1})}{1 - c_{31}Q_{13}(\lambda^{-1}) - c_{23}Q_{32}(\lambda^{-1}) + c_{12}^*\Pi Q_{32}(\lambda^{-1})Q_{13}(\lambda^{-1})}.$$

We will call the matrix T_{1L} in (5.24) a transfer matrix. Notice that v was any type 1 vertex. Therefore for any type 1 vertex v, we have

$$\begin{pmatrix} a_{L(v)} \\ b_{L(v)} \\ c_{L(v)} \end{pmatrix} = T_{1L} \begin{pmatrix} a_v \\ b_v \\ c_v \end{pmatrix}.$$

Similarly, it can be shown that their exist transfer matrices T_{1R}, T_{2L}, T_{2R}, T_{3L}, T_{3R}, T_{4L}, T_{4R}, T_{5L}, T_{5R}, T_{6L}, T_{6R} such that

$$\left.\begin{aligned} \begin{pmatrix} a_{L(v)} & b_{L(v)} & c_{L(v)} \end{pmatrix}^T &= T_{iL} \begin{pmatrix} a_v & b_v & c_v \end{pmatrix}^T, \\ \begin{pmatrix} a_{R(v)} & b_{R(v)} & c_{R(v)} \end{pmatrix}^T &= T_{iR} \begin{pmatrix} a_v & b_v & c_v \end{pmatrix}^T. \end{aligned}\right\} \begin{array}{l} \forall \text{ type } i \text{ vertices } v \\ \forall\ i \in \{1,2,3,4,5,6\} \end{array} \tag{5.25}$$

It turns out that $T_{5R} = T_{1L}$, $T_{4L} = T_{1R}$, $T_{3R} = T_{2L}$, $T_{6L} = T_{2R}$, $T_{6R} = T_{3L}$ and $T_{5L} = T_{4R}$, so that there are only six independent transfer matrices. Notice that T_{1L} has only one non-zero eigenvalue. Similarly, all transfer matrices have only one non-zero eigenvalue.

Now (5.25) is still not satisfactory because they depend on Q_α. However Q_α can be eliminated. Consider two vertices v and v', both of type 2. Because of (5.22), (5.23), we have

$$\begin{aligned} b_v &= (c_{13}a_v + c_{23}b_v + c_{33}c_v)Q_{32}, \\ c_v &= (c_{11}a_v + c_{21}b_v + c_{31}c_v)Q_{13}, \\ b_{v'} &= (c_{13}a_{v'} + c_{23}b_{v'} + c_{33}c_{v'})Q_{32}, \\ c_{v'} &= (c_{11}a_{v'} + c_{21}b_{v'} + c_{31}c_{v'})Q_{13}. \end{aligned}$$

Eliminating Q_{32} and Q_{13}

$$\begin{aligned} c_{13}\left(\frac{a_{v'}}{b_{v'}} - \frac{a_v}{b_v}\right) + c_{33}\left(\frac{c_{v'}}{b_{v'}} - \frac{c_v}{b_v}\right) = 0, \\ c_{11}\left(\frac{a_{v'}}{c_{v'}} - \frac{a_v}{c_v}\right) + c_{21}\left(\frac{b_{v'}}{c_{v'}} - \frac{b_v}{c_v}\right) = 0. \end{aligned} \tag{5.26}$$

Solving this for a_v and $a_{v'}$ assuming $b_{v'}/c_{v'} - b_v/c_v \neq 0$ gives

$$\begin{aligned} a_v &= -\frac{c_{21}}{c_{11}}b_v - \frac{c_{33}}{c_{13}}c_v, \\ a_{v'} &= -\frac{c_{21}}{c_{11}}b_{v'} - \frac{c_{33}}{c_{13}}c_{v'}. \end{aligned}$$

However these simple relations cannot be true. Therefore the correct solution is $b_{v'}/c_{v'} - b_v/c_v = 0$, which also implies $a_{v'}/c_{v'} = a_v/c_v$ via (5.26). Therefore

$$\{a_{v'}, b_{v'}, c_{v'}\} = \text{scale factor} \times \{a_v, b_v, c_v\},$$

which holds for any two vertices $v, v' \in \mathcal{T}\backslash r$ of type 2 (though not with the same scale factor each time). Similarly, we can show that for any two vertices $v, v' \in \mathcal{T}\backslash r$ of the same type,

$$\{a_{v'}, b_{v'}, c_{v'}\} = \text{scale factor} \times \{a_v, b_v, c_v\}. \tag{5.27}$$

This simple fact along with the existence of transfer matrices allows us to solve for the wavefunctions. Let $\mathbb{t} = \{v_1, v_2, v_{1'}, v_5, v_{2'}, v_6, v_{5'}, v_4, v_{6'}, v_3, v_{4'}, v_{1''}, v_{3'}\}$ be a sublattice of $\mathcal{T}$ defined as

$$\begin{aligned}
&v_1 = r', \qquad v_2 = L(v_1), \qquad v_{1'} = L(v_2),\\
&v_5 = R(v_2), \qquad v_{2'} = R(v_5),\\
&v_6 = L(v_5), \qquad v_{5'} = L(v_6),\\
&v_4 = R(v_6), \qquad v_{6'} = R(v_4),\\
&v_3 = L(v_4), \qquad v_{4'} = L(v_3),\\
&v_{1''} = R(v_3), \qquad v_{3'} = R(v_{1''}),
\end{aligned}$$

as shown in Fig. 5.8. For any vertex v_α in this set, let the wavefunction at that

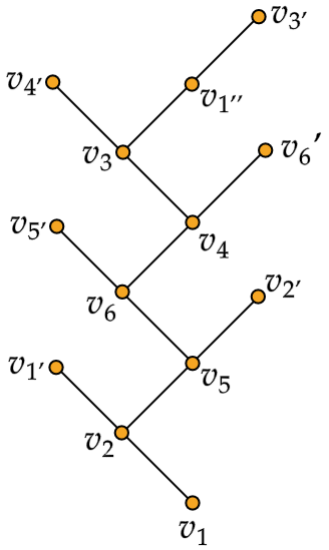

Figure 5.8: The sublattice $\mathbb{t}$.

site be written as $\{a_\alpha, b_\alpha, c_\alpha\}$. Now define Y and $\{X_i\}_{i=1}^6$ as

$$\begin{aligned}
\{a_{i'}, b_{i'}, c_{i'}\} &= X_i\{a_i, b_i, c_i\} \qquad \text{for } i = 1, ..., 6, \qquad (5.28)\\
\{a_{1''}, b_{1''}, c_{1''}\} &= Y\{a_1, b_1, c_1\}.
\end{aligned}$$

That such scale factors exist is because of (5.27). Analogous to (5.22) and (5.23) we can write two equations for the wavefunctions between any two vertices. On

our lattice $\mathbb{t} \cup \{r\}$ this lets us write down 26 equations:

$$\left.\begin{aligned} u_r &= \lambda a_1, \\ c_{13}a_1 + c_{23}b_1 + c_{33}c_1 &= \lambda u_r + 1; \end{aligned}\right\} \text{between } r \text{ and } r' \equiv v_1 \tag{5.29}$$

$$\left.\begin{aligned} a_1c_{11} + a_2(-\lambda) + b_1c_{21} + c_1c_{31} &= 0, \\ a_2c_{12} + b_2c_{22} + b_1(-\lambda) + c_2c_{32} &= 0; \end{aligned}\right\} \text{between } v_1 \text{ and } v_2 \tag{5.30}$$

$$\left.\begin{aligned} a_2c_{11} - a_1\lambda X_1 + b_2c_{21} + c_2c_{31} &= 0, \\ a_1c_{13} + b_1c_{23} - \tfrac{c_2\lambda}{X_1} + c_1c_{33} &= 0; \end{aligned}\right\} \text{between } v_2 \text{ and } v_{1'} \tag{5.31}$$

$$\left.\begin{aligned} a_2c_{13} + b_2c_{23} + c_5(-\lambda) + c_2c_{33} &= 0, \\ a_5c_{12} + b_5c_{22} + b_2(-\lambda) + c_5c_{32} &= 0; \end{aligned}\right\} \text{between } v_2 \text{ and } v_5 \tag{5.32}$$

$$\left.\begin{aligned} a_5c_{11} - a_2\lambda X_2 + b_5c_{21} + c_5c_{31} &= 0, \\ a_2c_{12} + b_2c_{22} - \tfrac{b_5\lambda}{X_2} + c_2c_{32} &= 0; \end{aligned}\right\} \text{between } v_5 \text{ and } v_{2'} \tag{5.33}$$

$$\left.\begin{aligned} a_5c_{13} + b_5c_{23} + c_6(-\lambda) + c_5c_{33} &= 0, \\ a_6c_{11} + a_5(-\lambda) + b_6c_{21} + c_6c_{31} &= 0; \end{aligned}\right\} \text{between } v_5 \text{ and } v_6 \tag{5.34}$$

$$\left.\begin{aligned} a_6c_{13} + b_6c_{23} - c_5\lambda X_3 + c_6c_{33} &= 0, \\ a_5c_{12} + b_5c_{22} - \tfrac{b_6\lambda}{X_3} + c_5c_{32} &= 0; \end{aligned}\right\} \text{between } v_6 \text{ and } v_{5'} \tag{5.35}$$

$$\left.\begin{aligned} a_6c_{12} + b_6c_{22} + b_4(-\lambda) + c_6c_{32} &= 0, \\ a_4c_{11} + a_6(-\lambda) + b_4c_{21} + c_4c_{31} &= 0; \end{aligned}\right\} \text{between } v_6 \text{ and } v_4 \tag{5.36}$$

$$\left.\begin{aligned} a_4c_{13} + b_4c_{23} - c_6\lambda X_4 + c_4c_{33} &= 0, \\ a_6c_{11} - \tfrac{a_4\lambda}{X_4} + b_6c_{21} + c_6c_{31} &= 0; \end{aligned}\right\} \text{between } v_4 \text{ and } v_{6'} \tag{5.37}$$

$$\left.\begin{aligned} a_4c_{12} + b_4c_{22} + b_3(-\lambda) + c_4c_{32} &= 0, \\ a_3c_{13} + b_3c_{23} + c_4(-\lambda) + c_3c_{33} &= 0; \end{aligned}\right\} \text{between } v_4 \text{ and } v_3 \tag{5.38}$$

$$\left.\begin{aligned} a_3c_{12} + b_3c_{22} - b_4\lambda X_5 + c_3c_{32} &= 0, \\ a_4c_{11} - \tfrac{a_3\lambda}{X_5} + b_4c_{21} + c_4c_{31} &= 0; \end{aligned}\right\} \text{between } v_3 \text{ and } v_{4'} \tag{5.39}$$

$$\left.\begin{aligned} a_3c_{11} + a_1\lambda(-Y) + b_3c_{21} + c_3c_{31} &= 0, \\ a_1c_{13} + b_1c_{23} - \tfrac{c_3\lambda}{Y} + c_1c_{33} &= 0; \end{aligned}\right\} \text{between } v_3 \text{ and } v_{1''} \tag{5.40}$$

$$\left.\begin{aligned} a_1c_{12} + b_1c_{22} - \tfrac{b_3\lambda X_6}{Y} + c_1c_{32} &= 0, \\ a_3c_{13} + b_3c_{23} - \tfrac{c_1\lambda Y}{X_6} + c_3c_{33} &= 0. \end{aligned}\right\} \text{between } v_{1''} \text{ and } v_{3'} \tag{5.41}$$

These are written in variables Y, $\{X_i\}_{i=1}^6$, $\{(a_i, b_i, c_i)\}_{i=1}^6$ and u_r – a total of 26 complex d.o.f.. Therefore all variables can in principle be determined from (5.29)-(5.41). How does one then determine the wavefunction at an arbitrary site

in $\mathcal{T}$ that isn't necessarily in $\mathbb{t} \cup \{r\}$? First one notices that (5.28) actually holds more generally:

$$\{a_{L^2(v)}, b_{L^2(v)}, c_{L^2(v)}\} = X_i\{a_v, b_v, c_v\} \qquad \begin{smallmatrix}\forall \text{ type } i \text{ vertices } v \\ \forall\ i\in\{1,3,5\}\end{smallmatrix}, \tag{5.42}$$

$$\{a_{R^2(v)}, b_{R^2(v)}, c_{R^2(v)}\} = X_i\{a_v, b_v, c_v\} \qquad \begin{smallmatrix}\forall \text{ type } i \text{ vertices } v \\ \forall\ i\in\{2,4,6\}\end{smallmatrix}, \tag{5.43}$$

$$\{a_{(RL)^3(v)}, b_{(RL)^3(v)}, c_{(RL)^3(v)}\} = Y\{a_v, b_v, c_v\} \qquad \forall \text{ type 1 vertices } v, \tag{5.44}$$

where $L^2(v) \equiv L\circ L(v)$, $R^2(v) \equiv R\circ R(v)$ and $(RL)^3(v) = R\circ L\circ R\circ L\circ R\circ L(v)$. This follows because of the existence of transfer matrices. For example let v be of type 1. Then $L^2(v)$ is also of type 1, so $\{a_{L^2(v)}, b_{L^2(v)}, c_{L^2(v)}\}^T = \text{scale factor} \times \{a_v, b_v, c_v\}^T = T_{2L}T_{1L}\{a_v, b_v, c_v\}^T$. So $\{a_v, b_v, c_v\}$ must be an eigenvector of $T_{2L}T_{1L}$ and the scale factor must an eigenvalue. However $T_{2L}T_{1L}$ has only one non-zero eigenvalue and its value is X_1, since (5.28) with $i = 1$ reads $\{a_{L^2(v_1)}, b_{L^2(v_1)}, c_{L^2(v_1)}\} = X_1\{a_{v_1}, b_{v_1}, c_{v_1}\}$ for $v_1 \in \mathbb{t}$. Therefore, X_1 is a universal scale factor and so (5.42) with $i = 1$ follows; similarly the other scale factors are universal and so (5.42)-(5.44) follow. Now, from the relations (5.42)-(5.44) it's not hard to show that the wavefunction at any site $v \in \mathcal{T}$ of type i (for any i) can be related to $\{a_i, b_i, c_i\}$ by a scale factor that is a function of only $\{X_i\}_{i=1}^6$ and Y.

Now we can address the question of when $(U - \lambda)^{-1}$ doesn't exist. For λ s.t. $(U - \lambda)^{-1}$ doesn't exist, $|u\rangle$ is non-normalizable. First, let's compute the norm-squared of $|u\rangle$:

$$P_1 \equiv \langle u|u\rangle - |u_r|^2 = \sum_{v\in\mathcal{T}\setminus r} (|a_v|^2 + |b_v|^2 + |c_v|^2). \tag{5.45}$$

Now we define sub-trees of $\mathcal{T}$:

$$\mathcal{T}_2 = \{v : v = \mathcal{O}(v_2)\},$$

$$\mathcal{T}_5 = \{v : v = \mathcal{O}(v_5)\},$$

$$\mathcal{T}_6 = \{v : v = \mathcal{O}(v_6)\},$$

$$\mathcal{T}_4 = \{v : v = \mathcal{O}(v_4)\},$$

$$\mathcal{T}_3 = \{v : v = \mathcal{O}(v_3)\},$$

$$\mathcal{T}_{3''} = \{v : v = \mathcal{O}(R(r'))\},$$

$$\mathcal{T}_{1'} = \{v : v = \mathcal{O}(v_{1'})\},$$

where $\mathcal{O}$ consists of all powers of L and R (for e.g. LRL^2R) including $\mathcal{O} = \mathrm{id}$. The roots of $\mathcal{T}_2, \mathcal{T}_5, \mathcal{T}_6, \mathcal{T}_4, \mathcal{T}_3, \mathcal{T}_{3''}$ and $\mathcal{T}_{1'}$ are $v_2, v_5, v_6, v_4, v_3, R(r')$ and $v_{1'}$ in that order. Now, define the norm-squared on these sub-trees:

$$P_i := \sum_{v \in \mathcal{T}_i} (|a_v|^2 + |b_v|^2 + |c_v|^2) \qquad \text{for } i = 2, 3, 4, 5, 6, 3'', 1'.$$

Note that $\mathcal{T} \backslash r$ can be decomposed as $\{r'\} \cup \mathcal{T}_2 \cup \mathcal{T}_{3''}$. Therefore $P_1 = |a_1|^2 + |b_1|^2 + |c_1|^2 + P_2 + P_{3''}$. However $P_{3''} = |X_6/Y|^2 P_3$ since $\{a_x, b_x, c_x\} = X_6 Y^{-1}\{a_3, b_3, c_3\}$ where x is the root of $\mathcal{T}_{3''}$. Similarly $\mathcal{T}_2$ can be decomposed as $\{v_2\} \cup \mathcal{T}_{1'} \cup \mathcal{T}_5$, so $P_2 = |a_2|^2 + |b_2|^2 + |c_2|^2 + P_{1'} + P_5$. However $P_{1'} = |X_1|^2 P_1$ because $\{a_{1'}, b_{1'}, c_{1'}\} = X_1\{a_1, b_1, c_1\}$. Using similar arguments, one finally arrives at a matrix equation:

$$\underbrace{\begin{pmatrix} 1 & -1 & -|X_6/Y|^2 & 0 & 0 & 0 \\ -|X_1|^2 & 1 & 0 & 0 & -1 & 0 \\ -|Y|^2 & 0 & 1 & -|X_5|^2 & 0 & 0 \\ 0 & 0 & -1 & 1 & 0 & -|X_4|^2 \\ 0 & -|X_2|^2 & 0 & 0 & 1 & -1 \\ 0 & 0 & 0 & -1 & -|X_3|^2 & 1 \end{pmatrix}}_{\equiv M} \begin{pmatrix} P_1 \\ P_2 \\ P_3 \\ P_4 \\ P_5 \\ P_6 \end{pmatrix} = \begin{pmatrix} |a_1, b_1, c_1|^2 \\ |a_2, b_2, c_2|^2 \\ |a_3, b_3, c_3|^2 \\ |a_4, b_4, c_4|^2 \\ |a_5, b_5, c_5|^2 \\ |a_6, b_6, c_6|^2 \end{pmatrix}, \tag{5.46}$$

where $|a_i, b_i, c_i|^2 \equiv |a_i|^2 + |b_i|^2 + |c_i|^2$. This allows P_1 and therefore $\langle u|u\rangle$to be computed. The radius of convergence of (5.45) is reached when $\det M = 0$. Outside of this surface, $|u\rangle$ is non-normalizable. Notice that this convergence criterion only depends on the scale factors.

Let us demonstrate this for the maximally symmetric coin (5.13). First the symmetry tells us that $X_1 = X_3 = X_5$, $X_2 = X_4 = X_6$ and $Y^2 = (X_1 X_2)^3$. Then we write (5.30)-(5.36), (5.38), (5.40) as a matrix equation for the vector $\vec{v} \equiv \{a_1, b_1, c_1, a_2, b_2, c_2, ..., a_6, b_6, c_6\}$: $M_1 \vec{v} = 0$. This implies that that $\det M_1 = 0$ which turns out to be a polynomial equation in just X_1 and X_2. Similarly, (5.30), (5.32)-(5.38), (5.40) can be written as matrix equation $M_2 \vec{v} = 0$, and $\det M_2 = 0$ gives another equation for X_1 and X_2. Eliminating X_2 between these equations leaves

$$\begin{aligned} &-4\left(\lambda^2 - 1\right)^2 \lambda^2 + 9\lambda^4 X_1^3 - 2\left(14\lambda^4 + 2\lambda^2 - 7\right)\lambda^2 X_1^2 \\ &+ \left(36\lambda^8 - 40\lambda^6 + 32\lambda^4 - 28\lambda^2 + 9\right) X_1 = 0. \end{aligned} \tag{5.47}$$

Because the coin matrix is real, it turns out that $|X_1| = |X_2|$. Using this fact to simplify $\det M = 0$ (M defined in (5.46)) gives $(1 - |X_1|^2)(1 - 4|X_1|^2) = 0$. This has a zero closest to the origin when $|X_1| = 1/2$. Therefore the criterion for normalizability of $|u\rangle$ is $|X_1| < 1/2$. Solving (5.47) with $|X_1| = 1/2$ gives

$$-72 + 88\lambda^2 - 23\lambda^4 + 88\lambda^6 - 72\lambda^8 = 0.$$

This has four roots on the circle and they coincide with the endpoints of the bands of the a.c. spectrum as computed in §5.4 (see (5.14)) because, around these values, λ changes from being in the spectrum to out of the spectrum.

5.6 Conclusions

As discussed in §2.3.1 and §5.3, the 2-Cayley tree has a maximum of two bands in the spectrum while the 3-Cayley tree appears to have a maximum of six bands. It is reasonable to conjecture that for the q-Cayley tree, the maximum number of bands in the spectrum is a function of q only; can we determine what this function is? If this is false, we wonder which property of the walk controls the maximum number of bands.

As shown in §5.4, the Verblunsky coefficients of the QRW on the 3-Cayley tree with symmetric coin matrix is asymptotically four-periodic. It is worthwhile determining if this model with general coin matrix also has asymptotically periodic Verblunsky coefficients – by the theorem at the end of §2.3.6 this would immediately provide an upper bound on the number of bands in the spectrum.

An open question is how to solve the eigenvalue equation $U|\lambda\rangle = \lambda|\lambda\rangle$. The obvious obstruction is that the number of equations aren't enough to fix the wavefunction, as discussed at the start of §5.5. In §5.5, we overcame this problem (to solve $U|u\rangle = \lambda|u\rangle + |r\rangle$) by taking advantage of properties of walks which start at the root; however, this same method can't be directly adapted to the eigenvalue equation so it remains open how to do this.

6 Summary

In this thesis, we aimed to solve three rather different problems.

In Chapter 3, we analysed Causal Dynamical Triangulations (CDT) coupled to hard-dimers in two dimensions (aka CDT+HD). CDT is a model of pure quantum gravity and it is a discretization of the path integral over metrics in quantum gravity. It is formulated as a sum over geometries constructed by the gluing of simplicial blocks in all possible ways subject to the constraint that the geometry admits a discrete time slicing. These geometries are discretized analogues of globally hyperbolic geometries. We reviewed pure CDT in §2.1.

Dimers on the other hand are a set of additional degrees of freedom that inhabit the triangulation. They are similar to Ising spins on the triangulation – the difference is that dimers are extended objects. The dimers interact with each other via the hard dimer rule which requires that no two dimers can inhabit the same triangle. This causes the dimers to interact with the underlying geometry in an interesting way. CDT+HD is then defined as the sum over all triangulations and dimer configurations with each triangle and dimer carrying an associated fugacity (or weight). Models of CDT coupled to extra d.o.f. are meant to imitate quantum gravity coupled to matter.

In the past, the partition function of a restricted version of CDT+HD (in which not all dimer types was allowed) was calculated. In this work, we included all

dimers types, subject to a single restriction and solved for the cylinder-amplitude (see §3.4) (which is the amplitude of transition of an initial spatial loop of fixed size at time zero to a final spatial loop of fixed size, at fixed time after zero, such that the topology of the 2-manifold is a cylinder), employing a bijection to labelled trees (§3.3). This also allows one to work out the grand-canonical partition function (which is the amplitude for a point (the zero spatial universe) to transition to a spatial loop of any size in any time). We found that the partition function is actually the root of a fourth-order polynomial whose coefficients are functions of the dimer and triangle fugacities (§3.5). We then worked out the phase diagram of this model (§3.5.4) in the space of coupling constants (aka the fugacities) by taking the scaling limit (the process in which the size of the triangles goes to zero while the total size of the triangulation is kept fixed) and computing the critical exponents. Critical points occur when the coupling constants are tuned such that this polynomial has either a double or triple-root (aka a tri-critical point). In the absence of dimers, the triangle fugacity can be tuned such that this polynomial has a double root, and this gives rise to the pure gravity (PG) phase of CDT. When the dimer weights are non-zero, in addition to the PG phase, the dimers interact strongly with the geometry and new phases appear: two tri-critical phases and two dense dimer phases, phases in which the dimer density diverges in the scaling limit. We analysed these phases in detail (§3.5.2, §3.5.1) and worked out the local and global Hausdorff dimensions (§3.5.3).

We found that the cylinder amplitude is constructed from the solutions to certain second or first order recurrence relations (§3.4). With certain dimer weights we managed to solve these relations but in general they are non-linear and not easily solved. However, by taking the scaling limit, these relations turn into differential equations of second or first order and are characteristic of each phase (§3.6.2). We managed to write down solutions to these differential equations and verified these solutions using the exact solutions of the recurrence relations, where they existed (§3.6.3, §3.6.4). This allowed us to construct the continuum cylinder amplitudes (and disk amplitudes which are gotten by taking the length of the initial loop to

zero, and are supposed to give the amplitude for a big-bang creation event [11]) in each of the phases. By studying the small-time expansion of these functions, we also determined the continuum Hamiltonian (or time-evolution operator) in some phases in which they exist (§3.7). We concluded with an argument for why unrestricted CDT+HD (i.e. with the last remaining constraint lifted) might not have any new phases beyond those that we determined (§3.8). Even then, it is still interesting from a combinatoric viewpoint to find a solution to unrestricted CDT+HD and to overcome the problem of non-local interactions on the tree model.

In Chapter 4, we calculated the soliton radius in the ϕ^4 model in two dimensions (we reviewed the classical aspects of this model in §2.2.1). As we discussed in the introduction, §1.2, this problem began from the 'bound states conjecture': we wanted to find a quantum field theoretic reason for why the radius of a generic stable bound state might be bounded below, by arguing along the lines of an instability caused by particle creation. However we were eventually led to attempt a rigorous calculation of the radius of a well-understood bound state. We settled on the ϕ^4 soliton in two dimensions and attempted to calculate its radius via quantum field theory techniques. Similarly to how the radius of the proton is determined from its electromagnetic form factors [78], the radius of the soliton must follow from an appropriate form factor (this point was suggested to us by *F. Caola*). The soliton has an extended energy distribution so we found it natural to study the form factor $\langle p'| \mathcal{H}(\boldsymbol{x}) |p\rangle$. We were then faced with the problem of determining the one-particle soliton state $|p\rangle$. If the soliton was an elementary excitation of the theory, then $a^\dagger_{\boldsymbol{p}}$ acting on the vacuum $|0\rangle$ would create the incoming (or outgoing) state. One of our contributions was to motivate soliton creation operators, fairly generally, so that acting with these on the vacuum gives an incoming one-particle soliton state, see §4.2, §4.3.

We then compared our results with a famous set of results by S. Mandelstam (§4.4). What he managed to do was derive soliton creation operators in the sine-Gordon (SG) model and show that the Heisenberg equations of motion satisfied by these operators are the same as those satisfied by the Thirring field in the Thirring model. Therefore, he derived, from first principles, the now well-known duality

between sine-Gordon and Thirring models. However, Mandelstam's justification why these operators describe the soliton is slightly heuristic; and his operators do not transform covariantly under Lorentz transformations, which suggests that they are actually being formulated in a particular frame of reference. We find that when our general soliton operators are adapted to the sine-Gordon model, that we can partially match onto Mandelstam's result by formulating our operator in the infinite-momentum frame. More precisely, we find that our operators match onto his *only* when $\beta^2 = 4\pi$ (where β is the coupling constant in the SG model). Therefore, while there is a duality between Mandelstam's operators and the Thirring field for all β, his operators describe the SG soliton only at $\beta^2 = 4\pi$.

To calculate the soliton form factor, we make a change of variables on the configuration space that maps a field configuration ϕ to a position variable X of the soliton and a leftover field configuration χ that is subject to constraints, as reviewed in §2.2.3. The incoming and outgoing soliton states assume a convenient form in these new variables. Moreover, the Hamiltonian can be re-expressed in these new variables. One then expresses the matrix element as a path integral over these new variables. We find that the integral over X and its dual P can be performed easily, leaving us with the integral over χ and its dual $\bar{\pi}$ (§B.1). As usual, we split the action into a free and interacting part and deduce the propagators and Feynman rules from this. We find that we have three propagators $\langle\chi\chi\rangle$, $\langle\chi\bar{\pi}\rangle$ and $\langle\bar{\pi}\bar{\pi}\rangle$ and an infinite set of interaction vertices (§B.2). Using these rules, we then explicitly computed $\langle p'|\,\mathcal{H}(\boldsymbol{x})\,|p\rangle$ and expressed it as the sum of a classical contribution $f_0(x)$ (of order $\hbar^0$) and a first-quantum contribution $f_1(x)$, of order $\hbar^1$ (§4.5). The zeroth moment of $f_0(x) + f_1(x)$ gave us the mass of the kink to order $\hbar^1$ – corroborating the accepted result – and the second moment of $f_0(x) + f_1(x)$ gave us the radius of the kink to order $\hbar^1$.

In Chapter 5, we investigated a quantum random walk on the Cayley tree. The Cayley tree is an infinite, uniformly branching tree of branching order three with a distinguished root vertex. There is a spin-one particle with three internal spin states (the number of spin states is chosen to be equal to the branching

order of the tree) and it is allowed to occupy sites on the tree. The configuration space of this theory consists of all spin states and positions of the particle. We defined a unitary time-evolution operator U_α (time in this system is discrete and takes on non-negative integer values) as the product of coin and shift operators (§5.1). The coin operator simply causes a unitary rotation on the spin states according to a 3×3 unitary 'coin' matrix, while the shift operator moves the particle from any site to one of its three neighbours depending on the spin state of the particle – this assignment of spins to neighbours all throughout the tree is called a 'labelling scheme' and we introduced six different such labelling schemes $\alpha \in \mathbb{L} = \{12, 13, 21, 23, 31, 32\}$. The entries of the coin matrix are considered as variables, and the model is considered a function of these.

An introduction to QRWs can be found in our review of the QRW on the 2-Cayley tree in §2.3 – in which we introduce generating functions, integration measures on the unit circle and solution of the spectrum, among other things.

We showed how matrix elements of U^n can be written as a sum over walks or paths of the particle. We investigated the return generating function (or Stieltjes function) $\mu_\alpha(z)$ and the closely related first return generating function $Q_\alpha(z)$ via the representation as a sum over walks (§5.2). We showed that $\mu_\alpha(z)$ has cuts when z lies in the absolutely continuous (a.c.) spectrum of U_α and $\mu_\alpha(z)$ has poles when z lies in the pure-point spectrum (§2.3.4). The a.c. spectrum typically decomposes into disconnected pieces called bands. We showed how one can derive six coupled polynomial equations for $\{Q_\alpha(z)\}_{\alpha\in\mathbb{L}}$ and outlined a procedure by which these equations can be reduced to a single eighth-order polynomial equation (§5.2). By simulating the solutions to this polynomial on a computer, we derived the analytic structure of $Q_\alpha(z)$ (§5.3). This showed that the number of bands of the spectrum is typically six. We commented that it is interesting to find a reason for this in terms of the properties of the walk. We also analysed a simple example in which the coin matrix was taken to be of a maximally symmetry form in §5.4. In this example we found that the Verblunsky coefficients are asymptotically

four-periodic. We commented that it is interesting to determine if this persists for more general coin matrices.

We then went on to solve for $|u\rangle = (U-\lambda)^{-1}|r\rangle$ (where $|r\rangle$ is the root state and $U \equiv U_{13}$) in §5.5. This provides an independent way to determine the spectrum of U because when λ lies in the spectrum of U, $(U-\lambda)^{-1}|r\rangle$ has infinite norm (the technical statement for this is that $(U-\lambda)^{-1}$ is unbounded when λ lies in the spectrum). We found that the equation for $|u\rangle$ appears to be under-determined. This problem was overcome by using an identity satisfied by walks starting at the root (see §C.1) to derive a closed set of equations for $|u\rangle$. We found that the appropriate ansatz for $|u\rangle$ is that of a function that decays exponentially along 'straight lines' through the tree, controlled by six different decay factors, one for each of the six types of 'straight lines' that can be defined. These decay factors satisfy a known set of coupled polynomial equations. The norm of $|u\rangle$ can be calculated, and the boundary of the region in which the norm is finite can be parametrized solely in terms of the decay factors. By studying the flow of the decay factors as a function of λ and their positions with respect to the boundary surface, one can work out the spectrum. In practice, for general coin matrices this is not easy to do because of the complexity of the polynomial equations. However, for the symmetric coin matrix we introduced in §5.4, the equations are tractable and we showed how this method can be carried through and matched onto the results for the spectrum as determined from the analytic structure of $\mu(z)$. We pointed out at the end that it is interesting to find out how the eigenvalue equation $U|\lambda\rangle = \lambda|\lambda\rangle$ can be solved since it suffers from the same problem of being under-determined and a work-around using properties of the walk cannot be directly applied.

We hope that the reader has enjoyed the direction we have taken through this work and that some of the techniques we have discussed can be used to solve more modern problems like the determination of the mass of the hadronic particles from first principles (through a change of QCD field-variables possibly). In recent times, through the work of Almheiri et. al. and Marolf et. al. [79, 80] (starting with an idea of S. Hawking [8]), it has become clear that topology change can provide

deep insights into the information paradox and the quantum dynamics of black holes. Can we employ this idea to fully resolve the ultraviolet nature of gravity, or will there still be some missing ingredients? We hope that the reader, like us, is inclined to believe that the answer to such questions is near.

Appendices

A

Appendices to Chapter 3

Contents

A.1 Proof that γ is a bijection

Proof. Injectivity follows from checking that the map γ^{-1} exists. This is constructed by combining $\beta^{-1} : \mathcal{P}_{t+1} \to \mathcal{T}_t$ with the labelling rules (i)-(vi) followed backwards. To check surjectivity we show that $\mathcal{RL}_{t+1}$ is indeed the image of $\mathcal{D}_t$ under the map γ, by verifying constraints (vii)-(x):

- (viia) and (viib) follow from the boundary conditions that there are no dimers dual to edges on $\partial_1 T$ and $\partial_2 T$ respectively.
- (viii) follows from the hard dimer rule. To deduce the rules, consider the local occurrence of any dimer type from Fig. 2.6 corresponding to the label $\ell(v)$ of vertex v. Then add a 'probe' dimer to the vacant edges in turn, thus violating the hard-dimer rule. Each time, attach a new triangle to that edge in all allowed ways and apply γ to map this segment of the triangulation to a

segment of a labelled tree; if the probe dimer corresponds to the labelling of a vertex w which is v itself or to the left or right of v, or a child of v, then there is a new constraint on $\ell(w)$, otherwise not. Figs. A.1, A.2 and A.3 show how the constraints (viiib), (viiic) and (viiid) respectively arise. (viiia) follows from applying the same procedure, starting with dimer type 1.

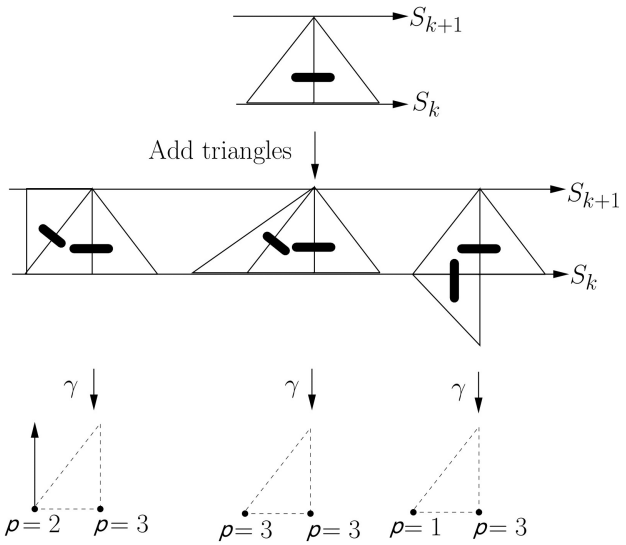

Figure A.1: We start with the definition of a specific dimer type and study the segment of the triangulation under the map γ. The dashed lines are the edges of the triangulation while the solid lines are those of the tree. The horizontal arrows indicate the clockwise direction of the circles.

- (ix) follows from restriction (I) – see Fig. A.4.

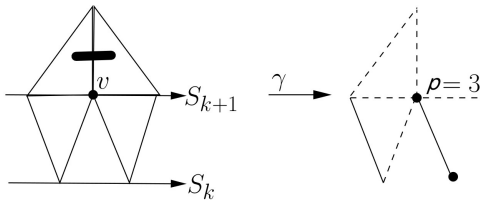

Figure A.4: We apply γ to a triangulation with $f(v)$ dual to a dimer, $\sigma_f(v) = 1$ and $\sigma_b(v) = 2$ to obtain (ix).

- (xa), (xb) and (xc) follow from the geometry of the dimer types – see Fig. A.5.

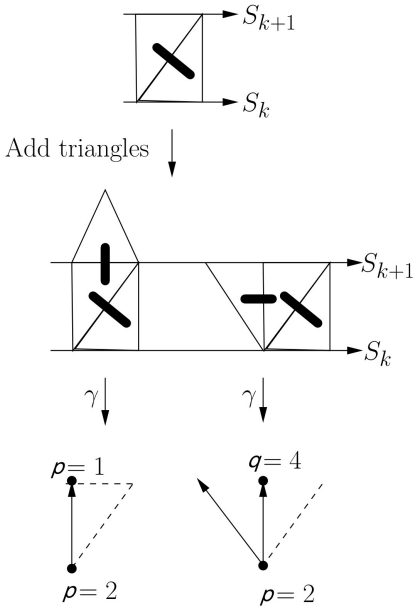

Figure A.2: Constraint (viiic).

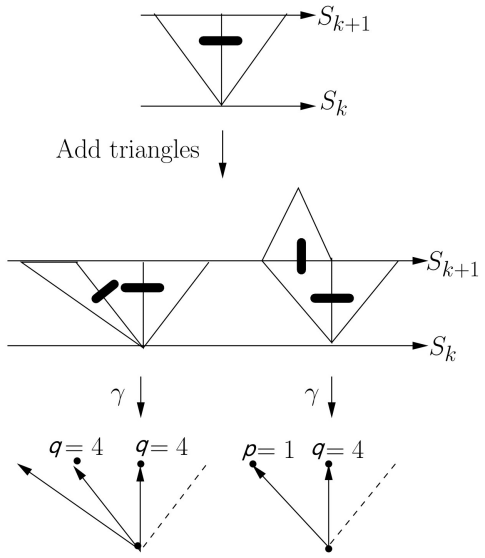

Figure A.3: Constraint (viiid).

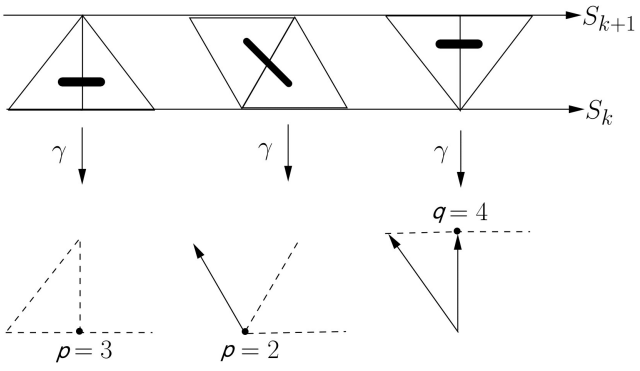

Figure A.5: Constraints (xa), (xb) and (xc).

□

A.2 Cylinder Amplitude Series for TCII

For TCII, the cylinder amplitude cannot be calculated in closed form so we record the series expansion at high and low T for completeness. The couplings

$$\xi_1 = \xi_2 = \xi_3 = 0, \quad \xi_4 = -1/3,$$

lie in TCII. Adopting these couplings and defining $g = g_c - \Lambda a^3/18$, $y = \sqrt{3} - aY$, the small T expansion of F takes the form

$$\begin{aligned} F(T,\Lambda,Y) = -Y + \frac{T}{3}\left(Y^3 - \Lambda\right) + \frac{T^2}{6}Y^2\left(\Lambda - Y^3\right) + \frac{T^3}{54}\left(Y^3 - \Lambda\right)\left(5Y^4 - 2\Lambda Y\right) \\ + \frac{1}{648}T^4\left(\Lambda - Y^3\right)\left(2\Lambda^2 + 35Y^6 - 28\Lambda Y^3\right) + \text{h.o.t.}. \end{aligned}$$

For large T, F can be expanded as a Taylor series in $\exp(-\Lambda^{2/3}T)$:

$$F(T,\Lambda,Y) = -\Lambda^{1/3}\sum_{n=0} a_n \left(\alpha\,\phi(Y)\right)^n e^{-n\Lambda^{2/3}T},$$

where

$$\begin{aligned} \phi(Y) &= \prod_i (-Y + \alpha_i)^{\alpha_i}, \\ \alpha &= -(-1+\alpha_2)^{-\alpha_2}(-1+\alpha_3)^{-\alpha_3}; \end{aligned}$$

the first few coefficients are $a_0 = 1, a_1 = 1, a_2 = 1, a_3 = 7/6, a_4 = 13/9, a_5 = 133/72, a_6 = 217/90$.

A.3 Discrete solution for TCI Cylinder Amplitude

On TCI, $\xi_4 = 0$, so eliminating f_t^2 from (3.12) and (3.13), f_t^1 can be seen to satisfy

$$\begin{aligned} &R(f_{t-1}, f_t, f_{t+1}) \equiv \\ &\quad g^4\xi_1\xi_2 f_{t-1}f_t f_{t+1} - g^2 f_t f_{t+1}\left(g^2\xi_3 + \xi_1 + \xi_2 + 1\right) + f_{t+1}\left(g^2\xi_2 + 1\right) - 1 = 0. \end{aligned}$$

The solution to this is

$$f_t^1 = \frac{c_1 p_1^{-t} + c_2 p_2^{-t} + c_3 p_3^{-t}}{c_1 p_1^{-t-1} + c_2 p_2^{-t-1} + c_3 p_3^{-t-1}}, \tag{A.1}$$

where c_i are unfixed constants and $\{p_i\}_{i=1}^3$ are the three roots of $R(p,p,p) = 0$. There is a simple set of critical couplings lying in TCI which we adopt: $\xi_3 = 0, \xi_1 = \xi_2/4 = -1/8$ for which $f_c^1 = f_c^2 = 4$ and $g_c = 1/\sqrt{2}$; and we take $g = g_c(1 - \Lambda a^3/4)$. First we impose the boundary conditions (3.11) to determine the constants c_i in terms of the fugacity y. Expanding p_i in powers of a gives $p_i = 4(1 - \alpha_i \Lambda^{1/3} a) + O(a^2)$, where $\{\alpha_i\}_{i=1}^3$ are the three roots of unity. Then the numerator and denominator of (A.1) at leading order read $4^{-t} \sum C_i \exp(\alpha_i \Lambda^{1/3} T)$ and $4^{-t-1} \sum C_i \exp(\alpha_i \Lambda^{1/3}(T+a))$ resp., where C_i is the leading term of c_i. With $u(T) := \sum_i C_i \exp(\alpha_i \Lambda^{1/3} T)$, (A.1) then becomes

$$f_{T/a}^1 = 4u(T)/u(T+a) = 4(1 - a\, u'(T)/u(T)) + O(a^2).$$

Comparing this with (3.32) we see that $F^1 = -4u'/u$. Calculating c_i using the boundary conditions, one finds that $c_i = \alpha_i + a\frac{\text{const.}}{y_c - 1/\sqrt{2}} + O(a^2)$. This indicates that the non-trivial scaling occurs at $y_c = 1/\sqrt{2}$. So setting $y = (1 - aY)/\sqrt{2}$, we get $c_i = \alpha_i(2Y + \Lambda^{1/3}\alpha_i) + O(a)$, i.e $C = \alpha_i(2Y + \Lambda^{1/3}\alpha_i)$. Therefore

$$F^1(T, \Lambda, Y) = -4\sqrt[3]{\Lambda} \frac{\sum_i (\alpha_i^2 Y + \sqrt[3]{\Lambda}/2) \exp(\alpha_i \sqrt[3]{\Lambda} T)}{\sum_i (\alpha_i Y + \alpha_i^2 \sqrt[3]{\Lambda}/2) \exp(\alpha_i \sqrt[3]{\Lambda} T)}. \tag{A.2}$$

Expanding (3.12) also shows that $F^2 = 3F^1/2$; together with (A.2), we then have agreement with (3.48).

B

Appendices to Chapter 4

Contents

B.1 Matrix Elements to Path Integrals

We begin by deriving expressions for the Hamiltonian and Hamiltonian density in a perturbative expansion in powers of λ^{-1}. For that purpose, we expand[1] (2.43):

$$\pi(x) = \bar{\pi}(x - X) - \frac{1}{2M_0}\left\{\phi'_{cl}(x - X), P + \int \chi'\bar{\pi}\right\} + O(\lambda^{-2}).$$

The Hamiltonian density of the theory is (see (4.14)) (where all operators in the following are at time zero)

$$\mathcal{H}(x) = \frac{1}{2}\left(\pi(x)^2 + \phi'(x)^2 - (1 + \delta_{m^2})\phi(x)^2 + \frac{\phi^4(x)}{2\lambda^2} + \frac{\lambda^2}{2}(1 + \delta_{m^2})^2\right) + C(x),$$

where

$$C(x) = -\frac{1}{2}\langle\Omega|\left(\pi^2(x) + \phi'^2(x) - (1 + \delta_{m^2})\phi^2(x) + \frac{\phi^4(x)}{2\lambda^2} + \frac{\lambda^2}{2}(1 + \delta_{m^2})^2\right)|\Omega\rangle\,. \tag{B.1}$$

[1] The order of λ can be counted by recalling $\phi_{cl} \propto \lambda$, $M_0 \propto \lambda^2$, and $\delta_{m^2} \propto \lambda^{-2}$.

Expanding this, we have $\mathcal{H}(x) = \tilde{\mathcal{H}}(x - X)$, where

$$\begin{aligned}
&\tilde{\mathcal{H}}(x) := a(x) + b(x) + c(x) + d(x) + \mathcal{O}(\lambda^{-2});\\
&\quad a \propto \lambda^2, \quad b \propto \lambda, \quad c \propto \lambda^0, \quad d \propto \lambda^{-1};\\
&a(x) := \frac{1}{2}\left(\phi_{cl}'^2 - \phi_{cl}^2 + \frac{\phi_{cl}^4}{2\lambda^2} + \frac{\lambda^2}{2}\right),\\
&b(x) := (\phi_{cl}'\chi)',\\
&c(x) := \frac{1}{2}\left(\bar{\pi}^2 + \chi'^2 - \chi^2 + \frac{3}{\lambda^2}\phi_{cl}^2\chi^2 - \delta_{m^2}(\phi_{cl}^2 - \lambda^2)\right) + C_0(x),\\
&d(x) := -\frac{1}{4M_0}\left\{\bar{\pi}, \left\{\phi_{cl}', P + \int \chi'(y)\bar{\pi}(y)\,dy\right\}\right\} - \delta_{m^2}\phi_{cl}\chi + \frac{\chi^3\phi_{cl}}{\lambda^2} + C_{-1}(x).
\end{aligned}$$

$C_0(x)$ and $C_{-1}(x)$ are defined as $C(x) = C_0(x) + C_{-1}(x) + \mathcal{O}(\lambda^{-2})$ s.t. $C_0(x) \propto \lambda^0$ and $C_{-1}(x) \propto \lambda^{-1}$. Integrating $\tilde{\mathcal{H}}(x - X)$ w.r.t. x, we get the Hamiltonian $H = M_0 + H_{free} + H_{int} + O(\lambda^{-2})$ (where $H_{free} \propto \lambda^0$ and $H_{int} \propto \lambda^{-1}$) with [30]

$$\begin{aligned}
H_{free} &= \int dx\, \frac{1}{2}\left(\bar{\pi}^2 + \chi'^2 - \chi^2 + \frac{3}{\lambda^2}\phi_{cl}^2\chi^2 - \delta_{m^2}(\phi_{cl}^2 - \lambda^2)\right) + C_0,\\
H_{int} &= \int dx \left(-\delta_{m^2}\phi_{cl}\chi + \frac{\chi^3\phi_{cl}}{\lambda^2}\right) + C_{-1},
\end{aligned}$$

where $C_i \equiv \int dx\, C_i(x)$ for $i = 0, -1$. To derive H_{int} we've used the constraint (2.42) and the fact that integration variables can be shifted by X provided that every factor under the integral commutes with X. We've also used the fact that $\phi_{cl}' \sim e^{-\sqrt{2}|x|}$ at large $|x|$, meaning that $\int b(x)\,dx = 0$.

Our goal is to calculate the first correction to the radius. A consistent truncation scheme is as follows: the highest term we will keep in $\tilde{\mathcal{H}}(x)$ is $c(x)$ and the highest term in H will be H_{int}. One can easily verify that $\mathcal{H}(x_1)\mathcal{H}(x_2)\mathcal{H}(x_3)$ when expanded to this order can be "left-right ordered" (see §2.2.4) without generating additional terms. Applying (2.45) we thus have[2]

$$\begin{aligned}
&\int \langle y, 0|\, e^{-HT}\mathcal{H}(x_1)\mathcal{H}(x_2)\mathcal{H}(x_3)e^{-HT}\,|x, 0\rangle\, dx\, dy\\
&= \int DXD\chi DPD\bar{\pi}\, \tilde{\mathcal{H}}(x_1 - X)\tilde{\mathcal{H}}(x_2 - X)\tilde{\mathcal{H}}(x_3 - X)\\
&\quad \times \exp\int_{-T}^{T} dt \left(iP\dot{X} + i\int dx(\bar{\pi}\dot{\chi}) - H\right).
\end{aligned}$$

[2] In this formula we have dropped the $\delta(\chi(t = \pm\infty))$ factors because it can be shown that it contributes only an overall factor. We have also dropped the Jacobian factor $J^{1/2}$ arising from $\psi_{in/out}$ which again contributes only an overall constant due to the constraint $\chi(t = \pm\infty) = 0$.

To the order of our calculation, H or $\tilde{\mathcal{H}}$ doesn't depend on X or P; so the integral over P gives $\delta(\dot{X})$. The integral over X is then restricted to constant paths $X(t) = x_0$, giving

$$\int D\chi D\bar{\pi} \int dx_0 \; \tilde{\mathcal{H}}(x_1 - x_0)\tilde{\mathcal{H}}(x_2 - x_0)\tilde{\mathcal{H}}(x_3 - x_0) \; \exp \int_{-T}^{T} dt \left(i \int dx (\bar{\pi}\dot{\chi}) - H \right).$$

Similarly we can show that

$$\int \langle y, 0| \, e^{-2HT} \, |x, 0\rangle \, dx \, dy = L \int D\chi D\bar{\pi} \; \exp \int_{-T}^{T} dt \left(i \int dx (\bar{\pi}\dot{\chi}) - H \right),$$

where the factor of L arises from the x_0 integral.

B.2 Propagators

Using the decomposition (2.34), (2.37), in (4.33), we have

$$S_{free} = \sum_{n=1}^{\infty} \int_{\infty}^{\infty} dt \left(i p_n(t) \dot{a}_n(t) - \frac{1}{2} p_n(t)^2 - \frac{\Omega_n^2}{2} a_n(t)^2 \right).$$

Consider $Z[\vec{J}, \vec{K}] = \int d^{\infty}\vec{a} \; d^{\infty}\vec{p} \; \exp(S_{free} + \sum_{n=1}^{\infty} \int dt (J_n(t) a_n(t) + K_n(t) p_n(t)))$. Integrating $\vec{p}$ out, and then integrating $\vec{a}$ out gives

$$Z[J, K] = const. \; \exp \sum_{n=1}^{\infty} \int_{-\infty}^{\infty} dt \; dt' \Bigg(\frac{1}{2} (i J_n(t) + \dot{K}_n(t)) \mathrm{Op}_n^{-1}(t, t') (i J_n(t') + \dot{K}_n(t'))$$

$$+ \frac{K_n^2(t)}{2} \delta(t - t') \Bigg),$$

where $\mathrm{Op}_n \equiv \partial_t^2 - \Omega_n^2$. Taking derivatives of $Z[J, K]$ w.r.t. to K and J gives the following propagators:

$$\begin{aligned}
\langle \chi(t, x) \chi(t', x') \rangle &= G(t - t'; x, x'), \\
\langle \chi(t, x) \bar{\pi}(t', x') \rangle &= i \partial_{t'} G(t - t'; x, x'), \\
\langle \bar{\pi}(t, x) \bar{\pi}(t', x') \rangle &= -\partial_t \partial_{t'} G(t - t'; x, x') + \Delta(t - t'; x, x'),
\end{aligned}$$

where

$$\begin{aligned}
G(t - t'; x, x') &:= -\sum_{n=1}^{\infty} \Psi_n(x) \Psi_n(x') \mathrm{Op}_n^{-1}(t, t'), \\
\Delta(t - t'; x, x') &:= \delta(t - t') \sum_{n=1}^{\infty} \Psi_n(x) \Psi_n(x').
\end{aligned}$$

Writing Ψ in terms of ψ – see §2.2.3 – gives [30]

$$G(t-t';x,x') = \sum_{n\in\{a,\mathbb{Z}\}} \int \frac{d\omega}{2\pi} e^{i\omega(t-t')} \frac{\psi_n(x)\psi_n^*(x')}{\omega^2+\omega_n^2}, \tag{B.2}$$

$$\Delta(t-t';x,x') = \delta(t-t') \sum_{n\in\{a,\mathbb{Z}\}} \psi_n(x)\psi_n^*(x'). \tag{B.3}$$

In the large L limit, for $m \in \mathbb{Z}$, $\psi_m(x)\psi_m^*(x')$ is given by (2.26), and $k_m = 2\pi m/L + O(L^{-1})$ (see (2.25)). This allows us to convert the sums in (B.2), (B.3), into integrals, which leads, in the $L \to \infty$ limit, to

$$\begin{aligned} G(t-t';x,x') = &\int \frac{d\omega}{2\pi} e^{i\omega(t-t')} \frac{\psi_a(x)\psi_a^*(x')}{\omega^2+\frac{3}{2}} \\ &+ \int \frac{d\omega\, dk}{4\pi^2} \frac{e^{i\omega(t-t')}e^{ik(x-x')}}{\omega^2+k^2+2} \left(1 + \frac{\sum_{l=0}^3 k^l\, A_l(x,x')}{2(k^2+2)(2k^2+1)}\right), \end{aligned} \tag{B.4}$$

$$\Delta(t-t';x,x') = \delta(t-t') \left(\psi_a(x)\psi_a^*(x') + \int \frac{dk}{2\pi} e^{ik(x-x')} \left(1 + \frac{\sum_{l=0}^3 k^l\, A_l(x,x')}{2(k^2+2)(2k^2+1)}\right)\right). \tag{B.5}$$

B.3 The Vacuum Subtraction

Recall that $C(x) = C_0(x) + \mathcal{O}(\lambda^{-1})$ s.t. $C_0(x) \propto \lambda^0$. From (B.1), we have[3]

$$C_0(x) = -\frac{1}{2} \frac{\int [d\phi][d\pi]\, (\pi^2(x) + \phi'^2(x) + 2\phi^2(x))\, e^{S'_{free}}}{\int [d\phi][d\pi] e^{S'_{free}}},$$

with $S'_{free} = \int \left(i\pi\dot{\phi} - \pi^2/2 - \phi'^2/2 - \phi^2\right)$. The equation above contains the product of two fields at the same point. To regularize the divergences associated with this, we need to 'point-split' the arguments:

$$\begin{aligned} C_0(x) &= \lim_{x'\to x} C_{0,ps}(x,x'), \\ C_{0,ps}(x,x') &= -\frac{1}{2} \frac{\int [d\phi][d\pi]\, (\pi(x)\pi(x') + (\partial_x\partial_{x'} + 2)\, \phi(x)\phi(x'))\, e^{S'_{free}}}{\int [d\phi][d\pi] e^{S'_{free}}}. \end{aligned}$$

To work this out, we need the propagators, for which we need to solve the following Schrödinger equation in a spatial box of size L with periodic boundary conditions:

$$\left(-\partial_x^2 + 2\right) \tilde{\psi}_m(x) = \tilde{\omega}_m^2 \tilde{\psi}_m(x).$$

[3] To obtain this we have used $|\Omega\rangle = \langle\Omega|\lambda\rangle_\phi^{-1} \lim_{T\to\infty} e^{-HT} |\lambda\rangle_\phi$ in (B.1), converted the result into a path integral, employed the shift $\phi(t,x) \to \lambda + \phi(t,x)$ in the path integral and expanded out the result to $O(\lambda^0)$.

This gives the following normalized eigenfunctions

$$\tilde{\psi}_m(x) = \frac{1}{\sqrt{L}} \exp(i2\pi mx/L) : \qquad m \in \mathbb{Z},$$
$$\tilde{\omega}_m = \sqrt{\left(\frac{2\pi m}{L}\right)^2 + 2}.$$

This gives the following propagators

$$\langle \phi(t,x)\phi(t',x')\rangle = \tilde{G}(t-t';x,x'),$$
$$\langle \phi(t,x)\pi(t',x')\rangle = i\partial_{t'}\tilde{G}(t-t';x,x'),$$
$$\langle \pi(t,x)\pi(t',x')\rangle = -\partial_t\partial_{t'}\tilde{G}(t-t';x,x') + \tilde{\Delta}(t-t';x,x'),$$

where

$$\tilde{G}(t-t';x,x') = \sum_{m\in\mathbb{Z}} \int \frac{d\omega}{2\pi} e^{i\omega(t-t')} \frac{\tilde{\psi}_m(x)\tilde{\psi}_m^*(x')}{\omega^2+\tilde{\omega}_m^2}, \tag{B.6}$$
$$\tilde{\Delta}(t-t';x,x') = \delta(t-t') \sum_{m\in\mathbb{Z}} \tilde{\psi}_m(x)\tilde{\psi}_m^*(x'). \tag{B.7}$$

Therefore

$$C_{0,ps}(x,x') = -\frac{1}{2}\left(\left(\partial^2 + \partial_x\partial_{x'} + 2\right)\tilde{G}(0,x-x') + \tilde{\Delta}(0,x-x')\right), \tag{B.8}$$

where ∂^2 is two derivatives w.r.t. the first argument of $\tilde{G}$. In the $L\to\infty$ limit, the sums in (B.6), (B.7) can be written as integrals, giving

$$\tilde{G}(t-t';x,x') = \int \frac{d\omega\, dk}{4\pi^2} \frac{e^{i\omega(t-t')}e^{ik(x-x')}}{\omega^2+k^2+2}, \tag{B.9}$$
$$\tilde{\Delta}(t-t';x,x') = \delta(t-t') \int \frac{dk}{2\pi} e^{ik(x-x')}. \tag{B.10}$$

B.4 Subtracted Propagators

Using (B.4), (B.5), (B.9), (B.10), we have, for the subtracted propagators,

$$G^s(t-t';x,x') = \int \frac{d\omega}{2\pi} e^{i\omega(t-t')} \frac{\psi_a(x)\psi_a^*(x')}{\omega^2+\frac{3}{2}} \tag{B.11}$$
$$+ \int \frac{d\omega\, dk}{4\pi^2} \frac{e^{i\omega(t-t')}e^{ik(x-x')}}{\omega^2+k^2+2} \frac{\sum_{l=0}^3 k^l\, A_l(x,x')}{2(k^2+2)(2k^2+1)}, \tag{B.12}$$
$$\Delta^s(t-t';x,x') = \delta(t-t')\left(\psi_a(x)\psi_a^*(x') + \int \frac{dk}{2\pi} \frac{e^{ik(x-x')}\sum_{l=0}^3 k^l\, A_l(x,x')}{2(k^2+2)(2k^2+1)}\right) \tag{B.13}$$

C

Appendices to Chapter 5

Contents

C.1 An identity for walks

We define $\mathcal{W}_v$ as the set of walks that start at the root and end at v. We define $\mathcal{W}_{v,v'}$ as the set of walks, w, s.t. $w(0) = r$, $w(|w|) = v$ and $w(|w| - 1) = v'$. To prove (5.22) and (5.23), we first note that

$$\begin{aligned} b_{v'} &= \langle v', 2| \left(U - \lambda\right)^{-1} |r\rangle = -\lambda^{-1} \sum_{n=0}^{\infty} \lambda^{-n} \langle v', 2| U^n |r\rangle \\ &= -\lambda^{-1} \sum_{w \in \mathcal{W}_{v',R(v')}} \lambda^{-|w|} P(w). \end{aligned} \tag{C.1}$$

However, any path in $\mathcal{W}_{v',R(v')}$ must pass through v' at least once before reaching v' at the final time. So, for a path $w \in \mathcal{W}_{v',R(v')}$ let us refer to the second-to-last time that the particle is at v' as τ_w. Then decompose w as two paths: w_1 and w_2; w_1 will be the path from time zero to τ_w; and w_2 will be the path from τ_w to $|w|$ i.e. $w_2(t) = w(\tau_w + t)$, defined for $0 \leq t \leq |w| - \tau_w$. Now note that

$w_1 \in W_{v'}$ and $w_2 \in \mathcal{L}_{v'}$. So we have

$$W_{v',Rv'} = W_{v'} \circ \mathcal{L}_{v'}, \tag{C.2}$$

where $\mathcal{A} \circ \mathcal{B}$ is meant to be the set of walks obtained by following any walk in $\mathcal{A}$ by any walk in $\mathcal{B}$. But $W_{v'} = W_{v',L(v')} \cup W_{v',R(v')} \cup W_{v',D(v')}$. Combining this with (C.2),

$$W_{v',Rv'} = \left(W_{v',L(v')} \circ \mathcal{L}_{v'}\right) \bigcup \left(W_{v',R(v')} \circ \mathcal{L}_{v'}\right) \bigcup \left(W_{v',D(v')} \circ \mathcal{L}_{v'}\right). \tag{C.3}$$

Similar to (C.1) we have

$$c_{v'} = -\lambda^{-1} \sum_{w \in \mathcal{W}_{v',L(v')}} \lambda^{-|w|} P(w), \tag{C.4}$$

$$a_{v'} = -\lambda^{-1} \sum_{w \in \mathcal{W}_{v',D(v')}} \lambda^{-|w|} P(w). \tag{C.5}$$

Note also that, by definition (see (5.1)),

$$Q_{32}(\lambda^{-1}) = \sum_{w \in \mathcal{L}_{v'}} \lambda^{-|w|} P(w). \tag{C.6}$$

Combining the decomposition (C.3) with (C.4), (C.5), (C.6) we finally get

$$b_{v'} = (c_{13} a_{v'} + c_{23} b_{v'} + c_{33} c_{v'}) Q_{32}(\lambda^{-1}),$$

which proves (5.22). (5.23) can be proved in a similar way.

References

[1] J. F. Wheater and P. D. Xavier. "The cylinder amplitude in the hard dimer model on 2D causal dynamical triangulations". In: *Classical and Quantum Gravity* 39 (2022).

[2] J. Ambjørn and R. Loll. "Nonperturbative Lorentzian quantum gravity, causality and topology change". In: *Nucl. Phys. B* 536 (1998), pp. 407–434. arXiv: hep-th/9805108.

[3] P. Hořava. "Quantum Gravity at a Lifshitz Point". In: *Phys. Rev. D* 79 (2009), p. 084008. arXiv: 0901.3775 [hep-th].

[4] B. Freivogel et al. "A Conjecture on the Minimal Size of Bound States". In: *SciPost Phys. 8, 058* (2020). arXiv: 1912.09485 [hep-th].

[5] M. Santha. "Quantum walk based search algorithms". In: vol. 4978 LNCS. (2008).

[6] S. Weinberg. *The Quantum theory of fields. Vol. 1: Foundations*. Cambridge University Press, (2005).

[7] Y. Harpaz. *The Classification Problem of Smooth Manifolds*. (2008). URL: https://www.math.univ-paris13.fr/~harpaz/manifolds.pdf.

[8] S. W. Hawking. "Wormholes in spacetime". In: *Physical Review D* 37 (1988).

[9] J. von Neumann and R. T. Beyer. *Mathematical Foundations of Quantum Mechanics*. Princeton University Press (1995).

[10] J. -L. Gervais and A. Jevicki. "Point Canonical Transformations in Path Integral". In: *Nucl. Phys. B* 110 (1976), pp. 93–112.

[11] J. B. Hartle and S. W. Hawking. "Wave function of the Universe". In: *Phys. Rev. D.* 28 (1983), pp. 2960–2975.

[12] P. Ramond. *Field theory: a modern primer*. Vol. 74. Addison-Wesley Publishing (1990).

[13] D. Giulini. "Canonical Gravity". In: *Lectures presented at the 16th Saalburg Summer School* (2010). URL: https://saalburg.aei.mpg.de/wp-content/uploads/sites/25/2017/03/giulini.pdf.

[14] E. Witten. "Topological quantum field theory". In: *Communications in Mathematical Physics* 117 (1988).

[15] R. Hagedorn. "Statistical thermodynamics of strong interactions at high energies". In: *Nuovo Cimento, Suppl.* 3.CERN-TH-520 (1965), pp. 147–186.

[16] J. -L. Gervais and B. Sakita. "Extended Particles in Quantum Field Theories". In: *Phys. Rev. D* 11 (1975). Ed. by K. Kikkawa, M. Virasoro, and S. R. Wadia, p. 2943.

[17] S. R. Coleman. *Aspects of Symmetry: Selected Erice Lectures*. Cambridge, U.K.: Cambridge University Press, (1985).

[18] R. Friedberg, T. D. Lee, and Y. Pang. "Mini-Soltion Stars". In: *Phys. Rev. D* 35 (1987). Ed. by H. -C. Ren and Y. Pang, p. 3640.

[19] K. E. Cahill. "Extended Particles and Solitons". In: *Phys. Lett. B* 53 (1974), pp. 174–176.

[20] P. D. Francesco, P. H. Ginsparg, and J. Zinn-Justin. "2-D Gravity and random matrices". In: *Phys. Rept.* 254 (1995), pp. 1–133. arXiv: hep-th/9306153.

[21] J. Ambjørn, B. Durhuus, and T. Jonsson. *Quantum Geometry: A Statistical Field Theory Approach*. Cambridge Monographs on Mathematical Physics. Cambridge Univ. Press, (2005).

[22] S. Weinberg. "Ultraviolet divergences in quantum theories of gravitation". In: *General Relativity – An Einstein Centenary Survey*. Ed. by S. W. Hawking and W. Israel. Vol. 31. Cambridge Univ. Press, (1980), pp. 790–831.

[23] J. Ambjørn et al. "Nonperturbative Quantum Gravity". In: *Phys. Rept.* 519 (2012), pp. 127–210. arXiv: 1203.3591 [hep-th].

[24] B. Durhuus, T. Jonsson, and J. F. Wheater. "On the spectral dimension of causal triangulations". In: *J. Statist. Phys.* 139 (2010), p. 859. arXiv: 0908.3643 [math-ph].

[25] M. R. Atkin and S. Zohren. "An Analytical Analysis of CDT Coupled to Dimer-like Matter". In: *Phys. Lett. B* 712 (2012), pp. 445–450. arXiv: 1202.4322 [hep-th].

[26] J. Ambjørn, B. Durhuus, and J. F. Wheater. "A restricted dimer model on a two-dimensional random causal triangulation". In: *J. Phys. A* 47 (2014), p. 365001. arXiv: 1405.6782 [hep-th].

[27] J. Ambjørn et al. "2d CDT is 2d Hořava–Lifshitz quantum gravity". In: *Phys. Lett. B* 722 (2013), pp. 172–175. arXiv: 1302.6359 [hep-th].

[28] G. M. Napolitano and T. Turova. "The Ising model on the random planar causal triangulation: bounds on the critical line and magnetization properties". In: *J. Statist. Phys.* 162 (2016), pp. 739–760. arXiv: 1504.03828 [cond-mat.stat-mech].

[29] R. Friedberg, T. D. Lee, and A. Sirlin. "A Class of Scalar-Field Soliton Solutions in Three Space Dimensions". In: *Phys. Rev. D* 13 (1976), pp. 2739–2761.

[30] J. -L. Gervais, A. Jevicki, and B. Sakita. "Perturbation Expansion Around Extended Particle States in Quantum Field Theory. 1." In: *Phys. Rev. D* 12 (1975). Ed. by K. Kikkawa, M. Virasoro, and S. R. Wadia, p. 1038.

[31] R. F. Dashen, B. Hasslacher, and A. Neveu. "Nonperturbative Methods and Extended Hadron Models in Field Theory 2. Two-Dimensional Models and Extended Hadrons". In: *Phys. Rev. D* 10 (1974), pp. 4130–4138.

[32] J. Goldstone and R. Jackiw. "Quantization of nonlinear waves". In: *Phys. Rev. D* 11 (1975).

[33] C. G. Callan Jr. and D. J. Gross. "Quantum Perturbation Theory of Solitons". In: *Nucl. Phys. B* 93 (1975), pp. 29–55.

[34] E. Tomboulis. "Canonical quantization of nonlinear waves". In: *Phys. Rev. D* 12 (1975), pp. 1678–1683.

[35] A. Ahlbrecht et al. “Asymptotic evolution of quantum walks with random coin”. In: *Journal of Mathematical Physics* 52 (2011).

[36] A. Bressler and R. Pemantle. “Quantum random walks in one dimension via generating functions”. In: *Proc. of the 2007 Conf. on Analysis of Algorithms, Juan des Pins, France (AofA 07)*. DMTCS Proceedings (2007), pp. 443–456.

[37] M. J. Cantero et al. “Matrix-valued Szegő polynomials and quantum random walks”. In: *Communications on Pure and Applied Mathematics* 63 (2010).

[38] D. A. Meyer. “From quantum cellular automata to quantum lattice gases”. In: *Journal of Statistical Physics* 85 (1996).

[39] N. Konno. “Quantum Walks”. In: *Quantum potential theory*. Springer, Berlin, Heidelberg, (2008), pp. 309–452.

[40] A. Ahlbrecht et al. “Asymptotic behavior of quantum walks with spatio-temporal coin fluctuations”. In: *Quantum Information Processing* 11 (2012).

[41] F. A. Grünbaum et al. “Recurrence for Discrete Time Unitary Evolutions”. In: *Communications in Mathematical Physics* 320 (2013).

[42] M. J. Cantero et al. “One-dimensional quantum walks with one defect”. In: *Reviews in Mathematical Physics* 24 (2012).

[43] B. Simon. *Orthogonal Polynomials on the Unit Circle*. Vol. 1. American Mathematical Society, (2005).

[44] T. D. Mackay et al. “Quantum walks in higher dimensions”. In: *Journal of Physics A: Mathematical and General* 35 (2002).

[45] A. Joye and L. Marin. “Spectral Properties of Quantum Walks on Rooted Binary Trees”. In: *Journal of Statistical Physics* 155 (2014).

[46] E. Hamza and A. Joye. “Spectral Transition for Random Quantum Walks on Trees”. In: *Communications in Mathematical Physics* 326 (2014).

[47] J. Kempe. “Quantum random walks: An introductory overview”. In: *Contemporary Physics* 44 (2003).

[48] F. Zähringer et al. “Realization of a quantum walk with one and two trapped ions”. In: *Physical Review Letters* 104 (2010).

[49] J. Weidmann. “Strong operator convergence and spectral theory of ordinary differential operators”. In: *Univ. Iagel. Acta Math.* 34 (1997), pp. 153–163.

[50] J. Ambjørn et al. “Shaken, but not stirred: Potts model coupled to quantum gravity”. In: *Nucl. Phys. B* 807 (2009), pp. 251–264. arXiv: 0806.3506 [hep-lat].

[51] J. Ambjørn et al. “The spectral dimension in 2D CDT gravity coupled to scalar fields”. In: *Mod. Phys. Lett. A* 30 (2015), p. 1550077. arXiv: 1412.3434 [gr-qc].

[52] J. Ambjørn et al. “A $c = 1$ phase transition in two-dimensional CDT/Hořava–Lifshitz gravity?” In: *Phys. Lett. B* 743 (2015), pp. 435–439. arXiv: 1412.3873 [gr-qc].

[53] J. Ambjørn et al. “The microscopic structure of 2D CDT coupled to matter”. In: *Phys. Lett. B* 746 (2015), pp. 359–364. arXiv: 1503.01636 [gr-qc].

[54] J. Ambjørn and A. Ipsen. “Two-dimensional causal dynamical triangulations with gauge fields”. In: *Phys. Rev. D* 88 (2013), p. 067502. arXiv: 1305.3148 [hep-th].

[55] P. D. Francesco, E. Guitter, and C. Kristjansen. "Integrable 2-D Lorentzian gravity and random walks". In: *Nucl. Phys. B* 567 (2000), pp. 515–553. arXiv: hep-th/9907084.

[56] L. Glaser, T. P. Sotiriou, and S. Weinfurtner. "Extrinsic curvature in two-dimensional causal dynamical triangulation". In: *Phys. Rev. D* 94 (2016), p. 064014. arXiv: 1605.09618 [hep-th].

[57] B. Durhuus et al. "Critical behaviour of loop models on causal triangulations". In: (Apr. 2021). arXiv: 2104.14176 [hep-th].

[58] J. Ambjørn et al. "New multicritical matrix models and multicritical 2d CDT". In: *Phys. Lett. B* 712 (2012), pp. 109–114. arXiv: 1202.4435 [hep-th].

[59] M. R. Atkin and S. Zohren. "On the Quantum Geometry of Multi-critical CDT". In: *JHEP* 11 (2012), p. 037. arXiv: 1203.5034 [hep-th].

[60] M. Staudacher. "The Yang-Lee Edge Singularity on a Dynamical Planar Random Surface". In: *Nucl. Phys. B* 336 (1990). Ed. by E. Brezin and S. R. Wadia, p. 349.

[61] V. G. Knizhnik, A. M. Polyakov, and A. B. Zamolodchikov. "Fractal Structure of 2D Quantum Gravity". In: *Mod. Phys. Lett. A* 3 (1988). Ed. by I. M. Khalatnikov and V. P. Mineev, p. 819.

[62] J. L. Cardy. "Conformal Invariance and the Yang-Lee Edge Singularity in Two-dimensions". In: *Phys. Rev. Lett.* 54 (1985), pp. 1354–1356.

[63] J. Ambjørn et al. "A note on the Lee–Yang singularity coupled to 2d quantum gravity". In: *Phys. Lett. B* 735 (2014), pp. 191–194. arXiv: 1406.1458 [hep-th].

[64] S. Mandelstam. "Soliton Operators for the Quantized Sine-Gordon Equation". In: *Phys. Rev. D* 11 (1975). Ed. by M. Stone, p. 3026.

[65] R. F. Streater and A. S. Wightman. *PCT, spin and statistics, and all that.* Princeton University Press (2016).

[66] C. Cheung and J. Mangan. *Scattering Amplitudes and the Navier-Stokes Equation,* (2020). arXiv: 2010.15970.

[67] G. Badel et al. "The epsilon expansion meets semiclassics". In: *Journal of High Energy Physics* (2019).

[68] G. Badel et al. "Feynman diagrams and the large charge expansion in 3-ε dimensions". In: *Physics Letters, Section B: Nuclear, Elementary Particle and High-Energy Physics* 802 (2020).

[69] G. 't Hooft. "On the Phase Transition Towards Permanent Quark Confinement". In: *Nucl. Phys. B* 138 (1978), pp. 1–25.

[70] T. H. R. Skyrme. "Particle states of a quantized meson field." In: *Proc. R. Soc. Lond. A* 262 (1961), pp. 237–245.

[71] S. R. Coleman. "The Quantum Sine-Gordon Equation as the Massive Thirring Model". In: *Phys. Rev. D* 11 (1975). Ed. by M. Stone, p. 2088.

[72] G. Benfatto, P. Falco, and V. Mastropietro. "Massless Sine-Gordon and Massive Thirring Models: Proof of Coleman's Equivalence". In: *Communications in Mathematical Physics* 285 (2008), pp. 713–762.

[73] D. Tong. *Quantum field theory - Lecture notes,* (2008). URL: https://www.damtp.cam.ac.uk/user/tong/qft/qft.pdf.

[74] L. D. Faddeev and V. E. Korepin. "Quantum theory of solitons". In: *Physics Reports* 42 (1978).

[75] T. Weidig. *Quantum Mass Correction of Solitons in (1+1)D via Numerical Methods.* (1999). URL: https://arxiv.org/abs/hep-th/9912005.

[76] R. Rajaraman. *Solitons and Instantons: An Introduction to Solitons and Instantons in Quantum Field Theory.* North-Holland Publishing Company, (1982).

[77] N. S. Manton. "Classical and Quantum Solitons - Lecture notes". In: *Mathematical Tripos, Part Three, DAMTP* (2017). URL: https://www.damtp.cam.ac.uk/user/examples/3P11e.pdf.

[78] I. Sick. *Proton charge radius from electron scattering* (2018). URL: https://arxiv.org/abs/1801.01746.

[79] A. Almheiri et al. "Replica wormholes and the entropy of Hawking radiation". In: *Journal of High Energy Physics* 13 (2020).

[80] D. Marolf and H. Maxfield. "The page curve and baby universes". In: *International Journal of Modern Physics D* 30 (2021).